1129

TRANSPORTATION RESEARCH RECORD

Soil-Structure Interaction

TRANSPORTATION RESEARCH BOARD
NATIONAL RESEARCH COUNCIL
WASHINGTON, D.C. 1987

Transportation Research Record 1129
Price $10.50

modes
1 highway transportation
3 rail transportation
4 air transportation

subject areas
25 structures design and performance
62 soil foundations
63 soil and rock mechanics

Printed in the United States of America

Library of Congress Cataloging-in-Publication Data
National Research Council. Transportation Research Board.

Soil-structure interaction.

(Transportation research record, ISSN 0361—1981 ; 1129)
1. Soil-structure interaction—Congresses. I. National Research Council (U.S.). Transportation Research Board. II. Series.
TE7.H5 no. 1129 380.5 s 88-5318
[TA711.5] [624.1'5136]
ISBN 0-309-04510-X

Sponsorship of Transportation Research Record 1129

GROUP 2—DESIGN AND CONSTRUCTION OF TRANSPORTATION FACILITIES
David S. Gedney, Harland Bartholomew & Associates, chairman

Soil Mechanics Section
Raymond A. Forsyth, California Department of Transportation, chairman

Committee on Subsurface Soil-Structure Interaction
Michael G. Katona, TRW Ballistic Missiles Division, chairman
George Abdel-Sayed, Baidar Bakht, Sangchul Bang, Mike Bealey, C. S. Desai, J. M. Duncan, Lester H. Gabriel, John Owen Hurd, J. Neil Kay, Raymond J. Krizek, Richard W. Lautensleger, L. R. Lawrence, G. A. Leonards, Donald Ray McNeal, Michael C. McVay, A. P. Moser, Samuel C. Musser, Thomas D. O'Rourke, Raymond B. Seed, Ernest T. Selig, H. J. Siriwardane, Mehdi S. Zarghamee

Neil F. Hawks, Transportation Research Board staff

The organizational units, officers, and members are as of December 31, 1986.

Transportation Research Record 1129

The **Transportation Research Record** series consists of collections of papers on a given subject. Most of the papers in a Transportation Research Record were originally prepared for presentation at a TRB Annual Meeting. All papers (both Annual Meeting papers and those submitted solely for publication) have been reviewed and accepted for publication by TRB's peer review process according to procedures approved by a Report Review Committee consisting of members of the National Academy of Sciences, the National Academy of Engineering, and the Institute of Medicine.

The views expressed in these papers are those of the authors and do not necessarily reflect those of the sponsoring committee, the Transportation Research Board, the National Research Council, or the sponsors of TRB activities.

Transportation Research Records are issued irregularly; approximately 50 are released each year. Each is classified according to the modes and subject areas dealt with in the individual papers it contains. TRB publications are available on direct order from TRB, or they may be obtained on a regular basis through organizational or individual affiliation with TRB. Affiliates or library subscribers are eligible for substantial discounts. For further information, write to the Transportation Research Board, National Research Council, 2101 Constitution Avenue, N.W., Washington, D.C. 20418.

Contents

Foreword

Structural analysis is one of the important considerations related to buried conduits. The first six papers included in this Record concern the structural design of buried conduits. The last paper in the Record is on earth pressure development behind retaining walls.

Rogers reports the results of full-scale tests conducted on the response of small-diameter flexible pipes to surface loadings. The parameters investigated were the type and compaction of side fill, and the depth of the bedding layer. The type of soil surrounding the pipe had most influence on its performance.

Watkins et al. describe structural design of buried corrugated polyethylene pipe. Their work established conditions for structural performance of the conduit and identified performance limits.

Gabriel and Blower report on how to predict performance of semirigid pipes such as thin-walled concrete pipes. Computer modeling of structural composites of pipes embedded in surrounding soil media provided information on thin-walled concrete pipes. Physical tests established parameters needed for the CANDE computer analysis program and spot-checked the computer studies.

Jeyapalan and Jiang investigated bedding factors of buried vitrified clay pipes using finite element analysis. The bedding factors were affected by the backfill material type, compaction density, backfill height, trench width, and pipe diameter.

Katona and Akl provide a set of design tables listing the maximum allowable fill heights for large-diameter corrugated steel pipes with slotted joints. The design methodology that led to the design tables is presented in detail.

James and Brown measured live-load earth pressures on a reinforced-concrete box culvert. These measurements were compared with existing theoretical and numerical methods and proposed empirical equations. The empirical equations predicted the measured data better than the theoretical and numerical methods.

Bang and Kim report an analytical solution method developed to estimate the magnitude and distribution of the passive lateral earth pressures behind a vertical rigid wall supporting cohesionless backfill soil. The results were compared with those of experimental model tests, with good agreement.

The Influence of Surrounding Soil on Flexible Pipe Performance

C. D. F. ROGERS

The response of 160-mm-diameter, shallowly buried, unplasticized polyvinylchloride (uPVC) pipes to surface loading has been investigated in full-scale tests. Standard installation and loading conditions were used to study the influence of the surrounding soil below, beside, and above the pipe on pipe performance. The type of soil used to surround the pipes was found to have a considerable influence on pipe behavior. Various uncompacted granular materials provided good support, whereas uncompacted silty clay and silty sand did not. Compaction of the surrounding soil had a variable influence wholly dependent on soil type. Silty clay performed well only when thoroughly compacted in thin layers. Light compaction of a broadly graded granular soil improved performance slightly, whereas uniform gravel is generally considered to be unresponsive to compaction. The use of a thin bedding layer was shown to be beneficial in reducing pipe deformation, whereas a thicker bedding layer was shown to be less beneficial. The problems of measuring pertinent soil properties on site for fill selection are discussed and assessment of two empirical methods is made.

The basic structural requirement of a buried pipe is the provision of an opening of dimensions and permanence suited to the function it is to perform. In general, it must maintain its size, shape, line, level, and integrity.

Two fundamental methods of meeting the structural, economic, and other requirements have developed. The first uses rigid pipes on a rigid bed such that the inherent strength of the pipes is sufficient to withstand applied loads by bending action in the pipe walls. Such pipes are subject to brittle fracture if the applied loads are too great or if significant differential settlement occurs.

The second method involves the use of flexible pipes that reach equilibrium in the ground by deforming under load. Such pipes rely on the properties of the surrounding materials to provide support and can fail by buckling, by excessive compressive hoop strain in surrounds providing relatively good support, or by excessive deformation. Failure of the pipe in these cases can be difficult to define if complete collapse does not result.

The division between rigid and flexible pipe behavior has become blurred with the advent of many new forms of pipeline construction. These include flexible pipes with a wide variety of strengths and stiffnesses, and flexible jointing systems for rigid pipes. The distinction between rigid and flexible pipes is not important, however, if the composite pipe-soil system is treated as the structure under consideration rather than as two distinct entities. In this way, loads are resisted by composite action according to the relevant stiffness.

From these ideas of relative flexibility, it can be seen that to design a pipeline an appreciation of both pipe and fill properties and their interaction is necessary. In the case of an inflexible pipe, design is primarily concerned with the structural properties of the pipe ring and the material on which the pipe is laid. Where the pipe has great flexibility, the structural properties of the material both beside and above the pipe also become important, particularly their ability to resist both vertical and horizontal pressures without large deformations. It is at this point that the relative costs of specific structural solutions must be considered. Because there is complex soil-structure interaction, the properties of the soil in this system and the cost of their provision must be carefully considered, particularly for more flexible pipes.

In 1842, John Roe, surveyor of the Holborn and Finsbury districts of London, put his mind to the design of sewer systems at the request of Edwin Chadwick (1800-1890), who was then secretary to the Poor Law Board set up in 1834. Roe's brief was to work on a series of experiments to ascertain for different discharges the most economical sizes of pipes and the best materials for their construction.

Chadwick wrote at that time:

> As the old formulae, now in use, are founded on imperfect data and experiments, and not only give results so far above what experience shows to be the fact, but which, even if they were correct, would be of most limited application, they are obviously uncertain guides, and it is better to trust to our observations of what actually takes place. This is in fact experimenting on the largest and safest scale.

In reply to later questioning on the value of these experiments, Chadwick replied that drainage was a matter of gauging and experimenting that if carefully conducted would eventually remove all grounds for differences of opinion. Although the technology has progressed in many ways over the last 140 years, Chadwick's words still have a relevance and no more eloquent apology for the work presented hereafter could be devised.

The research at Nottingham has concerned full-scale tests on 160-mm-diameter, shallow-buried, unplasticized polyvinylchloride (uPVC) pipe under conditions simulative of building drainage. The work was instigated and sponsored by the British Plastics Federation. Such pipes are considered to

Loughborough University of Technology, Loughborough, Leicestershire, LE11 3TU, England.

be flexible and in qualitative terms the results can be extrapolated to other forms of flexible pipe construction. The results are presented in general terms to facilitate this extrapolation.

When discussing the results of the work, the terminology shown in Figure 1 is used. The diametral strain is defined as the change in the diametral measurement divided by the original diameter.

RESEARCH PROGRAM

Research Philosophy

The development of the test facilities at Nottingham has been described in detail by Rogers (*1*) and only scant details will be presented herein. The British Plastics Federation wished to investigate the performance of small-diameter uPVC pipes when buried in various soil surrounds and subjected to the most serious conditions that were likely to occur on a building drainage site. Based on their experience of such sites, the pipes were buried in a 500-mm-wide trench at a cover depth of 500 mm below the underside of a granular site access road, which was assumed to be approximately 200 mm thick. Surface loads of 5.5 and 7.0 tonnes were applied both statically and cyclically to simulate the loads applied by the rear wheel arrangement of a construction lorry. The lower load was applied statically for 30 min, was removed for 45 min, and was then cycled 150 times at approximately 12 cycles/min, at the end of which pipe deformation was found to have stabilized. The installation was allowed to recover for 2 hr before the process was repeated with the higher load, the final recovery period being at least 18 hr.

The trenches were cut in Keuper Marl, a silty clay having a liquid limit of 32 percent and a plastic limit of 19 percent. The trenches were backfilled using the excavated silty clay placed in one layer and thoroughly compacted at the surface. In accordance with the wishes of the sponsors, no effort was made to vary the type of pipe used in the tests because the properties of uPVC pipe were not considered to vary

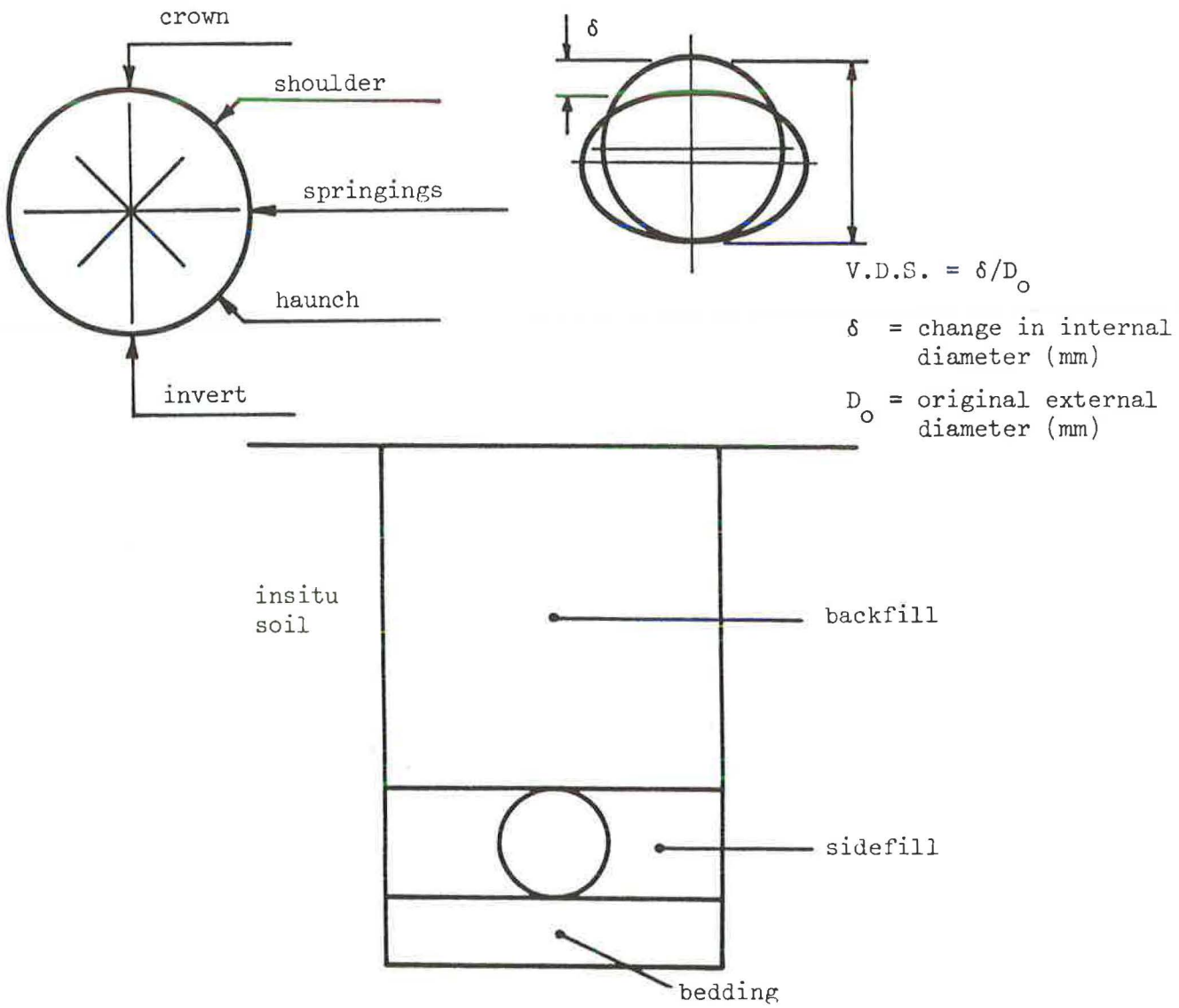

FIGURE 1 Terminology and definitions: (a) Pipe terminology, (b) Definition of VDS, and (c) Installation terminology.

significantly between manufacturers. The pipes were obtained from a local supplier. The parameters that were of most importance to the investigation were the type and compaction of the sidefill and the depth of the bedding layer. These were varied between tests and are described in greater detail in a later section of this paper.

Equipment and Instrumentation

The first requirement was a facility of sufficient size to permit pipes to be tested free from boundary influences. The pit had a testing area 3 m long, 2.1 m wide, and 1.9 m deep and an inspection chamber at one end to allow access to the pipes during tests (Figure 2). The pit was filled with Keuper Marl at its natural water content of 17.5 percent. Load was applied to the surface of the backfill through a 700-mm-diameter semiflexible platen by a hydraulic ram housed in a loading rig. The platen was designed to represent the stress at the base of a granular subbase layer. The load regime was applied at two points 1 m apart in succession along the surface of each installation in order that duplicate data could be obtained from each installation. Load was measured independently by a load cell.

Further tests were performed in a reinforced box from which comparative data were obtained under constant boundary influences. The box had internal dimensions 750 mm long, 500 mm wide, and 550 mm deep and pipes were buried with a cover depth of 250 mm (Figure 3). The same load regime was applied through a 480-mm-diameter rigid platen, a dead load being applied over the remaining area to simulate a total depth of cover of 500 mm. The loading was consequently considerably more severe in the box than in the pit.

The deformed shape of the pipe was recorded throughout each test using a ring flash camera developed at the Transport and Road Research Laboratory. The ring flash head was mounted on a boom and inserted into the pipe below the load platen. The head, which appears as a silhouette to provide a datum measurement, produced a thin band of light that was recorded photographically (Figure 4). Diametral change, shape of deformation, and settlement of the pipe invert were measured from the sequence of photographs. Vertical diametral change was also recorded by a linear potentiometer mounted on a self-righting sledge. Internal pipe wall strains were measured in the circumferential direction by eight equally spaced, single, active strain gauges glued directly to the wall of the pipes used in the box. Soil strain was measured at five strategic points in the trench cross section using inductance strain coils, and total pressures were measured at five points around the trench walls. Settlement of the load platen was measured using a linear potentiometer.

FIGURE 2 The test pit.

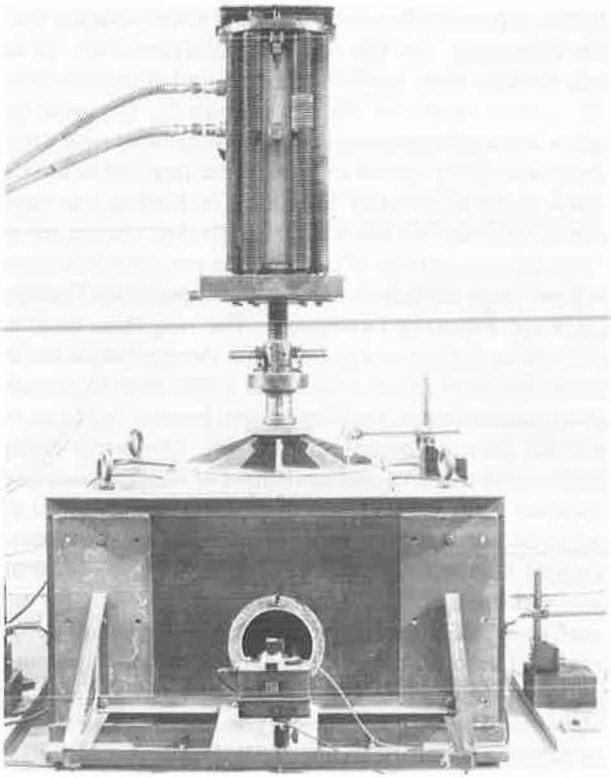

FIGURE 3 The test box.

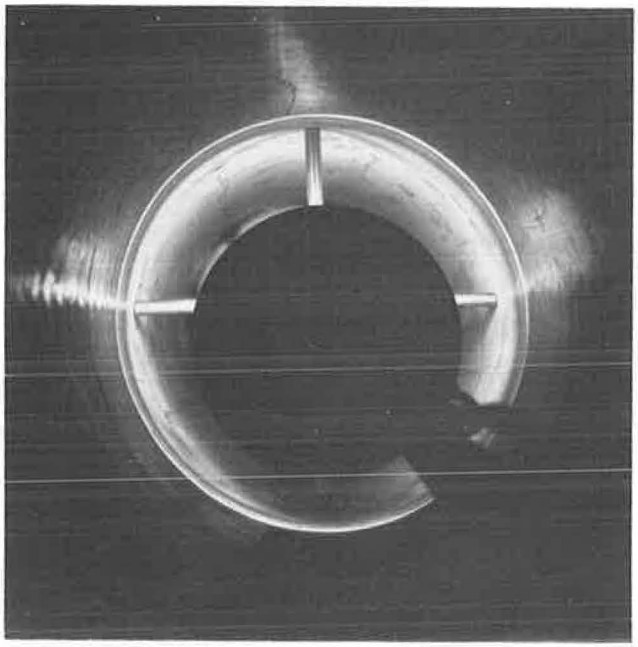

FIGURE 4 A ring flash photograph.

Experimental Program

The pit installations provided the most important research data, the pipe surround configurations for which are summarized in Table 1 and will be described first.

The installation representing current site practice was tested first and was used as a standard against which the performance of other installations was measured. The pipe was laid on a 100-mm-thick bedding of uncompacted 10-mm pea gravel and surrounded by uncompacted pea gravel to the level of the pipe crown. This installation was repeated towards the end of the test program to provide replicate data.

The influence of the bedding layer was investigated by repeating the standard installation configuration with a 50-mm-thick and no bedding layer. It was considered that hand trimming of the trench bottom, required where no bedding was laid, was likely to be impractical to specify and that a bedding layer of 50 mm would be necessary for leveling purposes. For this reason, only the more practical installation was repeated. The effect of removing a 50-mm-thick bedding layer from an uncompacted concrete ballast installation was also investigated.

Three levels of compaction were applied during the tests: thorough compaction by two passes of a pneumatic rammer, light compaction by treading, and no compaction. It has been shown by Gaunt et al. (*2*) in their tests on 300-mm-diameter uPVC pipe that a thoroughly compacted sandy clay sidefill performs comparably with uncompacted pea gravel, whereas an uncompacted sandy clay sidefill leads to large deformations. Performance in a poorer silty clay sidefill subjected to thorough compaction in one layer was thought to be a somewhat intermediate case and was measured in two installations. The effect of light compaction on concrete ballast was investigated.

Perhaps the most important series of tests concerned alternative imported pipe surround materials. The criteria for their choice were that they should be distinctly different in character, they should be widely available in Great Britain, and they should be relatively inexpensive. The materials chosen were concrete ballast (broad grading), washed quarry tailings, building sand (uniform), and reject sand (a silty sand). The grading curves for the coarse fractions of all the materials used in the tests are shown in Figure 5. Each of the materials was used as a 50-mm bedding layer and uncompacted sidefill, and each installation was repeated with the exception of reject sand, which was a marginal material.

The test box was used to gain comparative results from, and hence to indicate likely behavior in the pit of, several of the above installation types. Box installations were generally tested in advance of those in the pit. In addition to these tests, a further avenue of investigation was followed. A series of installations were tested in which good (pea gravel) and poor (silty clay) materials were juxtaposed around the pipe. This was done to isolate the areas in which good support to the pipe was most effective at reducing deformation. The configurations of all box installations are given in Table 2.

Associated soil testing, both in laboratory equipment and in situ, was performed concurrently with the experimental work, with several aims in mind. It was important to gain a good basic understanding of the soil properties in order to plan the test program. Soil properties were also necessary to prime a theoretical model, which was developed using a finite element program based on a linearly elastic soil model. A separate aim of the work was to investigate the means by which the relevant properties of soil that reduce deformation could be measured quickly and simply on site. The current method of soil selection in Great Britain refers only to the

TABLE 1 DETAILS OF EXPERIMENTAL INSTALLATIONS IN THE PIT

Reference	Bedding Type	Bedding Thickness (mm)	Sidefill Type	Sidefill Compaction	Comments
1A	Pea gravel	100	Pea gravel	none	standard practice
2	none	0	Pea gravel	none	
3A	none	0	Silty clay	thorough	insitu soil as sidefill
3B	none	0	Silty clay	thorough	insitu soil as sidefill
4	none	0	Concrete ballast	light	
5	none	0	Concrete ballast	none	clay refurbishment followed test No. 5
6A	Pea gravel	50	Pea gravel	none	
6B	Pea gravel	50	Pea gravel	none	
7A	Concrete ballast	50	Concrete ballast	none	
7B	Concrete ballast	50	Concrete ballast	none	
8A	Building sand	50	Building sand	none	
8B	Building sand	50	Building sand	none	
1B	Pea gravel	100	Pea gravel	none	standard practice
9A	Quarry tailings	50	Quarry tailings	none	
9B	Quarry tailings	50	Quarry tailings	none	
10	Reject sand	50	Reject sand	none	marginal material

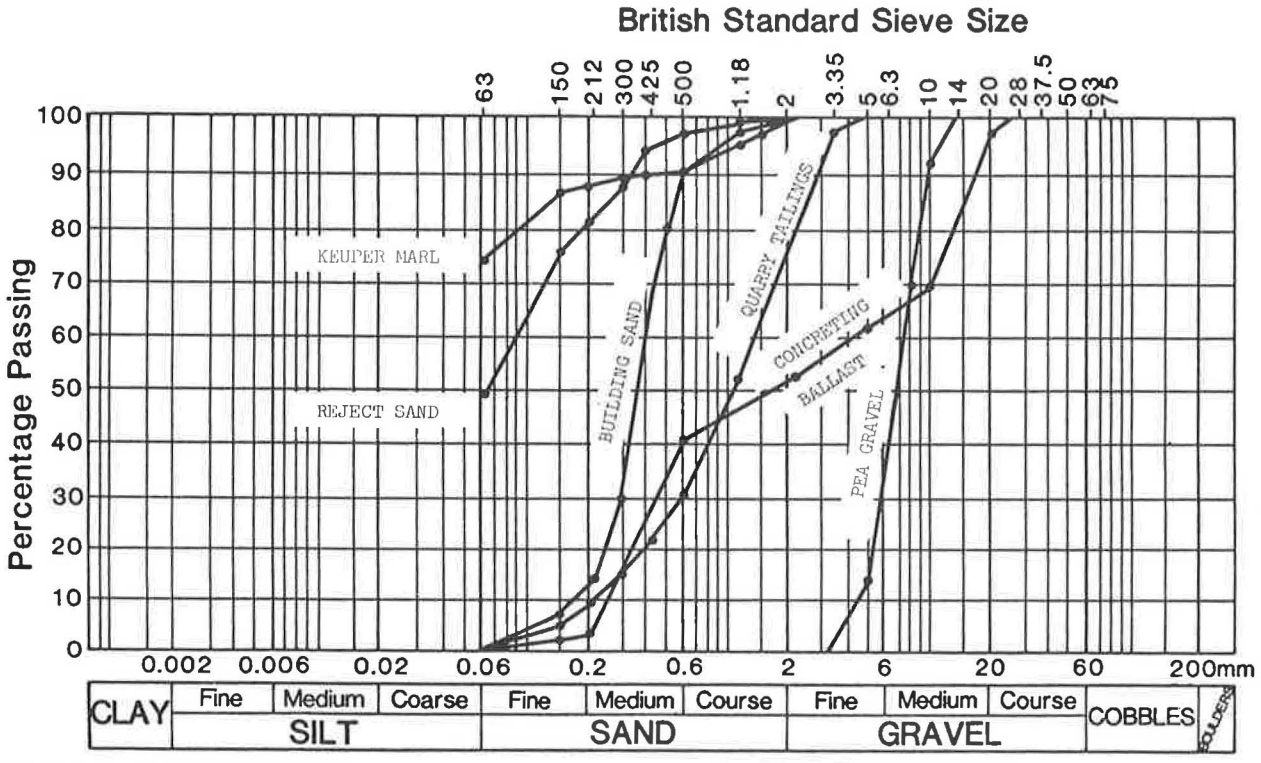

FIGURE 5 Particle size distribution curves.

TABLE 2 DETAILS OF EXPERIMENTAL INSTALLATIONS IN THE BOX

Reference	Bedding Type	Bedding Thickness (mm)	Sidefill Type	Sidefill Compaction	Comments
1	Pea gravel	100	Pea gravel	none	standard practice
2	Pea gravel	50	Pea gravel	none	
3	none	0	Pea gravel	none	
4	Pea gravel	50	Pea gravel to springings, silty clay above	none none	support to mid-height of pipe only
5	none	0	Pea gravel to springings, silty clay above	none thorough	split sidefill
6	none	0	Silty clay to springings, pea gravel above	thorough none	split sidefill
7	none	0	Silty clay to crown, pea gravel 50mm above	thorough none	arching layer over 9
8A and 8B	none	0	Silty clay to springings, pea gravel to 50mm above pipe crown	thorough none	arching layer over 6; 8A had low water content, 8B high
9	none	0	Silty clay	thorough	
10	none	0	Silty clay	thorough	compacted in 2 layers
11	none	0	Silty clay	light	
12	Pea gravel	100	Silty clay	thorough	
13	none	0	Concrete ballast	light	
14	none	0	Concrete ballast	none	
15	none	0	Reject sand	light	
16	none	0	Reject sand	none	

compaction properties of the material. The measurement of soil stiffness, or compressibility, has presented problems ever since Spangler (*3*) presented his classic work on deformation prediction and much effort has been expended to this end, notably by Watkins and Spangler (*4*), Watkins and Nielson (*5*), Bhandhausavee (*6*), Jaaskelainen (*7*), and Howard (*8*). While no immediate solution to the problem was expected from the work, some thoughts on the subject are presented later in the results section.

EXPERIMENTAL RESULTS

General Observations

Preliminary tests were conducted to provide information on loading rates and duration, recovery periods, and boundary conditions. These tests showed that for installations subjected to large static surface loads for several days there was no apparent increase in the magnitude of pipe deformation under load, but that permanent deformation on removal of the load was significantly increased. It was also discovered that when a long recovery period of 24 hr or more was introduced during the cyclic load sequences, elastic recovery of the pipe was greater and was not wholly removed on the immediate application of the next cyclic load. Thus, accelerated cyclic loading is significantly worse than that applied at the more normal rates experienced on site; extended static loads likewise provide a more severe case.

The internal pipe wall strain measurements were found to correlate well with the deformed shape of the pipes tested in the box. The shape of deformation varied significantly between tests, most deformation occurring above the springings of pipes buried in competent sidefills, whereas approximately elliptical deformation occurred in sidefills offering poor support.

When the results were assessed in terms of pipe deformation, an arbitrary load regime was necessarily adopted. Any extension of the results must consequently be based on engineering judgment and local experience of site conditions. Values of vertical diametral strain (VDS) quoted herein might differ slightly in certain cases from those published previously by Rogers et al. (*9*). This variation simply reflects better definition of deformation patterns from more detailed measurements, thereby illustrating inaccurate results.

Pipe deformation data use as the datum either that at the end of installation, representing deformation caused by the applied loads alone, or that when positioning the pipe. The installation process was found to produce somewhat variable pipe deformation, even in pipes with the same soil configuration, whereas deformation caused by the applied loads alone was remarkably consistent between tests.

The Influence of Soil Surround Type

The influence of sidefill type on the VDS of the pipe is demonstrated by the results of installations in which five uncompacted granular materials were used as sidefill and bedding, a summary of which is shown in Figure 6. In this

figure, VDS values at various stages of the tests are plotted using the point at which the pipe was positioned (PP) as the datum. Values thereafter are given at the end of installation (EOI), on application of the 55- and 70-kN loads (55 ON and 70 ON), and after they had been applied for 30 min (55/30 and 70/30). Values are also given after recovery at the end of the static load sequences (EO 55_s and EO 70_s) and the cyclic load sequences (EO 55_c and EO 70_c). The average curves for uncompacted pea gravel (UCPG) and concrete ballast (UCCB) are of similar type and magnitude throughout, with the cyclic loads having far more effect on the pipe-soil structure than the static loads. The average curve for washed quarry tailings (UCQT) exhibits greater strains at each stage, with a progressively increasing difference between it and the two mentioned, and in particular a greater susceptibility to creep under load. The average curve for the pipes buried in building sand (UCBS) shows higher strains still, with proportionally greater strain under static load, much of which was subsequently recovered. The average curve for uncompacted reject sand (UCRS), which was used in one installation only, exhibits strains of roughly twice those of the pipe in building sand. Installation deformation became progressively greater with poorer material, and it was apparent that creep effects under load were greater in materials having a broader grading or flatter grading curve.

The influence of sidefill type was further investigated in three pit installations in which no bedding layer was used. The pipe buried in uncompacted concrete ballast deformed least, with most deformation occurring under cyclic load. The pipe buried in uncompacted pea gravel was similarly more affected by the cyclic loads, but demonstrated a greater elastic response under static load. The pipe buried in well-compacted silty clay produced a deformation at the end of the test that was only slightly greater than the pea gravel installation, the pipe having a negative deformation at the end of installation caused by compaction of the soil beside the pipe. The permanent VDS caused by the static loads was relatively more significant to the overall value, with the pipe creeping considerably under load.

A further study of the influence of sidefill was conducted in the box in which the performance of three uncompacted granular materials was compared with that of silty clay thoroughly compacted in two layers (WCSC). A summary of the results is presented in Figure 7. In contrast to the pit results, the behavior of the pipes buried in the gravel and ballast was remarkably similar throughout the tests. The reason for this may lie in the inability of the pea gravel to bed in laterally in the box when loaded, whereas in the pit the gravel is found to penetrate the clay trench walls thereby allowing horizontal movement. Concrete ballast, being a broadly graded material, showed no tendency to bed in when used in the pit. Where the clay sidefill was used, a large negative VDS at the end of installation was followed by large positive deformation on application of the 55-kN load, and because of creep only a small part of this was recovered on removal of the load. Thereafter the installation behaved in a similar manner to the others, though with somewhat greater deformations. The curve for UCRS exhibited a large initial response to static load but little creep under load.

Several behavioral trends were apparent from this series of experiments. A pipe buried in an uncompacted sidefill that produced ultimately good performance tended to have a small positive VDS at the end of installation, relatively small deformations caused by static load application and creep effects, and a large elastic recovery on removal of the load. Cyclic load tended to produce greater permanent deformations than the static load. Where the sidefill was compacted, a negative VDS occurred at the end of the installation process. Where a cohesive material was used as sidefill, a large VDS tended to occur on application of the static load and this was increased considerably by creep movements. A relatively small proportion of this deformation recovered on removal

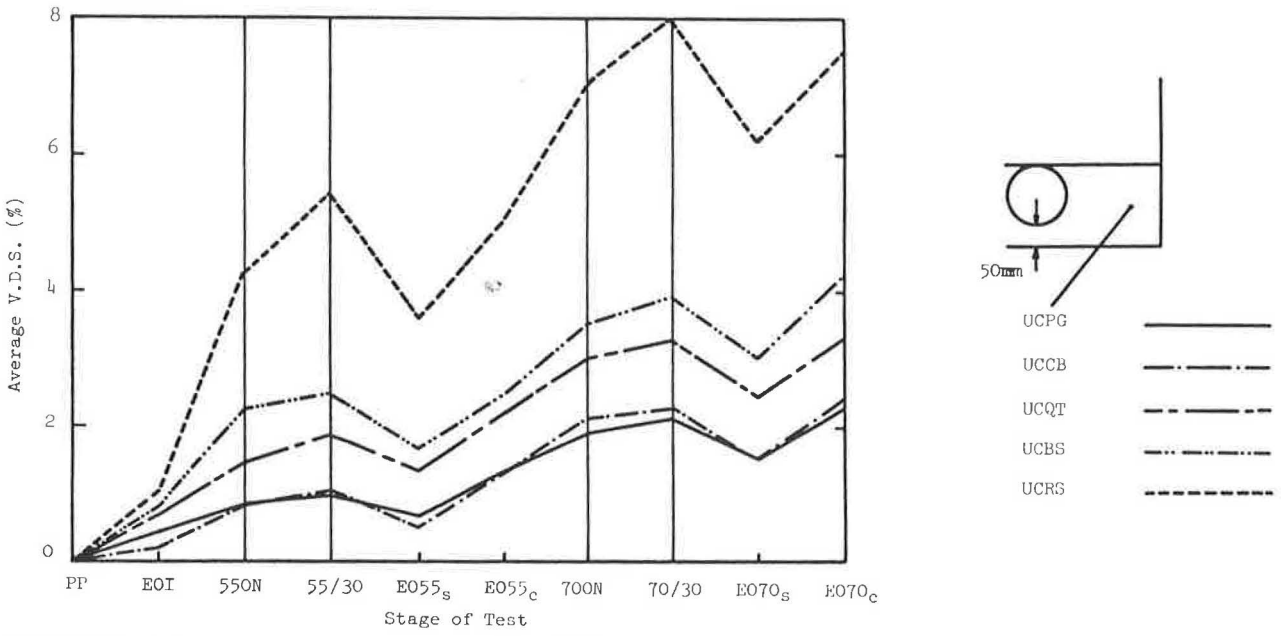

FIGURE 6 Vertical diametral strains (VDS) for five sidefill types in the pit.

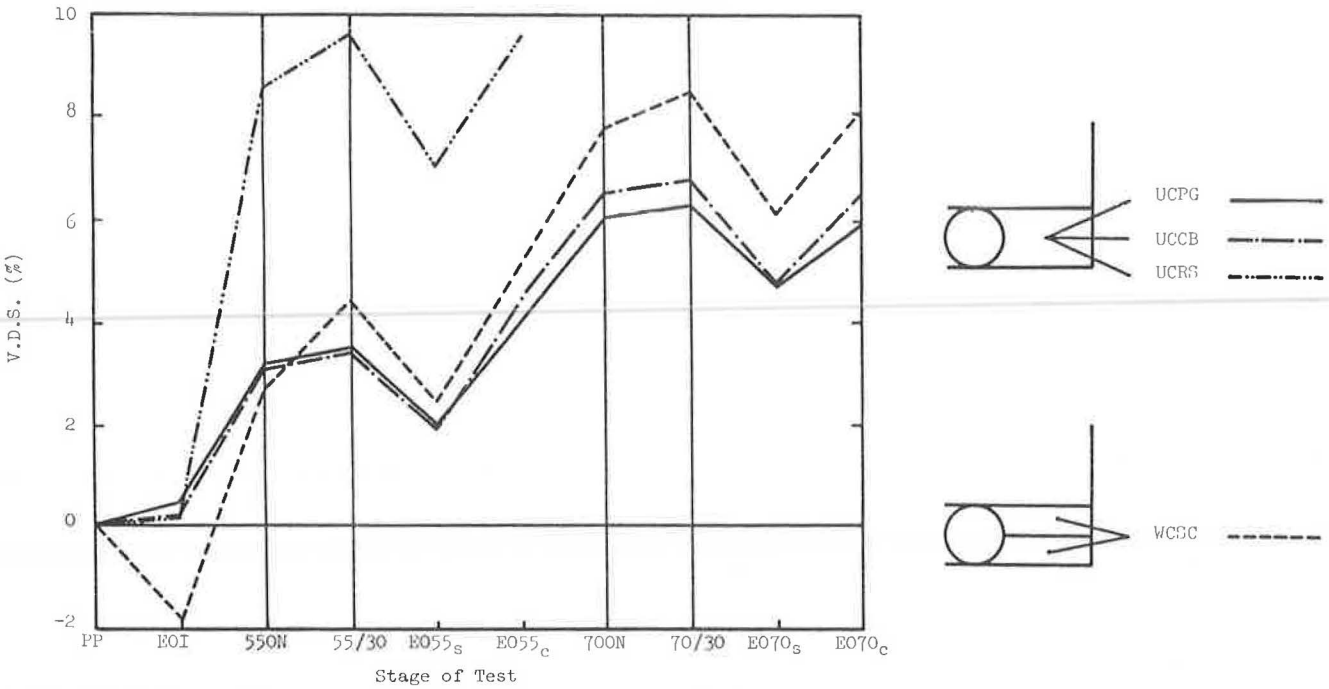

FIGURE 7 Influence of sidefill type on pattern of VDS measurements in the box.

of the static load, cyclic load causing a relatively small permanent increase in VDS in comparison with the static load.

The Influence of Sidefill Compaction

Where light compaction was applied to a concrete ballast sidefill (LCCB) beside a pipe with no bedding, the VDS at the end of the test reduced considerably from that where no compaction was applied (Figure 8). The reduction was mainly due to markedly reduced installation deformation and a lesser response to the 55-kN loads. Additional experiments in the box showed that a pipe supported by an uncompacted silty clay sidefill deformed excessively before the full 55-kN load could be applied. Compaction improved the performance of this material to the extent that thorough compaction of a silty clay sidefill in two layers produced a negative deformation at the end of installation of 1.8 percent and a subsequent deformation under surface loads that compared favorably with the better granular materials (Figure 7).

It was clear from these results that compaction of the sidefill, even that effected by systematic treading, was of considerable use in reducing the VDS of the pipe and that different soils respond to compaction by differing amounts. In a clay sidefill, where the voids between lumps had to be removed, thorough compaction in thin layers was necessary before suitable lateral restraint was mobilized. Where concrete ballast, a broadly graded material, was used, light compaction made a significant difference to an otherwise good material, a result confirmed by experience in highway engineering. Pea gravel, however, has proved in practice to be largely unaffected by compaction because a favorable soil structure would be taken up when laid, compaction probably only affecting the bedding in effect at the interface with the surrounding soil.

The Influence of Bedding

The influence of the bedding layer on pipe performance was investigated in three pit installations using uncompacted pea gravel sidefills with 0, 50-, and 100-mm-thick bedding layers (Figure 9). The pipes laid on the 50-mm-thick bedding produced the lowest VDS, with little response to static load. The pipes laid on the thicker bedding produced slightly higher deformations throughout, with a VDS of 2.7 percent at the end of the test compared with 2.3 percent for the 50-mm layer. The pipes on the thicker bedding showed a greater response to static loads, both elastic and permanent. Where no bedding layer was used, a final value of 4.4 percent occurred by progressively greater deformation throughout the test. This ranking of installation types was confirmed in the box (Figure 10), though with curves of similar form throughout and a closer grouping of results showing that the differences were less exaggerated.

A further investigation concerned pipes laid in uncompacted concrete ballast sidefills both with and without a 50-mm-thick bedding. Where no bedding layer was used, installation deformation was 0.6 percent greater, the curves being separated by an offset of roughly this magnitude thereafter (Figure 8). The average VDS values at the end of the tests were 3.0 percent without bedding and 2.4 percent with bedding.

These limited results indicate that where good support is afforded the performance of the pipe with a 50-mm-thick bedding layer is slightly better than that with a 100-mm-thick bedding. Omission of the bedding layer altogether leads to a

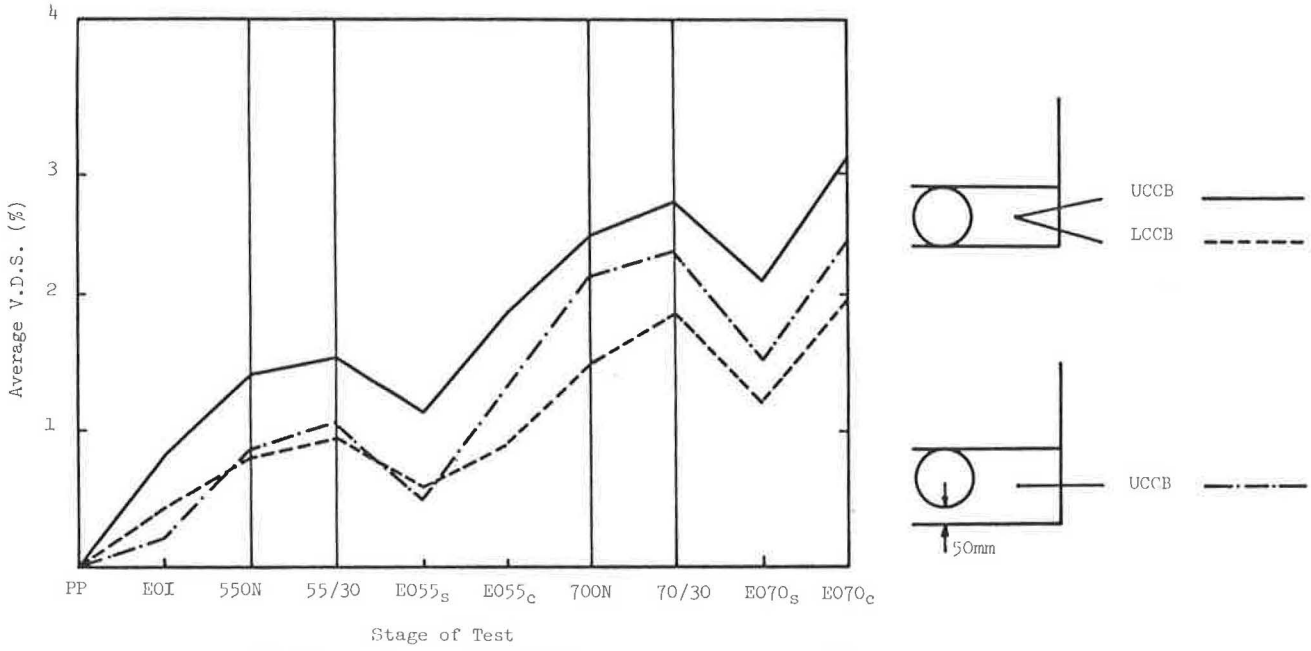

FIGURE 8 Influence of bedding and compaction on VDS for concrete ballast sidefill.

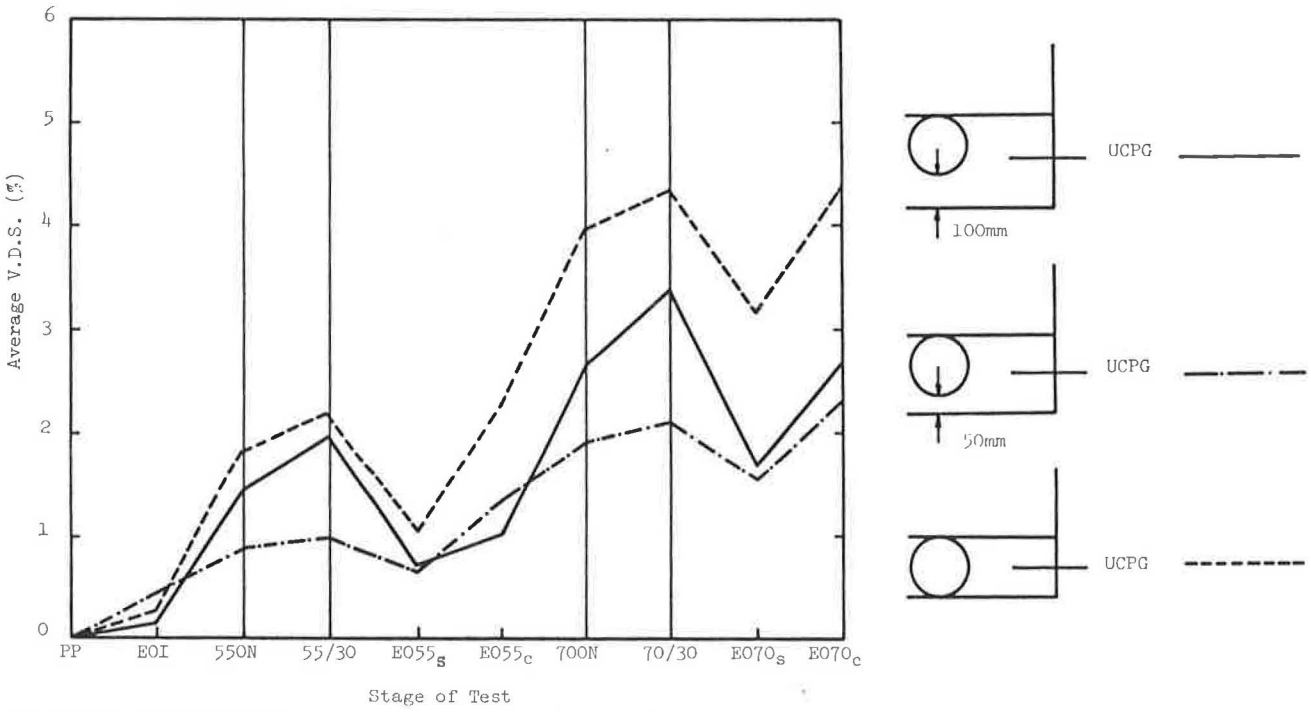

FIGURE 9 Influence of bedding on VDS measurements in the pit.

worse case, albeit perhaps only from installation effects. In practice, where a 50-mm-thick bedding layer is necessary to level the trench bottom, its increase to 100 mm on the grounds of structural performance would seem to be inappropriate.

Soil Investigations

The current British Standard (*10*) installation recommendations include the compaction fraction test, a method of fill selection, which relates the uncompacted and fully compacted heights of soil in a 250-mm-long, 160-mm-diameter tube. The difference between the two heights divided by the original height is known as the compaction fraction of the soil; judgments are made based on this figure. While this test is wholly concerned with the susceptibility of the soil to compaction (which is recommended for sidefill and bedding in the British Standard), it provides a method of ranking the

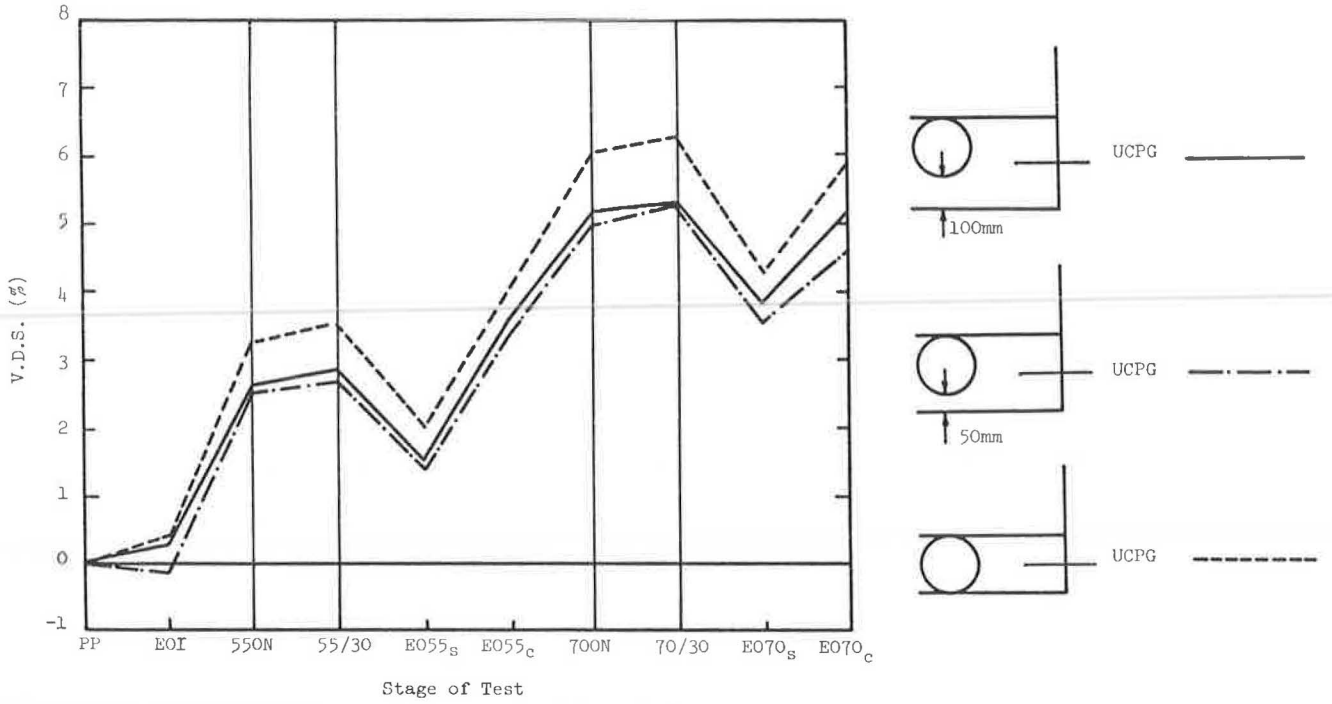

FIGURE 10 Influence of bedding on VDS measurements in the box.

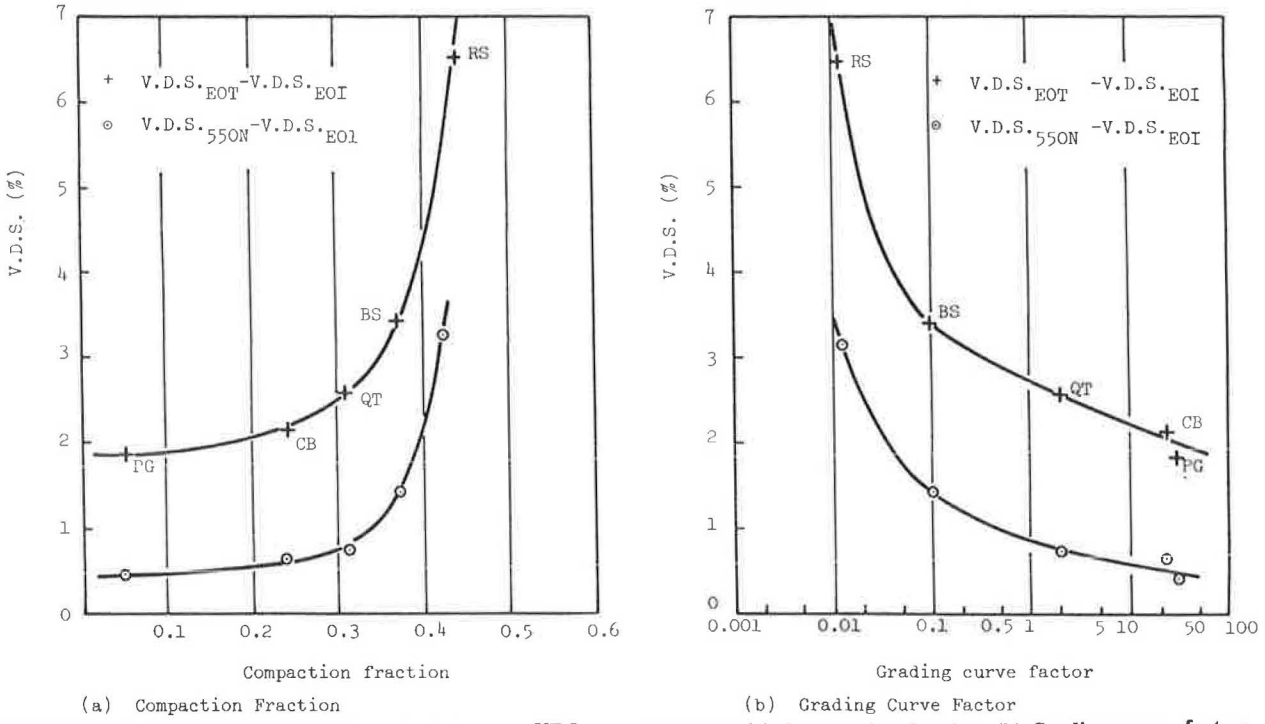

FIGURE 11 Influence of empirical soil factors on VDS measurements: (a) Compaction fraction, (b) Grading curve factor.

materials and a likely indication of their compressibility. With these considerations in mind, the ability of the compaction fraction to rank sidefill materials in order of performance was investigated. The average results of installations using five uncompacted granular materials as sidefill and 50-mm-thick bedding were used for the comparison. The average compaction fractions were plotted against the VDS caused by the application of the 55-kN static load (55 ON) and the VDS at the end of the test (EOT), both related to the strains at the end of installation (EOI). These are presented in Figure 11(a), in which a clear relationship is apparent.

Both the grading and the particle size of the soil surround were found to influence the performance of the pipes. A second method of ranking the soils based on the grading curves of the soil (Figure 5) was sought. The product of the difference between the diameters below which 80 and 20 percent (D_{80} and D_{20}) of the particles lie (which reflects the gradient of the curves) and D_{50} (which reflects the absolute

size) was used. Plotting this factor on a logarithmic scale against VDS produced smooth curves [Figure 11(b)], as before.

Although no serious conclusions should be drawn from these limited results, the findings perhaps add some ideas to the debate on soil selection.

CONCLUSIONS

The type of soil used to surround the pipe has most influence on its performance. Various uncompacted granular materials were shown to provide good support to the pipe. In order of performance, these included pea gravel, concrete ballast, washed quarry tailings, and building sand. Relatively large deformations were obtained in silty sand and silty clay. The better, granular surrounds were more affected by the cyclic loads than the static loads, whereas the pipes in poorer soils were influenced more by the static load sequences.

The benefit of sidefill compaction was wholly dependent on the soil type. Thorough compaction of a silty clay sidefill in thin (80-mm) layers greatly improved the support afforded by this soil, the performance being comparable to that of the better uncompacted granular soils. Light compaction of a broadly graded soil (concrete ballast) produced a significant improvement in pipe performance, whereas a more uniform soil (pea gravel) has proved to be largely unaffected by compaction.

A bedding layer was found to be beneficial in reducing pipe deformation, although deformation increased as the bedding thickness increased from 50 to 100 mm. A thin bedding layer would appear to be the optimum design solution from these limited data.

Two empirical methods for ranking soils in order of performance, based on compactability and grading, produced encouraging results.

ACKNOWLEDGMENTS

The research described herein was carried out in the Civil Engineering Department of the University of Nottingham under a contract with the British Plastics Federation, whose help and guidance are gratefully acknowledged. The author is grateful to P.S. Pell, Head of the Civil Engineering Department, for providing the necessary facilities, and particularly to S.F. Brown, who both supervised and contributed greatly to the work. The author also wishes to acknowledge the help of M.P. O'Reilly and his colleagues at the Transport and Road Research Laboratory.

REFERENCES

1. C. D. F. Rogers. *The Response of Buried uPVC Pipes to Surface Loading.* Ph.D. dissertation, University of Nottingham, England, May 1985.
2. J. Gaunt, J. J. Trott and J. B. Stevens. Static and Dynamic Load Tests on Shallow-Buried Flexible Pipes. *Ground Engineering,* Vol. 9, No. 3, April 1976.
3. M. G. Spangler. *The Structural Design of Flexible Pipe Culverts.* Bulletin 153. Engineering Experiment Station, Iowa State College, Cedar Falls, 1941.
4. R. K. Watkins and M. G. Spangler. Some Characteristics of the Modulus of Passive Resistance of Soil—a Study in Similitude. *HRB Proc.,* Vol. 37, 1958, pp. 576-583.
5. R. K. Watkins and F. D. Nielson. Development and Use of the Modpares Device. *Journal of the Pipeline Division, ASCE,* Jan. 1964.
6. C. Bhandhausavee. *Modulus of Soil Reaction as Determined from the Hveem Stabilometer Test (R-Value).* New Mexico State University, Las Cruces, 1968.
7. H. Jaaskelainen. *Modulus of Passive Resistance for the Protective Material of Flexible Pipes.* Building Technical and Community Development Publication 6. Technical Research Center of Finland, Otaneimi, 1973.
8. A. K. Howard. Modulus of Soil Reaction Values for Buried Flexible Pipes. *Journal of the Geotechnical Engineering Division, ASCE,* Vol. 103, No. GT1, Jan. 1977, pp. 33-43.
9. C. D. F. Rogers, S. F. Brown, and G. Boyle. The Influence of Bedding and Sidefill on the Response of uPVC Pipes to Surface Loading. *Proc., 6th International Plastics Pipe Conference,* The University of York, England, March 1985.
10. British Standards Institute. *The Installation of uPVC Pipework for Gravity Drains and Sewers.* British Standard BS-5955, Part 6, London, 1980.

Structural Design of Buried Corrugated Polyethylene Pipes

R. K. WATKINS, J. M. DWIGGINS, AND W. E. ALTERMATT

Test sections of corrugated polyethylene pipe (CPEP) were buried, as in typical drainage installations, in competent, compacted, granular backfill. Both dead load (soil cover) and surface live load (truck dual wheels) were applied. The objectives of the tests were to (a) observe performance of the pipes under load, (b) identify performance limits, (c) resolve some of the questions unanswered by present design methods, and (d) propose improved methods for the structural design of buried CPEP. The objectives were achieved. Experimenters agreed that tests confirmed the complementary interaction of pipe and backfill. Minimum soil cover was investigated under multiple passes of live loads. Conditions for structural stability of the pipe were identified. An analytical procedure was developed for predicting the minimum height of soil cover to assure ring stability under multiple passes of live loads. Maximum soil cover tests confirmed the ring compression analysis as the primary basis for design but also revealed a need to include the effects of ring deflection. An observable performance limit was identified, and a method of design was developed that combined the effect of ring deflection and ring compression on the performance limits of CPEP buried under maximum height of soil cover.

Corrugated polyethylene pipe (CPEP) is used primarily for nonpressurized buried conduits. Structural design must establish the conditions for adequate structural performance of the conduit and must identify the performance limits. Structural performance of a buried pipe is the interaction of the pipe and the soil in providing a useful conduit. If the pipe is flexible, it depends upon the soil to support it. The soil depends upon the pipe to retain the conduit cross section. The basic performance limit is excessive deformation. Excessive deformation could lead to yielding and even to fracture, but for most flexible pipes, excessive deformation is either too much longitudinal beam deflection or too much ring deformation. In the case of CPEP, because of the corrugations, longitudinal beam deflection does not cause pipe damage. Performance limit is simply too much beam deflection either from the standpoint of impeded flow due to beam bending or to sedimentation, or too much differential settlement of the soil surface. Longitudinal deflection is controlled by controlling the soil bedding elevation.

Excessive ring deformation may be so much ring deflection that flow is impeded, or it may be flattening or reversal of curvature of the ring. Reversal of curvature is considered to be excessive deformation, even though collapse does not occur, because the ring can no longer provide its full contribution to the pipe-soil conduit. Once the ring curvature is reversed, fluctuations in soil pressures can cause progressive ring deformation, sometimes called ratcheting, which could lead to eventual collapse. Soil pressure fluctuations are caused by surface loads and also by cycles of temperature changes, water level variations, freezing and thawing, and earth tremors.

In the summer of 1985, a series of minimum soil cover tests sponsored by Hancor, Inc., was conducted in Findlay, Ohio. The objective was to discover the minimum soil cover needed to protect CPEP. The independent variables were soil density and surface dual-wheel load. The backfill soil was crushed rock passing a 3/4-in. mesh screen and referred to in Findlay as 411 crushed limestone. Soil density was reported for its initially compacted state as a percent standard Proctor density (AASHTO Specification T-99). Except as noted, the load was provided by the single rear axle of a truck trailer with dual wheels carrying about 105-psi tire pressure. In each test, the loaded axle was run back and forth over the buried pipe (passes) in approximately the same tracks. Ruts formed. A graph of approximate rutting is shown in Figure 1, where rut depth H'' is a function of dual-wheel load W and soil density. The values of H'' are conservative, that is, 90 percent of all observed values in the field are estimated to be less than the plots. Rut depth H'' is the depth after the first pass. After the first pass (or up to three or four passes to establish the rut), H'' did not increase significantly, except directly over the pipe at performance limit. The equation from the plots of Figure 1 is

$$H'' = 0.315(\log W - 0.34)(103.9 - \rho)$$

where W is in kips, ρ is in percent, and H'' is in inches of soil cover.

Performance limit was identified as instability; i.e., progressive increase in ring deformation with each successive pass of the load. Multiple passes could lead to pipe damage.

Maximum soil cover tests were conducted on CPEP in a soil cell at Utah State University in Logan, Utah. The soil cell was a container in which a section of pipe was buried and then loaded vertically by 16 hydraulic cylinders to simulate high soil cover. The cell could accommodate pipes up to 2 ft in

R. K. Watkins, Civil and Environmental Engineering Department, Utah State University, Logan, Utah 84322-4110. J. M. Dwiggins and W. E. Altermatt, Hancor, Inc., 401 Olive Street, Findlay, Ohio 45840.

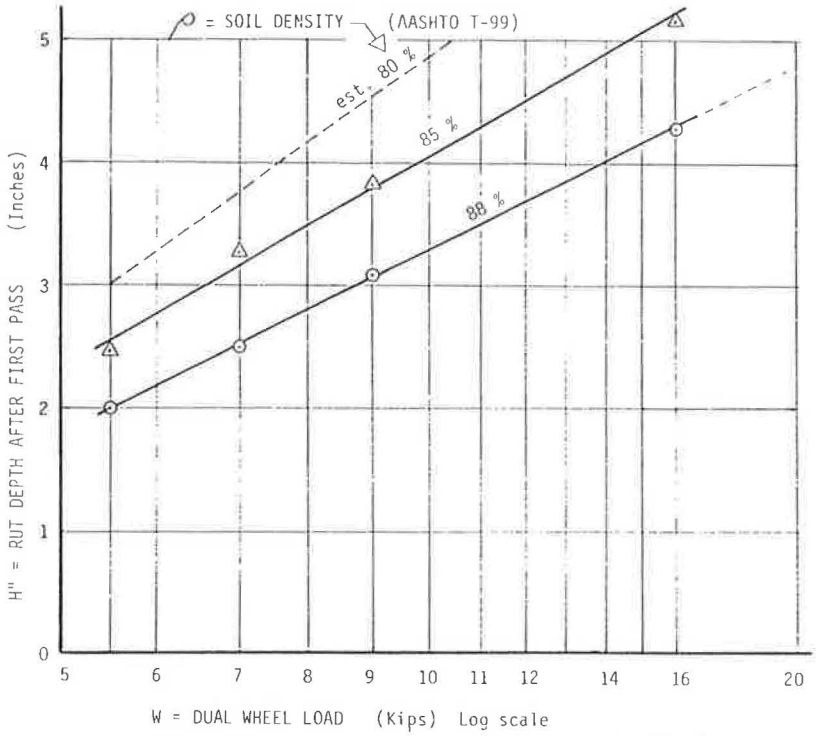

FIGURE 1 Depth of dual-wheel ruts H'' in crushed limestone backfill after the first pass. (Standard deviation of H'' is 0.5 in. The dotted plot for 80 percent soil density is estimated from single-tire ruts.)

diameter in lengths up to 5.5 ft. Soils of various types could be compacted to various densities, and loads in increments up to 16 kips/ft^2 could be applied to simulate soil loads including surface live loads. (See Figure 2.)

The independent variables were the density of the backfill soil and the vertical soil pressure at the top of the buried pipe. Two different diameters of CPEP were tested to verify similitude. The dependent variables, that is, performances were measured ring deflection and observed dimpling. The test section of pipe was buried in silty sand, Unified Soil Classification SM. Vertical soil pressure in the soil cell simulated high soil cover plus surface loads. After each increment of load, ring deflections were measured.

Performance limit in these tests was identified as vertical soil pressure P at dimpling of the crests of the corrugations at 9 and 3 o'clock as viewed from inside the pipe. The dimpling portended plastic hinging as a result of wall buckling and crushing. Plastic hinges could develop if the vertical soil pressure were increased past the performance limit.

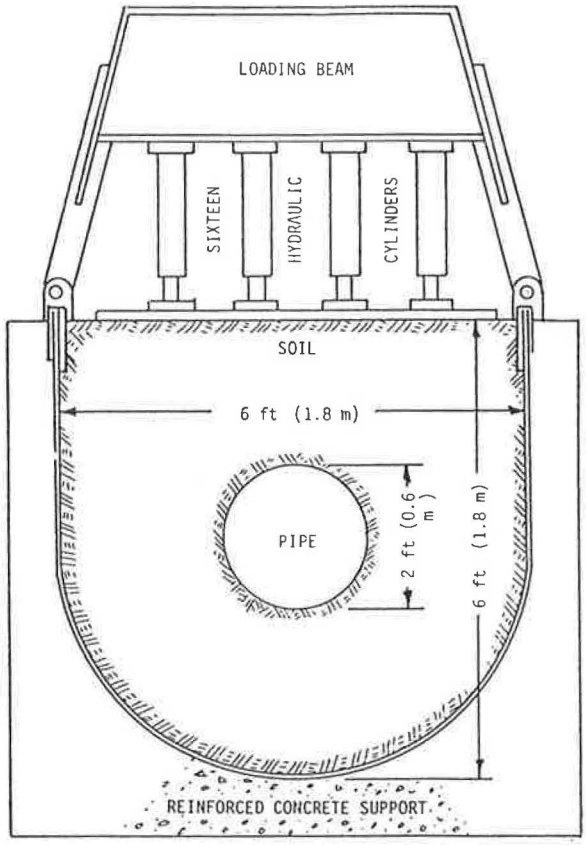

FIGURE 2 Cross section of small Utah State University soil cell in which pipes can be buried in soil and loaded vertically.

DESIGN

For design, it is traditional to evaluate performance as stress σ and to equate it to strength S as a performance limit. Including sf as a safety factor, $\sigma = S/sf$. In this paper, stress is analyzed as a function of deformation. Strength S is the stress at the limit of deformation, which may or may not occur at yield point. Elastic theory is used because it is generally understood and because it is conservative.

PERFORMANCE LIMITS FOR CPEP

In the design of CPEP, two performance limits must be considered: ring deflection and ring buckling. Ring deflection is the change in ring cross section from a circle to an approximate ellipse due to vertical compression of the pipe zone backfill soil. Ring deflection is defined as percent reduction in vertical mean diameter from the original mean circular diameter, that is,

d = Δ / D = ring deflection,
Δ = decrease in vertical diameter, and
D = mean circular diameter of pipe, to the neutral surface of the corrugations.

Design engineers specify the maximum allowable ring deflection d. A conservative maximum d = 5 percent is sometimes specified for culverts and storm drains. A proposed AASHTO deflection limit is 7.5 percent and many engineers permit 10 percent for pipe of this type.

Ring buckling in CPEP is usually identified by the first visible evidence of formation of plastic hinges in the pipe wall. Under maximum soil cover, plastic hinging is incipient when dimples appear on the crests of corrugations at approximately 9 and 3 o'clock. This is called dimpling. Under minimum soil cover with surface wheel loads passing over, this dimpling appears on the outside of the pipe near the crown, at 12 o'clock.

A special case of ring buckling is conduit instability. Under maximum soil cover, if the vertical soil pressure is so great that shear planes form in the soil at 9 and 3 o'clock, or if the ring compression stress in the pipe wall exceeds yield point, then the conduit is unstable. Progressive ring deformation could proceed. Under minimum soil cover, the conduit is unstable if multiple passes of a surface wheel load increase ring deformation with each successive pass. This multiple pass instability is discussed later.

PERFORMANCE OF CPEP

With performance limits identified, analysis must predict the structural performance of the buried CPEP ring under external soil pressures. The familiar stress theory is useful for conservative analysis. Stress is analyzed at performance limits of excessive deformation. Performance limit, then, becomes the maximum circumferential compressive stress developed in the pipe wall by vertical soil pressure P at the top of the pipe when the pipe is at the point of excessive deformation. Two conditions for vertical soil pressure are considered in this analysis: minimum soil cover and maximum soil cover. Under minimum soil cover, an approaching surface wheel load is critical. Under maximum soil cover, the surface wheel load is either negligible or only adds to the dead weight of soil.

Not included in this analysis are the conditions (a) for hydrostatic collapse of the ring, (b) for longitudinal beam deflection, and (c) for indentations or crushed corrugations due to a hard object bearing against the pipe. It is assumed that specifications for the pipe zone backfill will exclude rocks of such size that an indentation becomes a perforation or an impedance to flow. Usually, specifications exclude rocks over 1.5 in. from bearing against the pipe. It is assumed that intense surface loads such as superhigh-pressure tires over a less-than-minimum soil cover will be avoided.

Minimum Soil Cover

Minimum soil cover over buried CPEP is of concern only when a surface wheel load passes over it. In the following examples, the load is a truck dual-wheel load up to an HS-20 load of 16 kips. Similar analyses could be accomplished for different loads such as those due to tracked vehicles.

Because most buried CPEP is supported by compacted, granular pipe zone backfill, any ring deformation is associated with soil slip along shear planes. In the case of minimum soil cover, if the surface wheel load is applied over a rectangular surface area of width B and length L and if load W is great enough to cause soil compression, then soil shear planes form as indicated in Figure 3, isolating a truncated pyramid of soil. The pyramid angle $\theta = 45° - \phi/2$, where ϕ is the soil friction angle. At depth H, the surface wheel load W is distributed over the base area as indicated in Figure 3(a). For compacted, crushed-stone backfill, the soil friction slope is about 1:2, for which the base area is $(B + H)(L + H)$. The vertical soil pressure on the pipe with soil cover H [Figure 3(b)] is

$$P = W/[(B + H)(L + H)] \quad (1)$$

For a dual-wheel load, the surface area is approximately a 7- by 22-in. rectangle, for which tire pressures vary with load as follows:

Dual-Wheel Load W (kips)	*Tire Pressure (psi)*
5.5	36
7	45
9	58
16	104

The analysis can be adjusted to different dual-tire contact areas. However, the 7- × 22-in. contact area gives results in agreement with the Findlay field tests. For such loads, the minimum soil cover is so small (a few inches) that dead load due to soil cover can be neglected.

A useful model for evaluating minimum cover is the following as adjusted by field test results. The geometry is shown in Figure 4 and the notation is as follows:

Notation			*Values for 18-in. CPEP*
ID	=	inside diameter of pipe,	18 in.
D	=	mean diameter of pipe $= ID + 2c$,	19.8 in.
r	=	mean radius of pipe $= ID/2 + c$,	9.9 in.
c	=	distance from the neutral surface of corrugations to the crest on the inside of the pipe,	0.86 in.

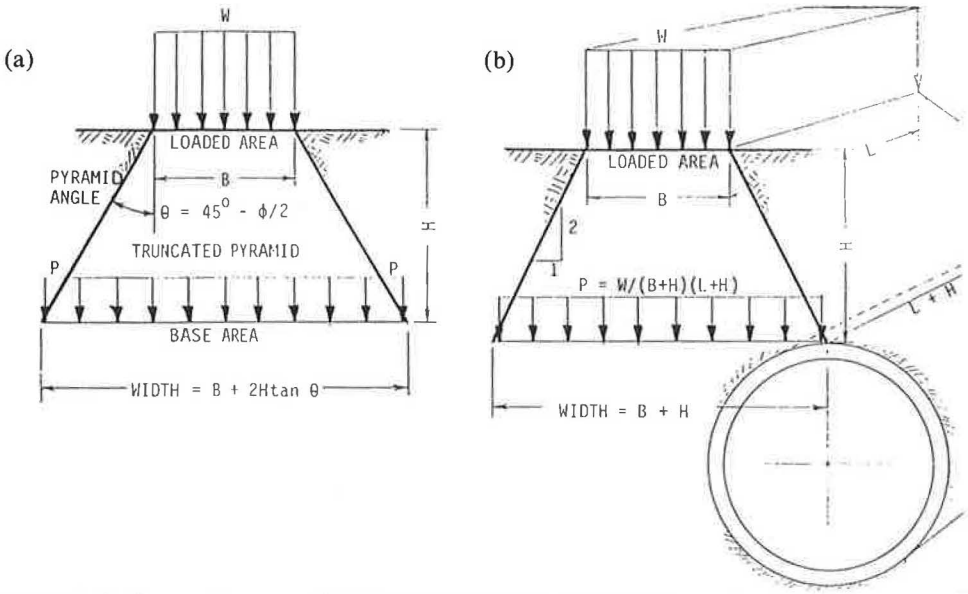

FIGURE 3 Truncated pyramid isolated by the formation of shear planes under a heavy surface load W with minimum soil cover H: (a) Vertical soil pressure P at depth H as load W is transferred through the truncated pyramid to the base area, and (b) approximate pyramid for compacted granular soil cover.

A	=	cross sectional area of pipe wall per unit length of pipe,	0.195 in.^{2}/in.
I	=	moment of inertia of the pipe wall per unit length of pipe,	0.077 in.^{4}/in.
S	=	strength of pipe wall material for quick loads such as wheel loads passing over,	3 ksi
H	=	installed height (in.) of soil cover (see Figure 4),	
H'	=	rutted height (in.) of soil cover after multiple passes of load W have stabilized the system,	
H''	=	depth of rut (in.),	
W	=	load on a truck dual wheel crossing over the pipe (kips),	
ρ	=	soil density in percent standard Proctor density (AASHTO Specification T-99) of granular soil cover and pipe zone backfill (percent),	
σ	=	circumferential stress in the pipe wall, and	
P	=	vertical soil pressure at the level of the top of the pipe due to passing dual-wheel load = $W/[(B + H)(L + H)]$ from Figure 3.	

The minimum height of cover is that soil cover H less than which the pipe-soil system is unstable under multiple passes of dual-wheel load W. Instability is incipient when stress equals yield point strength of the pipe.

From Figure 4, values of H are evaluated by $H = H' + H''$. For crushed limestone wet from precipitation, the rut depths H'' for dual-wheel loads W in granular soil cover are as shown in the following table. These values are from the Findlay field tests.

The rutted height of soil cover H' after multiple passes to stability is that cover less than which the stress in the pipe exceeds the quick-load strength of material S. For CPEP, the quick-load strength is usually greater than 3 ksi. So S = 3 kips/in.^{2}. Quick-load strength is used, rather than 50-year strength, because live loads are quick loads. The maximum stress in the pipe wall is less than the sum of ring compression stress and flexural stress due to nonuniform vertical soil pressure. To be conservative, then, the two are added as follows:

	Rut Depth H″ (in.)			
Soil Density	*W (kips)*			
ρ	*5.5*	*7.0*	*9.0*	*16.0*
80	3.0	3.8	4.6	6.5
85	2.4	3.0	3.7	5.1
90	1.8	2.2	2.7	3.8
95	1.1	1.4	1.7	2.4

$$\sigma = Pr/A + Mc/I$$

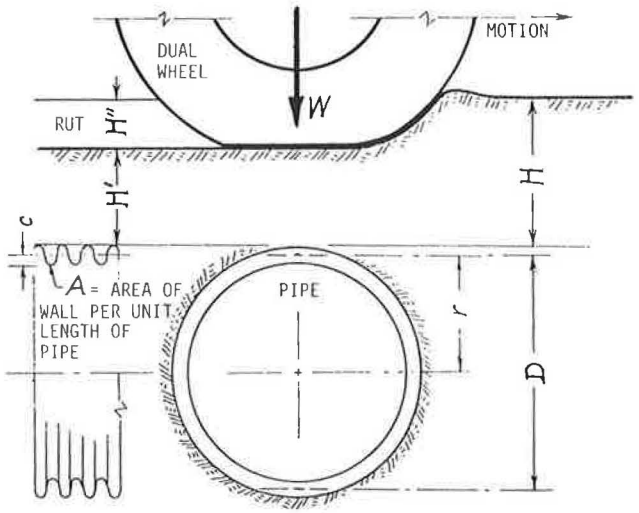

FIGURE 4 Sketch of a dual-wheel load W passing over a buried pipe with granular soil cover of height H.

Moment M can be evaluated by arch analysis. From the Findlay field tests, and from observations of minimum cover failures of flexible pipes, performance limit is identified as incipient plastic hinging that results in reversal of curvature of the pipe. When reversal of curvature does occur, it occurs within the top 80° arc of the ring. To be conservative, assuming 90° of top arch, see Figure 5 where $\alpha = 45°$, with ends of the arch fixed, and with a uniformly distributed vertical soil pressure P approaching from one side as shown,

$$M = 0.022Pr^2$$

The resulting stress equation is

$$\sigma = Pr(1/A + 0.022rc/I) \quad (2)$$

where, by pyramid soil stress analysis under a dual-wheel load distributed over a 7- × 22-in. rectangle,

$$P = W/[(7 + H')(22 + H')] \quad (3)$$

The rutted soil cover H' can be evaluated by substituting Equation 3 into Equation 2 and solving the resulting quadratic equation for H'.

The minimum granular soil cover, conservatively estimated (with 90 percent confidence), but without safety factor, is (see Figure 2)

$$H = H' + H'' \quad (4)$$

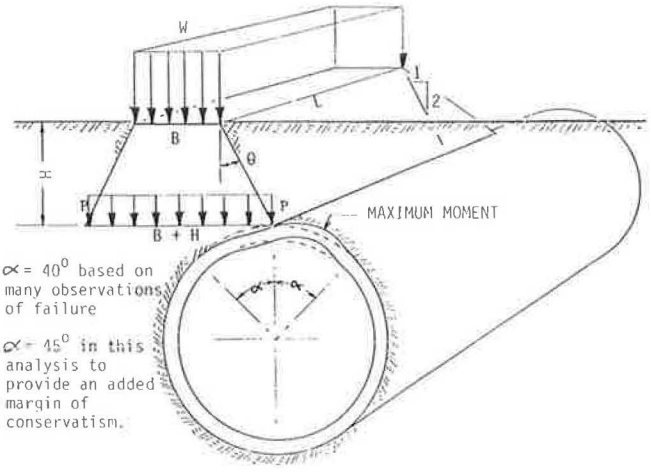

FIGURE 5 Pyramid live-load soil pressure P due to an approaching surface dual-wheel load W crossing over a pipe buried at depth H.

Example: Minimum Soil Cover

Suppose that minimum cover H of granular soil is to be evaluated for 18-in. CPEP in 85 percent dense backfill. Substituting Equation 3 into Equation 2 and including values of r, A, and I/c for 18-in. CPEP,

$$(H' + 14.5)^2 = 25W + 56.25$$

Solutions for 18-in. CPEP are as follows:

Dual-Wheel Load W (kips)	*Rutted Soil Cover H' (in.)*
5.5	-0.6
7	0.7
9	2.3
16	6.9

The negative value at $W = 5.5$ kips indicates that soil cover is not needed. The pipe can carry a 5.5-kip dual-wheel load even though the ruts expose the pipe. Of course, enough soil cover H should be provided to allow for rutting H'', to prevent surface rocks from indenting the pipe, and to avoid crushing of corrugations.

For soil at 85 percent density and with multiple passes of a 16-kip dual-wheel load, the minimum height of cover is (from Equation 4) $H = 12$ in. This example yields a conservative minimum soil cover in approximate agreement with field tests. In the Findlay field tests, instability was observed after multiple passes of a 16-kip dual-wheel load over an 18-in. CPEP with 85 percent dense granular soil cover and with an installed height of soil cover of $H = 10$ in. Rutting was found to be about 5 in. maximum after many passes.

This analysis is valid for CPEP up to and including 24-in. diameter. Conditions of similitude should be reviewed for pipes larger than 24 in. in order to consider changes required for installation and possible differences in the properties of the yet-to-be tested large pipes.

For 24-in. CPEP, the equation for rutted height of cover H' becomes

$$(H' + 14.5)^2 = 25.36W + 56.25$$

This result is based on $r = 13.24$ in., $A = 0.2775$ in.^{2}/in., and $I/c = 0.136$ in.^{3}/in. Solutions for 24-in. CPEP are as follows:

Dual-Wheel Load W (kips)	*Rutted Soil Cover H' (in.)*
5.5	-0.5
7	0.8
9	2.4
16	7.0

These values are essentially the same as for 18-in. CPEP.

Ring deflection under minimum soil cover comprises two components: permanent ring deflection d' and rebound ring deflection d''. The rebound ring deflection is elastic and so rebounds fully after each pass of the dual-wheel load.

In Figure 6, results are summarized of the Findlay field tests on 18-in. CPEP under the least favorable backfill conditions tested. Backfill was crushed limestone. The soil density was 85 percent of the standard Proctor density (AASHTO Specification T-99), the lowest density tested; the height of soil cover was 7 in., the least cover tested. Two observations are noteworthy from Figure 6:

1. Ring deflection is small, less than 2 percent, for the first pass of the dual-wheel load. Permanent ring deflection and

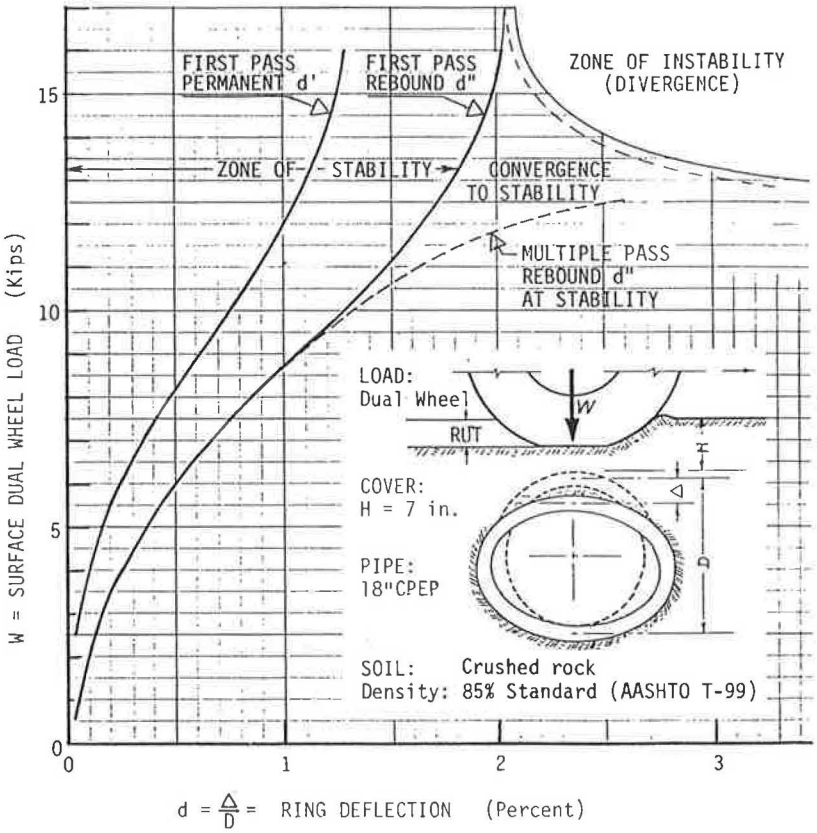

FIGURE 6 Typical load-deflection diagram for 18-in. CPEP under 7 in. of soil cover of 85 percent standard Proctor density (AASHTO T-99), comparing permanent ring deflection *d'* and rebound ring deflection *d"* and showing approximate zone of instability.

rebound ring deflection are both less than 2 percent for dual-wheel loads up to 16 kips.

2. For multiple passes, the rebound ring deflection stabilizes if dual-wheel loads are less than about 12.5 kips. The stabilized ring deflection is greater than the first-pass ring deflection (see the lower dotted graph of Figure 6). At dual-wheel loads greater than about 12.5 kips, rebound ring deflections may increase progressively toward instability.

For minimum soil cover of 12 in., no instability occurred. Ring deflections are much less than 2 percent.

For multiple passes of HS-20 loads over buried CPEP, the recommended minimum soil cover is 12 in. To assure a successful installation, it may be prudent to specify pipe zone backfill up to the ground surface of crushed rock passing the 1.0-in. sieve or less and compacted in 8-in. layers to at least 90 percent standard Proctor density (AASHTO Specification T-99). The 12-in. soil cover includes some surfaces such as asphalt. In fact, a good surface eliminates the rutting. For a reinforced-concrete slab, the minimum cover may be reduced. If the preceding conditions are met, ring deflection is not a performance limit unless it causes unacceptable cracking of the surface over the pipe. Slight cracking of the surface is possible above both rigid and flexible pipes under minimum soil cover. The remedies are to increase the soil cover over the minimum, to use concrete backfill, to densely compact the select pipe zone backfill, or to cast a reinforced concrete slab on the surface.

For minimum cover, these observations apply to all pipe diameters if all length dimensions are scaled proportionately. Ring deflections d and dimpling remain unchanged for all diameters of pipe under the same soil, density, cover, and load. Pipes larger than 24 in. should be studied further.

Maximum Soil Cover

Maximum soil cover is the height of soil cover H for greater than which ring deformation is excessive. Excessive ring deformation is the basic performance limit. It is identified as either (a) ring deflection d so great that flow is impeded, or (b) visible dimpling of the crests of corrugations at 9 and 3 o'clock inside the pipe. Dimpling portends wall crushing or wall buckling. Both effects can lead to the formation of plastic hinges, a condition for instability.

In terms of stress, dimpling occurs when compressive stress exceeds the strength of material. Critical compressive stress σ is the sum of ring compression stress and ring deflection stress, that is,

$$\sigma = Pr/A + 3Ecd/[r(1 - 2d)] \quad (5)$$

where

σ = circumferential compression stress,
Pr/A = ring compression stress,
$3Ecd/[r(1\text{-}2d)]$ = ring deflection stress as the circular ring deforms into an ellipse,
E = modulus of elasticity,
r = mean radius of the pipe,
A = area of cross section of pipe wall per unit length of pipe,
P = vertical soil pressure at the level of the top of the pipe,
c = distance from neutral surface of the corrugation cross section to the inside corrugation crest, and
d = ring deflection.

If ring deflection is controlled so that $d = 0$, then stress σ is simply ring compression stress. However, the contribution of ring deflection toward dimpling is usually significant.

Ring deflection is determined by pipe stiffness and compaction of the backfill. However, the effect of pipe stiffness is negligible if the backfill is dense and if ring deflection does not include initial ring deflection due to soil compaction. Such ring deflection becomes

$$d = \varepsilon \tag{6}$$

where

d = Δ/D = ring deflection excluding ring deflection due to soil compaction;
Δ = decrease in vertical diameter due to vertical soil pressure P;
D = initial, vertical, mean diameter with dense backfill already in place about the pipe;
ε = soil compression, i.e., vertical soil strain due to load P;
P = vertical soil pressure at the level of the top of the pipe;
P = $P_d + P_l$;
P_d = γH = dead weight of soil cover;
P_l = $f(W)$ = vertical live-load soil pressure on the pipe due to surface load W, usually calculated by Boussinesq formula;
H = height of soil cover over the pipe;
γ = unit weight of the soil cover; and
W = surface live load crossing over pipe.

Because maximum soil cover H is usually more than 8 ft, the live-load pressure due to an HS-20 dual-wheel load is less than $P_l = 100$ lb/ft^2, and so can be neglected. If live-load pressure is included, it is not treated as an approaching load. P_l is simply added to P_d. If a vertical load-deflection (P versus ε) diagram is available for the compacted backfill, then at the anticipated vertical soil pressure P the corresponding soil strain ε can be read directly. From Equation 6, the approximate ring deflection $d = \varepsilon$ can be predicted. Figures 7 and 8 show typical plots of high soil cover tests performed at Utah State University on CPEP. The plot relates ring deflection d to vertical soil pressure P in granular backfill compacted to 85 percent standard Proctor density (AASHTO Specification T-99). The most important observation is that the pipe-soil conduit is stable up to a vertical soil pressure of $P = 7.5$ kips/ft^2. At this pressure, the ring deflection is roughly $d = 13$ percent. Figure 8 shows the relationship of ring deflection to soil pressure in loose backfill at 75 percent density for which the pipe-soil conduit is stable up to soil pressure of $P = 4$ kips/ft^2. Equation 5 is of the form $\sigma = Pr/A + Kcd/r(1 - 2d)$, where K includes modulus of elasticity E and a number of minor variables. From Figures 7 and 8 assuming the same σ at dimpling in each, $K = 0.329$ ksi, and apparent yield point stress is $\sigma = 3.57$ ksi. Substituting these values into Equation 5 and solving for P,

$$P = A\{3.57 - [0.239cd/r(1 - 2d)]\}/r$$

For 18-in. CPEP, this equation reduces to

$$P = [10.1 - 15d/(1 - 2d)]ksf$$

The following is a table of values for 18-in. CPEP.

d (%)	P (ksf)	H (ft)	H/sf (ft)
0	10.1	84.4	33.8
5	9.3	77.2	30.9
10	8.2	68.5	27.4
15	6.9	57.4	23.0
20	5.1	42.5	17.0
25	2.6	21.7	8.7

The values for H are based on unit weight of soil of 120 lb/ft^3. The allowable values of H/sf are based on a safety factor of $sf = 2.5$. Figure 9 is a plot of P as a function of d from the table. The safety factor of $sf = 2.5$ is higher than necessary if the backfill is good granular soil. On the other hand, if the backfill is marginal, or if the pipe is installed carelessly, a generous safety factor may be justified because of the high cost of repair or replacement.

The use of quick-load strength rather than 50-year strength is appropriate for design. If polyethylene is held under constant deformation, such as the ring deformation of a pipe buried in select pipe zone backfill under a high soil cover, stresses in the polyethylene relax. The highest stresses are the initial stresses generated at the time of installation.

Example: Maximum Soil Cover

What is the maximum height of soil cover H allowed for 18-in. CPEP pipe if the backfill is to be granular soil at 90 percent standard density? Figure 10 is a hypothetical graph of a laboratory compression test on the granular backfill. The answer to the question is simply the point of intersection of the graph of Figure 9 and the 90 percent graph of Figure 10. This is easily done by inspection or by plotting Figure 9 on Figure 10. $P = 9.7$ kips/ft^2. If the soil unit weight is 120

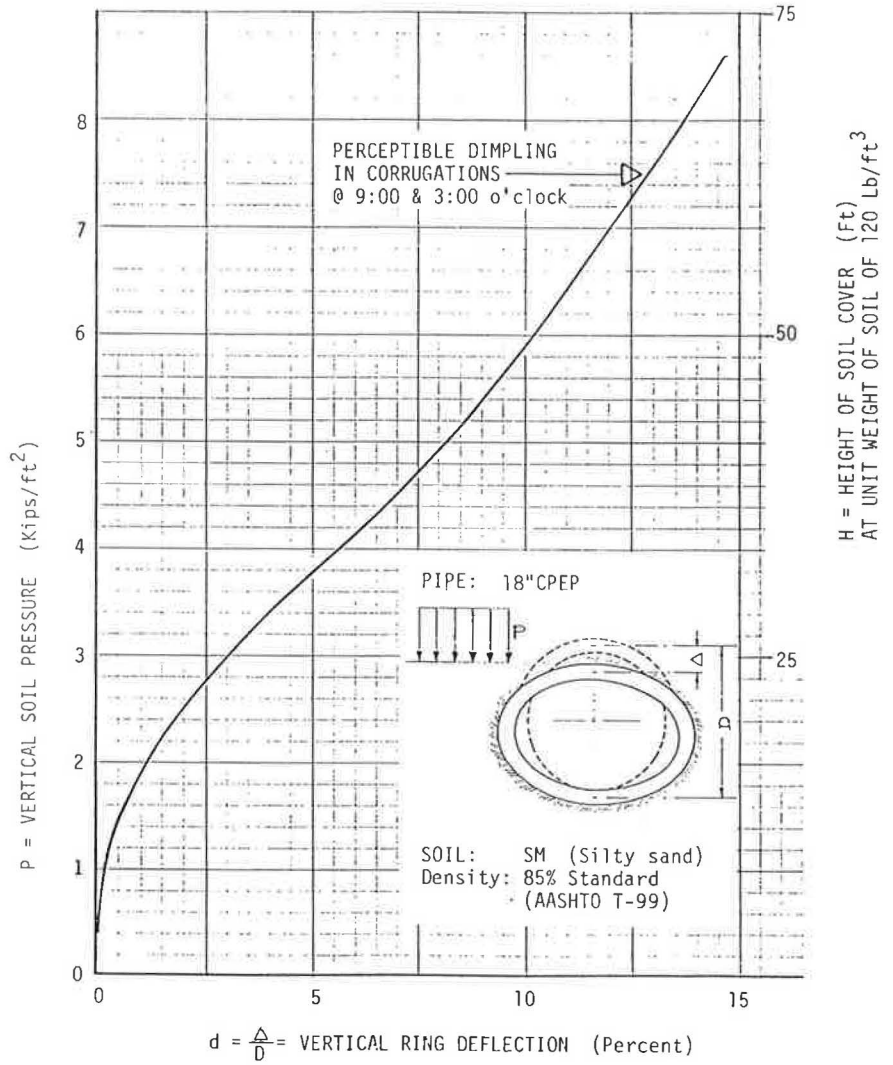

FIGURE 7 Typical load-deflection diagram for 18-in. CPEP buried under high soil cover *H*. (Vertical soil pressure *P* is a function of *H*).

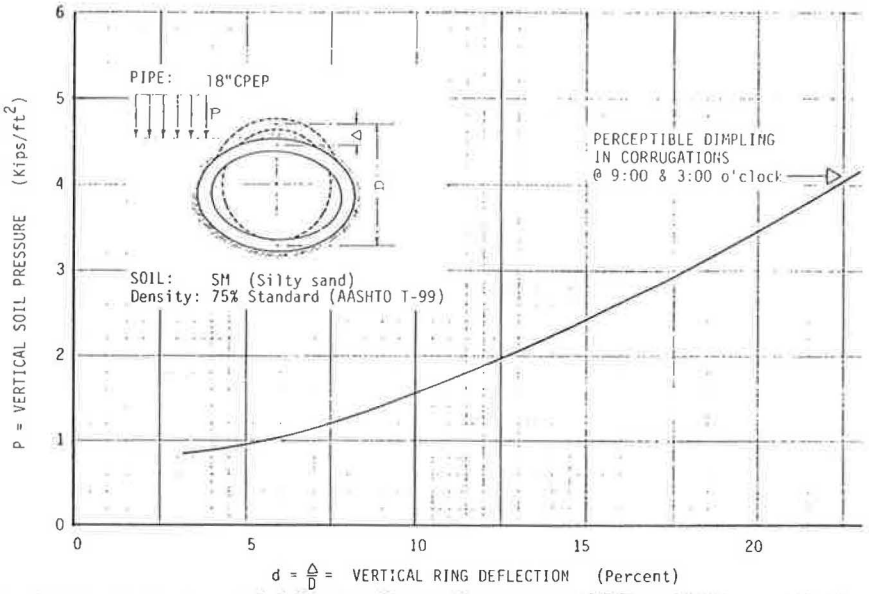

FIGURE 8 Typical load-deflection diagram from a test on 18-in. CPEP under high soil cover where load is the calculated vertical soil pressure *P* at the top of the pipe, but where the backfill is uncompacted.

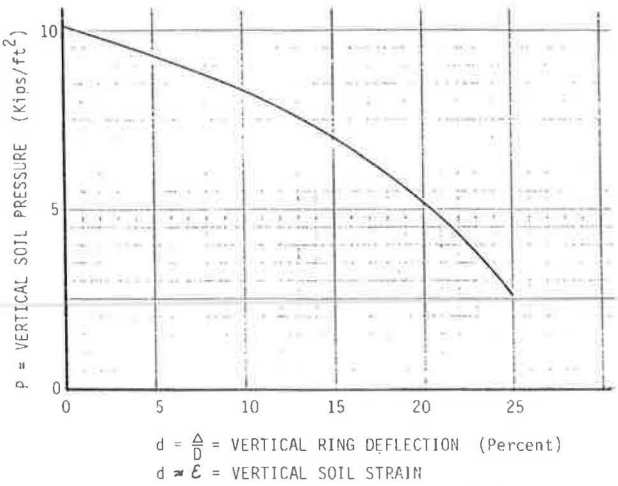

FIGURE 9 Vertical pressure at performance limit (dimpling at 9 and 3 o'clock) as a function of ring deflection for 18-in. CPEP.

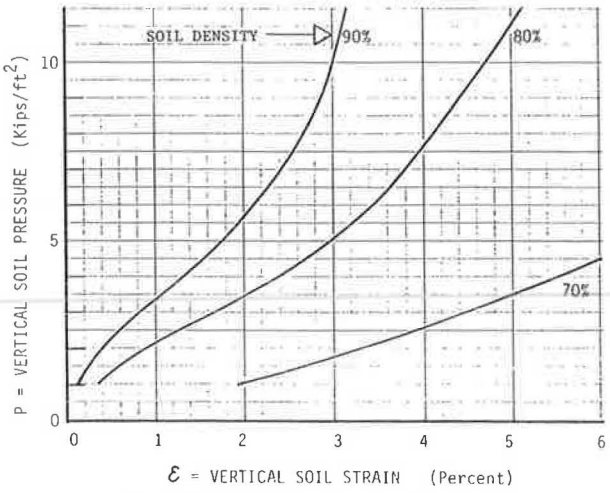

FIGURE 10 Hypothetical graphs of vertical soil stress as a function of vertical soil strain for granular soil from compression tests in the laboratory.

lb/ft^3, then at dimpling, the maximum height of soil cover is H = 81 ft. If a safety factor of 2.5 is called for, H/sf = 32 ft of allowable soil cover.

It is clear that the best control of the pipe-soil conduit under maximum soil cover is control of the backfill. Specifications should establish minimum values for compacted density and should assure competent granular material.

ACKNOWLEDGMENT

This paper is the outcome of the two testing programs referred to as the Findlay field tests and the Utah State University soil cell tests. The test program was sponsored by Hancor, Inc., Findlay, Ohio. The funding and cooperation by Hancor, Inc., is acknowledged with appreciation.

Performance of Thin-Wall Concrete Pipe

L. H. GABRIEL AND H. E. BLOWER

An analytical and experimental study was conducted of thin-wall unreinforced-concrete pipes of dimension ratios 16 through 70 under surcharge loads equivalent to 30 ft of fill. Special attention was directed towards bedding and trench properties and geometries. The advantages and efficiencies of matching the stiffnesses of the bedding with that of the soil envelope are discussed. Narrow trench widths are shown to be more efficient when trench fill is of lesser stiffness than trench walls. Recommendations for practice are made.

Concrete pipes are generally classified as rigid pipes. Thin-gauge metal pipes and plastic pipes are generally classified as flexible pipes. Each has its own strategies for design. As one criterion of performance, ring compression theory for flexible pipes anticipates a stress response to a service load. Stress is not employed as a criterion of performance in the case of ring deflection theory for flexible pipes, except as a parameter related to the possibility of a buckling failure. With the D-load method, neither is stress response to service loads a criterion for the design of rigid pipes.

In recent years, with the introduction of plastic pipe with stiffnesses between the extremes of flexible and rigid, the profession and industry have faced the difficulty of nesting a design strategy for semirigid (or semiflexible) pipe between the existing extremes. Neither design strategy may be extrapolated for application to the semirigid pipe.

As regards the use of rigid pipe theory for plastic pipes, the three-edge bearing test as a measure of performance cannot be adopted. The nonbrittle nature of plastic precludes the possibility of a 0.01-in. crack being used as a criterion (*1*). Rigid-pipe theory as a basis for semirigid pipe design has therefore been rejected.

A number of problems exist should either of the two common flexible pipe theories be adopted as a basis for the design of semirigid pipes. The ring compression theory has all the virtues of a theory rooted deeply in the principles of structural mechanics, including a stress response. The presumption of membrane action of an easily altered geometry of a thin shell under service loads rejects bending in favor of an in-plane thrust. Only a flexible pipe is flexible enough to satisfy this criterion; a semirigid pipe does not qualify.

The inconsistencies encountered in the backcalculations leading to articulation of soil stiffness E' provide the necessary empirical evidence for the rejection of the ring deflection theory as a means of predicting the performance of thin-wall concrete pipe. Gabriel and Blower (*2*) showed that the coupling of soil and structure stiffnesses in the denominator of the equation for the prediction of deflection under service load is more complicated than the arithmetic summation of the two. The extrapolation of the ring deflection method for purposes of semirigid pipe design may lead to gross errors of prediction (*3*).

The industry and profession await a consistent theory that may be applied to all classes of pipe. Loads are attracted to the stiffer elements of the composite structure. The greater the stiffness of the pipe relative to its embedment, the greater the internal force responses of thrust, moment, and shear within the pipe wall. Alternatives of bedding and trench geometries, materials, and compactions add complexity to the problem. The distribution of normal and shear pressures at the pipe-soil interface are important determinants of the mode of pipe response to service loads. The ideal always is a uniform normal pressure that precludes the excitement of flexural stresses within the wall of a circular cross section.

The larger purpose of the studies was to obtain a sense of some favored alternatives for thin-wall concrete pipes. The studies were supported by the California Department of Transportation (Caltrans) and the FHWA (*4*).

EXPERIMENTAL DESIGN

Models of structural analysis always include the assumption of reasonable correspondence with the material, geometric, and connective features of those structural elements being modeled. Computer modeling of structures composed of a multiplicity of structural elements follows the same prescription.

Computer modeling of structural composites of pipes embedded in surrounding soil media was adopted as the strategy for gaining, and maximizing, experience with thin-wall concrete pipes. Physical tests were performed to establish the parameters needed for the computer analyses and to spot check the computer studies. Surcharge loads equivalent to 30 ft of fill were superimposed on buried pipes in test frames designed and built at California State University, Sacramento.

CANDE (*5*) was selected as the program for the computer analyses. Its three levels of solution include the elasticity solution of Burns and Richard (*6*) and two finite element solutions, one of which has self-generating elements.

The experimental design was as follows:

1. Model concrete pipes of 9-in. outer diameter (OD) and wall thicknesses 1/8 in. to 1/2 in. (nominal dimension ratios

Department of Civil Engineering, California State University, Sacramento, Calif. 95814.

DR = 70 to 16, correspondingly) were buried in one of two loading cells with sand of uniform material and compaction. Surcharge loadings up to 25 psi, equivalent to over 30 ft of fill, were introduced in steps of 2.5 psi. Changes in vertical and horizontal diameters were measured (Figure 1).

2. With the assumed mechanical properties of pipe material to be described later and for a range of mechanical properties of the sand fill, CANDE was run for the same surcharge loadings as were physical experiments.

3. The outcomes of the physical experiments and the computer modeling of these same experiments were compared. The mechanical properties of the sand were defined when the outcomes matched.

4. Knowledge of the mechanical properties of the sand completed the information required for subsequent computer modeling of a buried pipe in the load frames. Parametric studies of pipe thickness and bedding and trench geometry were conducted with computer models and spot checked by physical experiment.

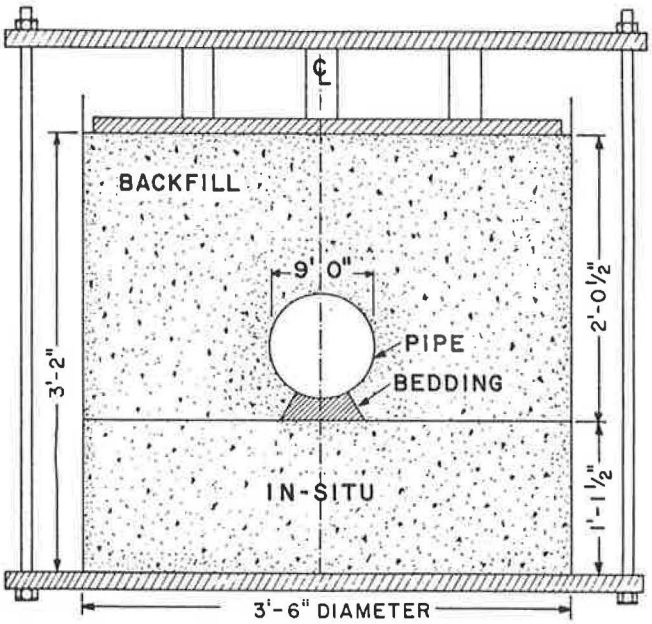

FIGURE 1 Test frame and computer model (schematic).

EQUIPMENT AND INSTRUMENTS

Each of the two load frames consists of 4-ft-high concentric sections of 42- and 48-in.-diameter (nominal) corrugated steel pipe sections forming and enclosing a nominal 3-in. concrete wall. The inside wall corrugations were filled, smoothed, and overlaid with two sheets of lubricated plastic to minimize wall friction on the boundary of the highly stressed soil. Force is transmitted to a rigid plate floating on the composite of buried pipe and surrounding soil by means of instrumented (with three strain gauges at 120° around the circumference of each rod) and calibrated tension rods. These rods, anchored below and attached above to a loading platform, are mechanically loaded by tightening nuts at the rod ends. The reactions to the motion of the loading platform deliver point loads to the rigid floating plate, positioned so as to deliver a uniformly distributed load to the entire soil surface of the soil-surface composite.

Contractions and extensions of the vertical and horizontal diameters were measured by means of a two-axis floating deformation sensor and transducer designed for continuous reading (Figure 2). The device is a pair of independent instruments with axes perpendicular to one another and mounted on a common frame. Each gauge is composed of a pair of spring steel bows of negligible bending stiffness, clamped at the ends, responding to displacements in a bending mode. Each bow has two opposing strain gauges, one centered on the convex side and the other on the concave side. The four gauges of each instrument are wired as a full bridge. Initial contact between a steel ball and a smoothened inner wall of the pipe was made with an adjusting screw at each outboard end. The instrument was able to sense motion to 0.0001 ± 0.00005 in.; its response was linear. The sensing arrangement for the vertical pipe diameter change was similar to that for the horizontal pipe diameter change.

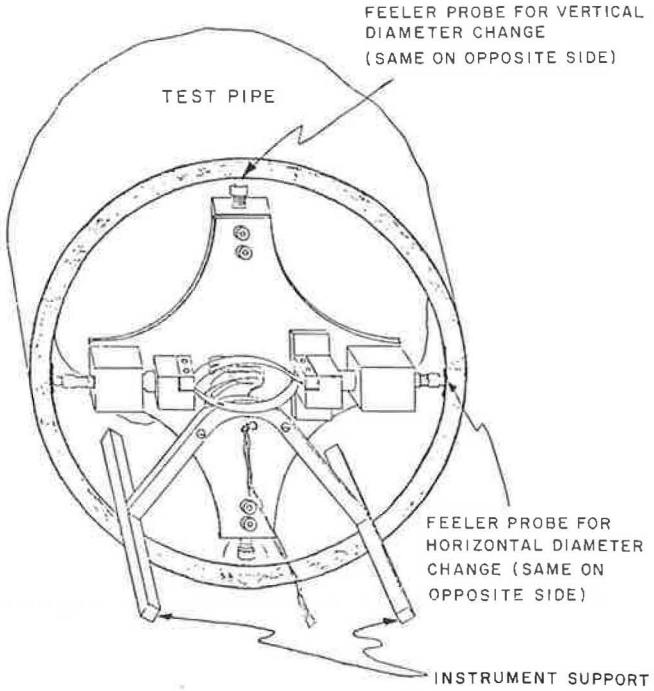

NOTE: SENSING ARRANGEMENT FOR VERTICAL PIPE DIAMETER CHANGE SIMILAR TO THAT FOR HORIZONTAL PIPE DIAMETER CHANGE.

FIGURE 2 Two-axis deformation sensor and transducer.

CONCRETE MODULUS

The property of stiffness of a stressed structural element is a function of the material, geometry, and mode of response. Recall that the deflection of a beam is inversely proportional to its material and geometric moduli EI; the extension of a bar is inversely proportional to EA/L; and the diametral change of a ring is inversely proportional to EI/R^3; where E is the material stiffness and I, A, L, and R are geometric parameters of the element.

Whereas I, A, L, and R are well defined, E is difficult to evaluate when it is other than linearly elastic. The surrounding soil and the embedded pipes are both of nonlinear inelastic materials. The potential for significant error exists for the prediction of the performance of the soil-structure composite.

In Figure 3, a secant modulus E_s and a tangent modulus E_t are both shown operating at some prescribed limit of working stress f of a nonlinear strain-softening material. Because the tangent modulus, at any level of stress and at all points in the pipe, governs the deflection (the secant modulus is only a convenience for design), the assumption of modular values has significant effect on the prediction of deflection. The nonconstant stress levels within the pipe imply further variation in modulus.

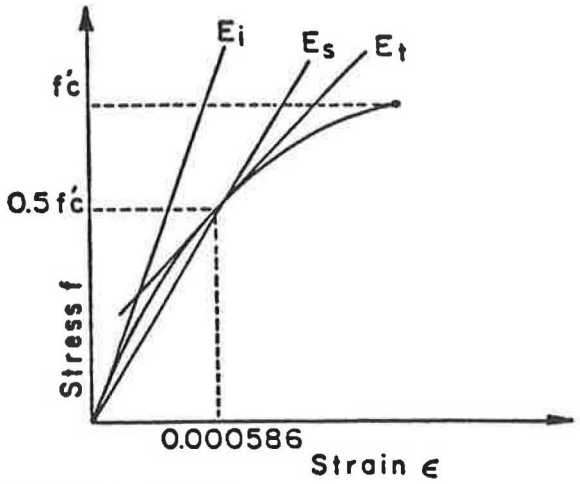

FIGURE 3 Moduli alternatives.

TANGENT MODULUS FOR CONCRETE

Obtaining the measure of tangent modulus is subject to the further disability that for soils and concrete the functional form of the curve is not generally known. The nonsmoothing nature of differentiation necessary to evaluate the tangent modulus adds further difficulty. For concrete, the properties of the stress-strain curve depend, in part, on the choice of materials, manner of preparation and casting, water content, method of curing, functional use, and rate of loading of test samples. Data developed by Ramaley and Henry (*6*) (Figure 4) suggest the appropriateness of a parabolic response between zero and a vertex of ultimate strength f'_c at a strain of 0.002. The equation for such a curve is

$$f = [1 - 250{,}000(\varepsilon - 0.002)^2]\, f'_c \qquad (1)$$

The tangent modulus at any point is

$$E_t = df/d\varepsilon = (f'_c/2)(0.002 - \varepsilon)(10^6) \qquad (2)$$

The measure of the initial modulus is

$$E_i = E(0, 0) = 1{,}000 f_c \qquad (3)$$

To judge the reasonableness of these equations, the results are compared with the estimate of secant modulus for concrete of f'_c = 5,000 psi based upon the American Concrete Institute (ACI) formula

$$E_s = 33 w^{1.5} f'_c$$

Note in Figure 3, the secant modulus lies between the tangent modulus and the initial modulus.

E_t = 3,535,000 psi (from Equation 2);
E_s = 4,074,000 psi (from ACI); and
E_i = 5,000,000 psi (from Equation 3).

The stress-strain curve described by Equation 1 was adopted.

In application, an iterative process was introduced into CANDE to establish an appropriate value for the stress-dependent tangent modulus. At each level of load, a tangent modulus was assumed. With the other parameters of the analysis held fixed, CANDE was run and the maximum stress at springline was noted. This stress was then introduced into the stress-strain law, Equation 1, and the strain was calculated. A revised tangent modulus was then computed from Equation 2, and the process was repeated until convergence, which was rapid.

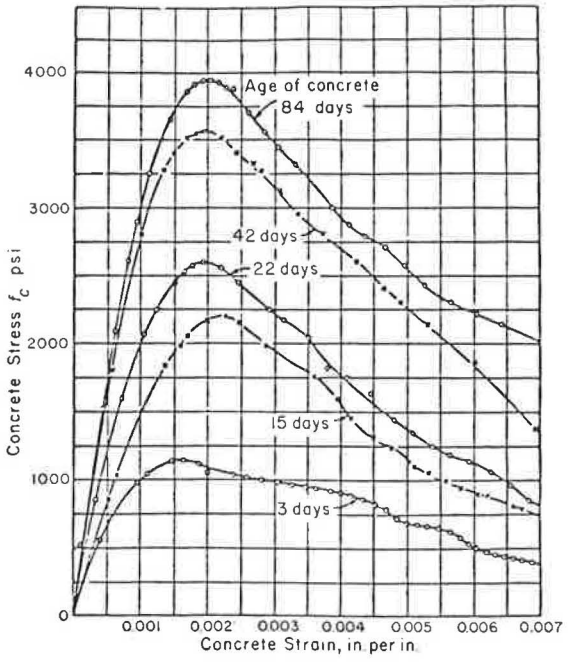

FIGURE 4 Concrete stress-strain curves from compression cylinders.

SOIL MODULUS

Pointwise definition of the mechanical properties of a solid at varying levels of stress permits linear elastic models of analysis to be used as reasonable approximations with nonlinear inelastic materials. A granular soil, however, is not a solid. Movements dissipative of the energy that deforms the soil mass inhibit it from being effectively modeled as a solid. Slippage not only has the potential to occur at the pipe-soil

interface, but also at all points of contact within the granular soil mass.

In spite of this, perhaps because of the absence of alternative forms of analysis, the pretense of the solid is carried forth. If the pointwise mechanical properties of a soil were known, then an elastic solid of precisely those same properties would be expected to perform in the same manner, enabling the latter to be modeled to predict the former. The burden then becomes one of properly defining the mechanical properties of the soil.

SELECTION OF SOIL PROPERTIES

For the purpose of learning the in-place property of soil modulus, the following conditions were applied to both the computer analyses and, where appropriate, the physical tests:

1. Nine-inch pipes, of wall thickness varying from 1/8 to 1/2 in. were buried in a homogeneous soil mass.
2. The Burns and Richard (*7*) elasticity solution was assumed operative.
3. The height of cover above springline was twice the *OD* of the pipe.
4. The compaction and density of the sand was taken as unvarying, achieved in the physical tests by uniform free-fall deposition of the sand grains transported with the assistance of an industrial vacuum.
5. Uniform surcharge was added in increments of 2.5 psi to a maximum of 25 psi.

The following quantities were extracted from the computer analyses:

- Center-crown displacement D_v (in.)
- Crown moment M (in.-lb/in.)

Input into the computer analyses includes:

- Wall thickness t (in.)
- Average pipe radius r (in.)
- *OD* D_0 (in.)
- Presumed operating soil modulus E_s (psi)
- Acting concrete tangent modulus E_c (psi)
- Surcharge pressure p (psi)
- Poisson's ratio ν

The calculated items include

- Pipe modulus $E_p = E_c(t/r)^3/12 = (2/3)E_c/(DR)^3$ (psi)
- Dimension ratio DR
- Soil stiffness ratio $K_2 = 100E_s/(E_p + E_s)$
- Displacement ratio $\%Y = 100D_v/r$

Sample results are presented in Table 1. Note that E_s varies from 1,100 to 1,800 psi. Other results were for presumed values of soil modulus increasing with surcharge pressure (5 to 25 psi) for the following additional ranges: 2,350-3,850; 3,600-5,900; 4,850-7,950; and 6,100-10,000 psi.

TABLE 1 STUDY OF MOMENTS AND DEFLECTIONS—CANDE (LEVEL 1)

cltrns5 STUDY OF MOMENTS AND DEFLECTIONS - CANDE (LEVEL 1)

	surch press p psi	soil mod Es psi	conc mod Ec psi x10**6	pipe mod Ep psi	crown mom M in-#/in	vert disp Dv in	K1	Dv/r x10**-3	Ep/Es x10**-3	slope:K1 K2 vs Ep/Es x10**-3	
t (in) = .125	5	6100	5.80	10.60	0.45	.00323	2.51	0.73	1.77	99.82	1417
r (in) = 4.438	10	7200	5.59	10.41	0.81	.0055	2.28	1.24	1.45	99.86	1580
DR = 71.81	15	8300	5.40	10.05	1.10	.0078	1.88	1.76	1.21	99.88	1556
	20	9150	5.21	9.70	1.37	.01003	1.66	2.26	1.06	99.89	1561
code:850107-151718	25	10000	5.02	9.35	1.61	.01209	1.48	2.72	0.93	99.91	1578
t (in) = .25	5	6100	5.79	90.03	3.15	.00271	21.17	0.61	14.76	98.55	1435
r (in) = 4.375	10	7200	5.58	86.76	5.79	.00508	17.59	1.14	12.05	98.81	1460
DR = 35.00	15	8300	5.40	83.97	7.93	.00709	14.97	1.60	10.12	99.00	1480
	20	9150	5.22	81.17	9.94	.00904	13.35	2.04	8.87	99.12	1505
code:850107-152051	25	10000	5.05	78.52	11.73	.01035	12.01	2.44	7.85	99.22	1530
t (in) = .375	5	6100	5.79	317.14	7.84	.00194	73.61	0.44	51.99	95.86	1416
r (in) = 4.313	10	7200	5.59	306.19	14.72	.00371	61.23	0.84	42.53	95.92	1440
DR = 23.00	15	8300	5.40	295.73	20.56	.00528	52.13	1.19	35.64	96.56	1463
	20	9150	5.22	285.92	26.10	.00682	46.47	1.54	31.25	96.97	1487
code:850107-152729	25	10000	5.04	276.06	31.15	.00828	41.30	1.87	27.61	97.31	1514

Ep = Ec*I/r**3 = (Ec*(t/r)**3)/12 = (2/3)*(Ec)*(1/DR)**3
K1 = (M/(Es*Dv*Do))*100 , where Do = outer dia = 9 in.
Dv = vert dia disp - crown/center
DR = Dimension Ratio = 2*r/t
K2 = (Es/(Ep+Es))*100

For the dense silica sand of their study, Duncan and Chang (*8*) assumed a value for Poisson's ratio of 0.3 for all values of a full range of confining pressure. The silica sand of this study is also very dense; a relative density of 98 percent was determined by the Caltrans Transportation Laboratory. Based upon the comparisons of the sands, a value for Poisson's ratio of 0.3 was adopted for all values of confining pressure.

Within the bounds of the noted presumed operating values of soil moduli, there is assumed to exist one set of modular values that closely represents the conditions operating in the test frames of the physical experiments. The outcomes of the experiments are sets of vertical and horizontal diameter changes for increasing surcharge pressures. The plots of deflection versus stiffness ratio (Figure 5) are a result of the computer analyses. Introduced into these charts are the measured vertical diameter deflections of the physical experiments. For example, the vertical deflection, when the surcharge pressure is increased from 10 to 15 psi in the physical experiment, should be laid out on a template to the same scale as the appropriate chart and then placed vertically so that it is precisely intercepted at its endpoints by the 10- and 15-psi lines drawn on the chart. Where the extension of this line intersects the horizontal axis, the relative stiffness K_2 compatible with the performance of the pipe-soil structure of the physical test is evaluated. With E_p known, E_s is evaluated. That process, extended to the full range of testing, leads to a calculation of acting soil moduli. With modification reflecting smoothing of results and the adoption of a midrange of values between the last two of those developed by analysis, the assigned values of soil moduli for varying surcharge pressures are noted in the following table.

Surcharge (psi)	*Acting Soil Modulus (psi)*	*Assigned Soil Modulus (psi)*
5.0	5,150	5,090
7.5	5,900	5,570
10.0	6,920	6,040
15.0	8,100	6,930
20.0	8,200	7,670
25.0	—	8,350

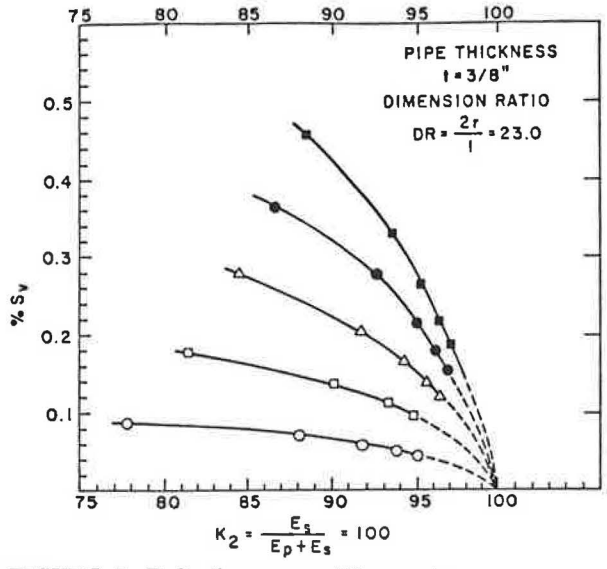

FIGURE 5 Deflection versus stiffness ratio.

BEDDING STUDY

Practice holds that the D-load strength requirement for a rigid concrete pipe, as determined by the three-edge bearing test (*1*), increases as the quality of bedding falls from Class A to Class D. A concrete cradle, bedding of the highest quality, may be required to longitudinally support a pipe over incompetent or irregular ground supports. The cradle shape is intended to distribute the reaction across the pipe-bedding interface.

A study was conducted on the influence of bedding on the performance of 9-in.-*OD* pipes of varying wall thickness (also, varying stiffness) interacting with bedding of varying stiffness including cradle spans of *OD*/2 and flat bedding. Figure 6 shows the geometric layout of the computer model using CANDE, Level 3. Note that 12 pipe elements make up the half-circle. Input to CANDE includes the measures of pipe and soil stiffnesses previously discussed. A shell structure is known to be sensitive to sharp changes in curvature and sharp changes in loading, in that each gives rise to large moments and the associated flexural stresses. Because the curvature of a circular pipe is constant, a preferred design would be one in which the loading around the pipe circumference would also be constant. The study established an understanding of the relationships between relative stiffnesses of pipe, bedding, and surrounding soil, and resulting interface loads, moments, and stresses.

Analyses were made for the embankment condition of 9-in.-*OD* pipes of wall thickness 1/8, 1/4, and 1/2 in. (of

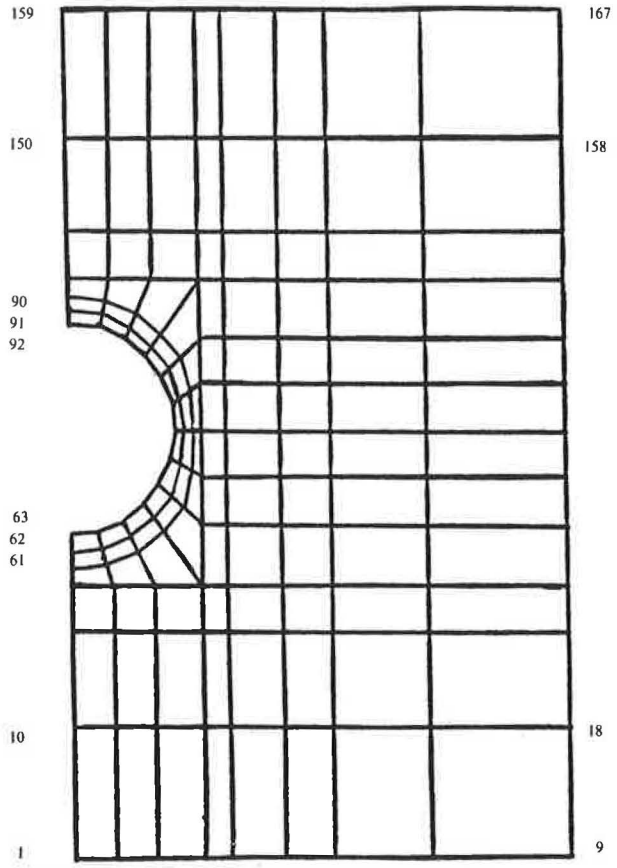

FIGURE 6 Finite element network nodal points.

DR = 70, 34, and 16, respectively); overburden pressures 5 to 25 psi; and bedding stiffness 1,000 to 4,090,000 psi.

For shaped bedding and surcharge loads of 25 psi, Figures 7 and 8 show the normal pressure at the interface and bending moment in the wall. All data pertained to an embankment condition with bedding of stiffnesses 1,000, 8,000, 512,000, and 4,090,000 psi. A plot of maximum tensile stress at any circumferential location along the pipe versus bedding stiffness for varying wall thicknesses is shown in Figure 9. Results for less pressures are closely proportional to those of 25 psi. A comparison of normal pressure and bending moment for shaped and flat bedding, of stiffnesses closely matched to the backfill soil, is shown on Figure 10. Results and inferences follow.

1. For the case of shaped bedding, for pipes of all dimension ratios and for all levels of surcharge pressure, the preferred condition of the smoothest distribution of normal pressure occurs when the stiffness of the bedding and the stiffness of the backfill are closely matched (8,000 and 8,350 psi, respectively, for the study of this report).
2. Shaped bedding of lesser stiffness than the backfill (e.g., urethane foam of stiffness 1,000 psi) results in a less smooth distribution of normal pressure around the pipe than the case of nearly matched stiffnesses.
3. As the shaped bedding stiffnesses increase beyond the favored condition of matched with the backfill, the departure from the preferred smooth distribution of normal pressure becomes more significant. With the higher stiffness shaped bedding ($E_s > E_p$), separation occurs between the pipe and the bedding except at the two endpoints of the bedding, due to the ovality of the pipe cross section. The unyielding endpoints of stiff shaped bedding introduce the undesirable condition of point loads.
4. Higher moments, at the edge of the bedding, always attend the less uniform loads.
5. For the condition where the bedding stiffness nearly matches the backfill stiffness, flat bedding with pockets of softer fill at the 5 and 7 o'clock regions due to poor compaction results in less uniform pressure and higher moments than shaped bedding.

TRENCH STUDY

One design strategy for minimizing loads attracted to a buried conduit is to place the conduit in a trench and backfill with a material less stiff than the soil forming the walls of the trench. The trench width is the variable of interest for the

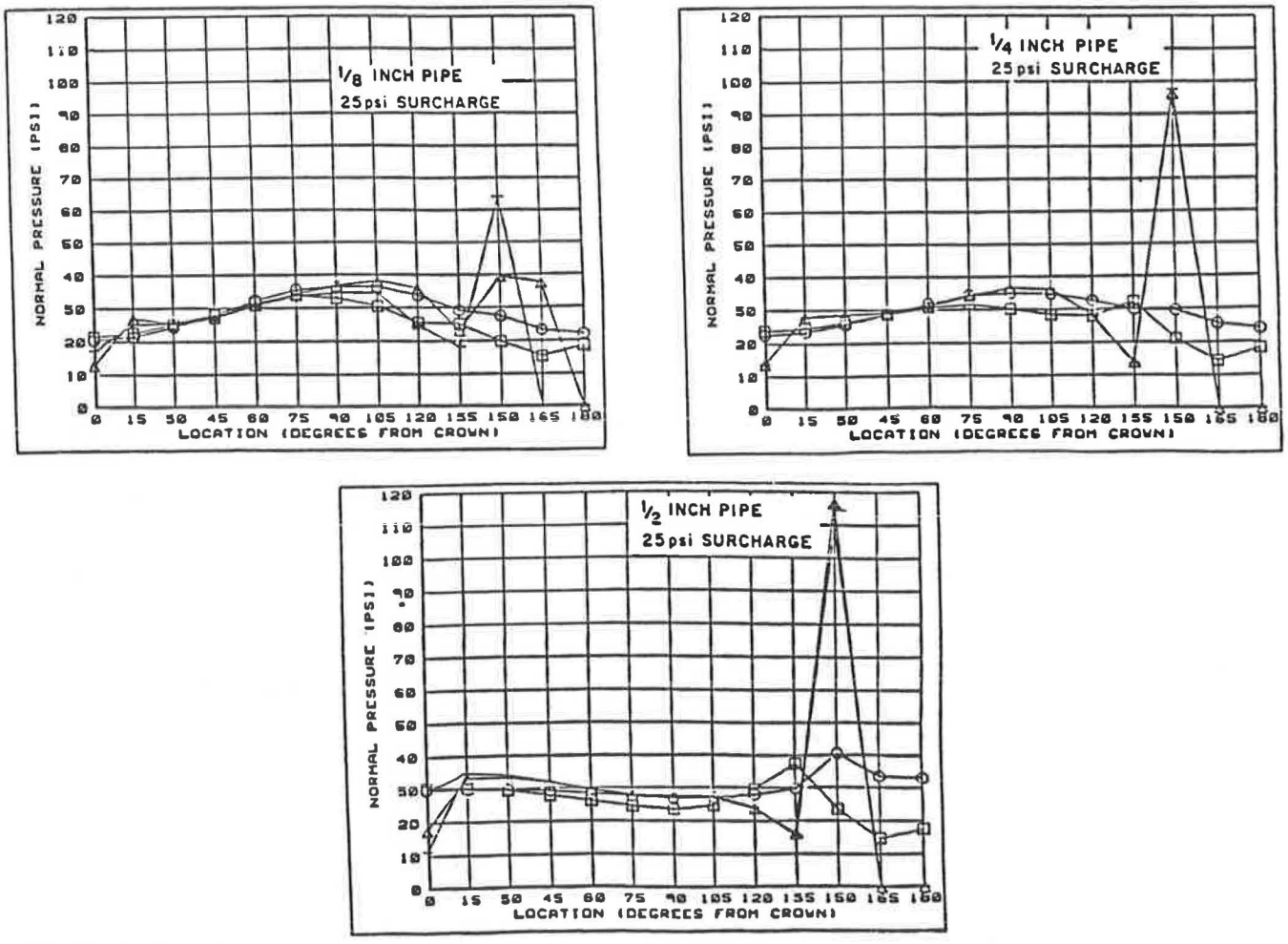

FIGURE 7 Normal pressure versus location on pipe.

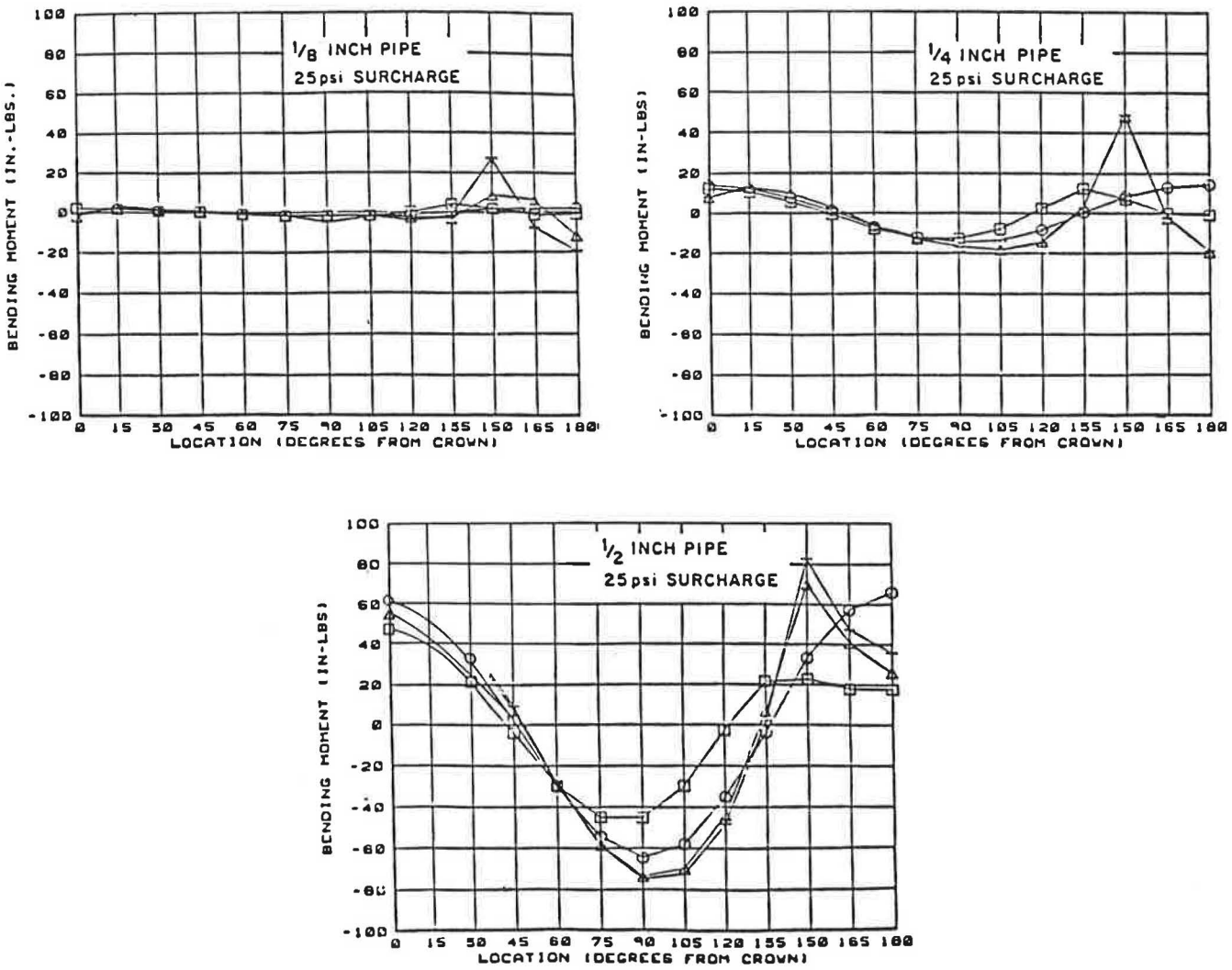

FIGURE 8 Maximum bending moment versus location on pipe.

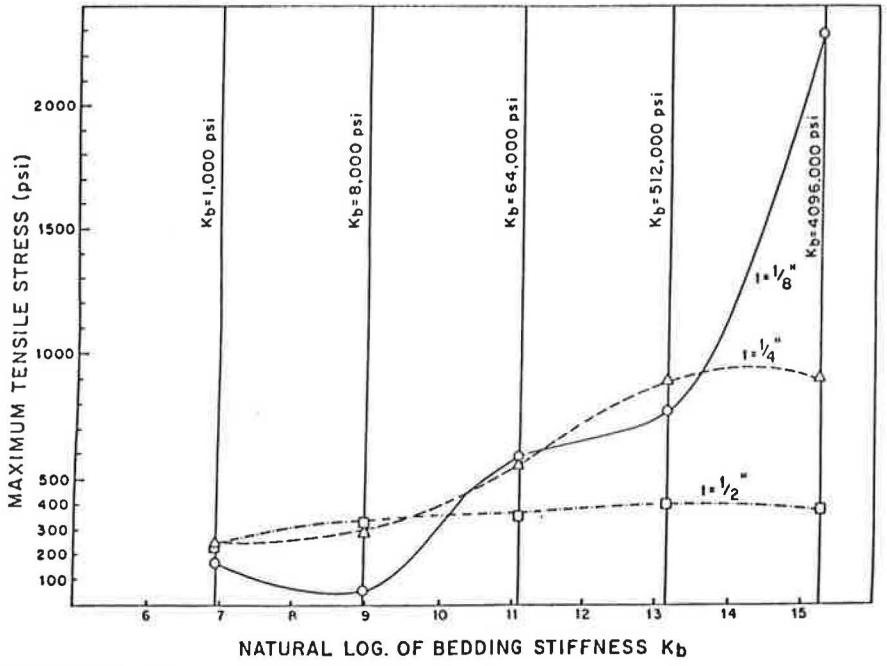

FIGURE 9 Maximum tensile stress versus bedding stiffness.

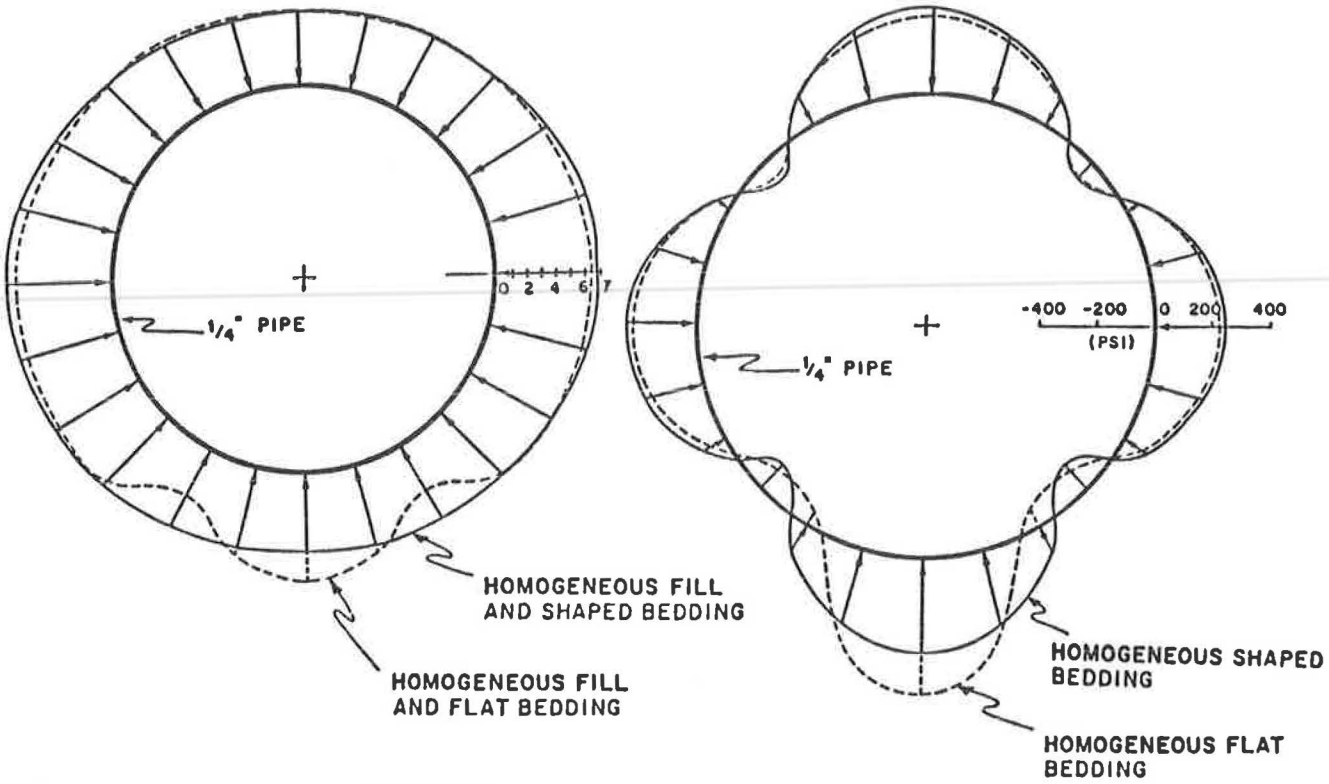

FIGURE 10 (a) Normal pressure diagram for pipe on shaped and flat beddings, and (b) Tensile stress diagram for 1/4-in. pipe on shaped and flat beddings.

studies reported herein. The support at the invert was always taken as shaped bedding with its stiffness nearly matching that of the side walls. The thickness of the pipe wall (a measure of the stiffness of the pipe) was varied. The measure of performance is the maximum tensile stress in the wall, chosen because of the brittle fracture characteristics of unreinforced concrete, and arrived at by the algebraic sum of the thrust and bending stresses. CANDE, Level 3, was the instrument of analysis with spot checks by physical testing.

The results point to the incompleteness of the notion that reducing the portion of the load attracted to the buried conduit by means of less competent trench fill is in general a preferred design. Again, as it was with the bedding study, the character (distribution) of the loading may dominate its performance. Analyses were conducted for the trench condition with one diameter (9 in.) of trench fill cover over the crown of the pipe. Pipe wall thicknesses were 1/8, 1/4, and 1/2 in. (DR = 70, 34, and 16, respectively). Trench widths were 1.25 × OD, 1.50 × OD, and 2.0 × OD, respectively. Stiffness of the trench wall, shaped bedding, and the material beyond was 5,090 psi; stiffness of the trench fill was 1,000 psi. Surcharge pressure was 5 psi. See Figures 11 and 12 for the following results and inferences.

1. The 1/8-in. pipe developed less tensile stress, both in magnitude and extent around the pipe for all conditions of trench width, than the thicker 1/4- and 1/2-in. pipes. A thinner, more compliant pipe more readily alters its geometry under load, thereby reducing load and moment.

2. The narrowest trench, 1.25 × OD, always presented the most favorable performance, independent of the wall thickness. The greater likelihood of the effective development of passive pressure in a narrow trench favors the development of a more uniform normal pressure at the soil-pipe interface. Less bending is implied.

3. The level of tensile stress was always significant enough to require tensile reinforcement.

In this study, it was not possible to get the pipe to survive the full 5 psi of surcharge load in the physical test for the noted conditions of bedding, backfill, and trench geometry. This is consistent with the analytical predictions of tensile stress on the unreinforced concrete sections.

IMPLICATIONS FOR THIN-WALL CONCRETE PIPE

The work of this study has shown that thin-wall concrete pipe can survive loadings that would unlikely ever be predicted by the usual design practice. Because thin-wall concrete pipe may be expected to fail quite early in its loading history when subjected to that test, D-load rigid-pipe theory will, most likely, not be extended to thin-wall concrete pipes.

Should thin-wall concrete pipe ever become thin enough to be judged semirigid, as is the case for some of the sections considered in this study, and for reasons previously stated, it is unlikely that the flexible pipe theories of ring compression and ring deflection will be successfully extended to include such pipes.

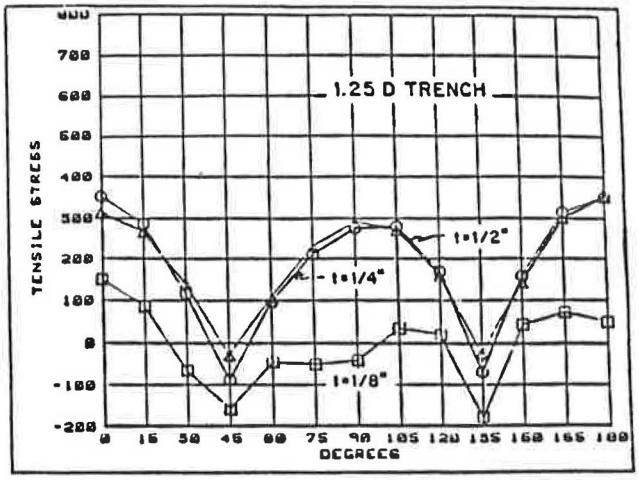

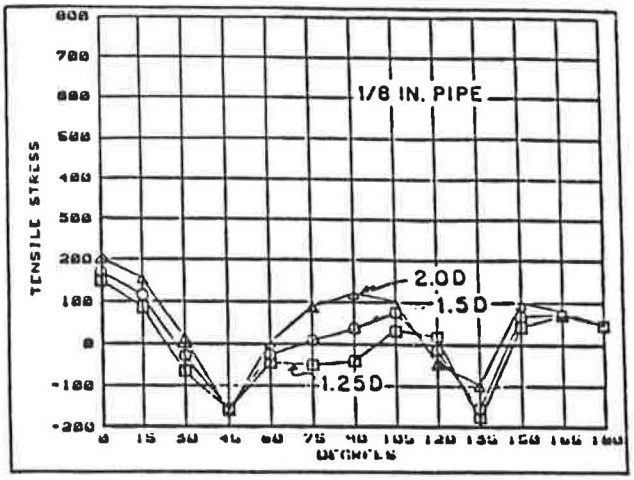

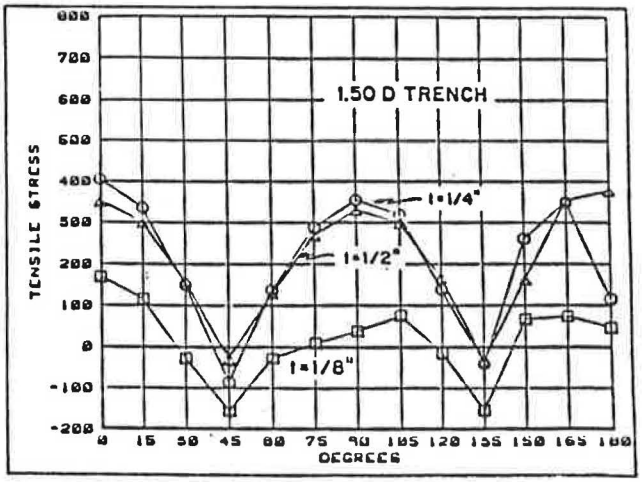

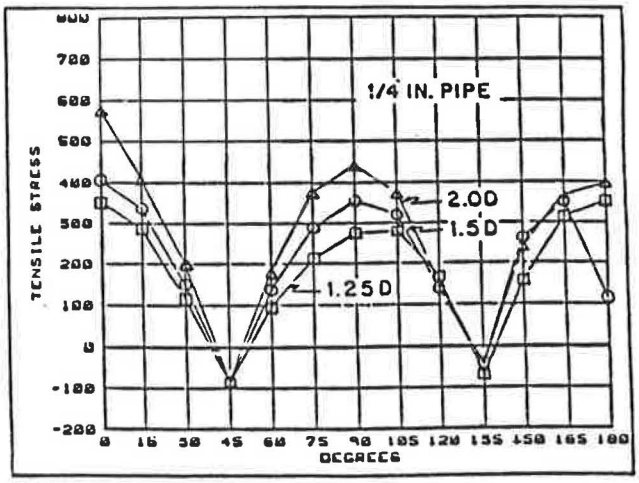

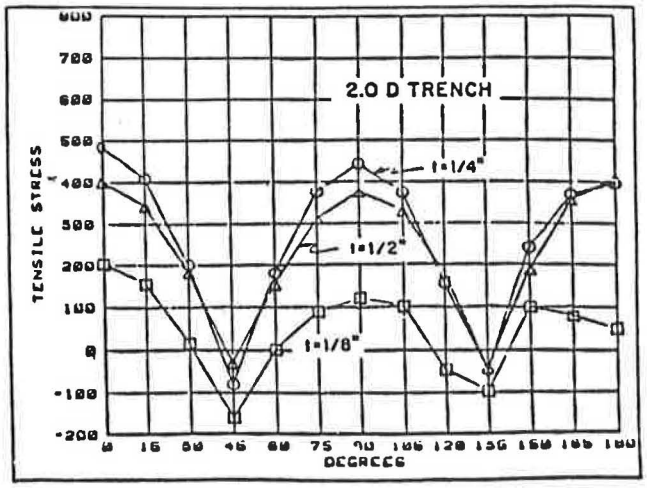

FIGURE 11 Maximum tensile stress versus location on pipe as function of trench diameter.

Note: D = Outer diameter. Surcharge = 5 psi.

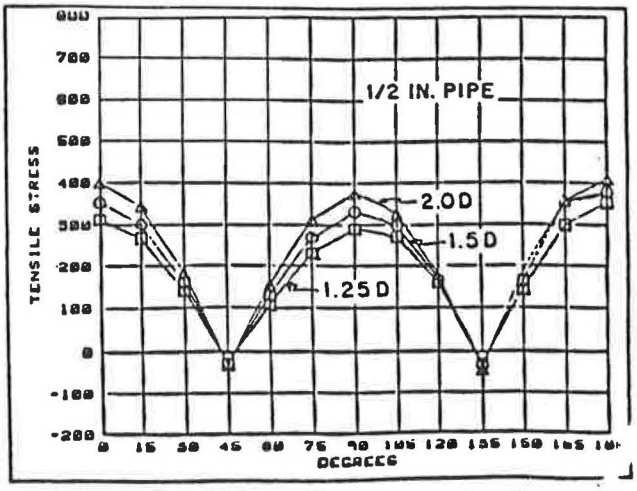

FIGURE 12 Maximum tensile stress versus location on pipe as function of pipe thickness.

Note: D = Outer diameter. Surcharge = 5 psi.

The industry and the profession await a consistent theory for semirigid pipe. In principle, this theory should be broad enough to include pipes of all materials and pipes of all stiffnesses (including both flexible and rigid) interacting with the surrounding soil matrix. The computational power to achieve this end is in place.

CONCLUSIONS AND RECOMMENDATIONS

The following apply to all concrete pipes:

1. Shaped bedding (supporting a surface of approximately $OD/2$) that is of greater stiffness than that of the surrounding soil is likely to require greater pipe strengths than shaped bedding of stiffness matching that of the surrounding soil. Such shaped-concrete beddings should be rejected for any purpose other than longitudinal support of the pipe, if required.
2. Shaped beddings more compliant than the surrounding soil offer little advantage, and possibly some disadvantage, in the performance of an embedded pipe.
3. The most favorable bedding is one that is shaped and has a stiffness approximating that of the soil envelope around the pipe. Standards ought to reflect this principle.
4. Narrow trenches, backfilled with material less stiff than the outer soil envelope, perform more efficiently than wider trenches with the same trench fill. Standards should specify a maximum trench width, compatible with reasonable construction practice, rather than a minimum trench width as is sometimes the case.

REFERENCES

1. *Determining Physical Properties of Concrete Pipe or Tile.* ASTM C497-74, 1974.
2. L. H. Gabriel and H. E. Blower. Composite Pipe-Deflection Response. International Conference on Underground Plastic Pipe, ASCE, New Orleans, La., 1981.
3. T. J. McGrath and R. E. Chambers. Field Performance of Buried Plastic Pipe. International Conference on Underground Plastic Pipe. ASCE, New Orleans, La., 1981.
4. L. H. Gabriel and H. E. Blower. *A Study of the Performance of Thin Wall Concrete Pipe.* California Department of Transportation/U.S. Department of Transportation, March 1986.
5. CANDE User Manual. Report FHWA-RD-77-6. FHWA, U.S. Department of Transportation, Oct. 1976 (updated 1980).
6. Ramaley and Henry. *Stress-Strain Curves for Concrete Strained Beyond Ultimate Load.* U.S. Bureau of Reclamation Laboratory Report, SP-12, Denver, Colo., 1947.
7. J. Q. Burns and R. M Richard. Attenuation of Stresses for Buried Cylinders. *Proc., Symposium on Soil-Structure Interaction,* University of Arizona, Tucson, 1964.
8. J. M. Duncan and Y-Y. Chang. Nonlinear Analysis of Stress and Strain in Soils. *Journal of the Soil Mechanics and Foundations Division, ASCE,* Vol. 96, No. SM5, Sept. 1970.

New Bedding Factors for Vitrified Clay Sewer Pipes

JEY K. JEYAPALAN AND NAIYI JIANG

The present bedding factors used by the clay pipe industry are dependent only on the bedding type. This practice has led to extremely conservative designs of these buried pipes and to their perceived inability to support deep covers of soil. Due to this conservative approach, clay pipe installations under deep fills were considered to be impossible and other materials have been used instead despite the many advantages clay pipe has offered for these projects. In this study, new bedding factors were predicted by the finite element analyses of buried vitrified clay pipes with four types of backfill and bedding materials. These bedding factors were calculated as the ratio of the maximum tensile strain in the computer-simulated three-edge bearing test of vitrified clay pipes to that in the finite element analyses of buried pipes. The new bedding factors are generally higher than those given in the current ASTM specifications. It is shown that the bedding factors are affected by the backfill material type and compaction density, backfill height, trench width, and pipe diameter. Design practice around the world is also summarized in this paper.

The design of buried vitrified clay pipes involves determining the maximum loads to which the vitrified clay pipes will be subjected in service and ensuring that the installed vitrified clay pipes under a certain bedding condition will provide field-supporting strength great enough to withstand the loads with a reasonable degree of safety. For vitrified clay pipes transporting sewage and other industrial effluents, the backfill loads, which were discussed in another paper (*1*) by the same authors, are usually the most important loads to be considered. The purpose of this paper is to study the field-supporting strength of buried vitrified clay pipes.

The field-supporting strength of vitrified clay pipes is influenced by many factors, such as physical properties of the vitrified clay pipes, bedding materials, depth of soil cover, trench width, degree of compaction of the trench materials, and workmanship. The physical properties of vitrified clay pipe determine its inherent strength (*2*). The bedding factor is the ratio of the field-supporting strength to the three-edge bearing test strength of the vitrified clay pipe. The three-edge strength of the pipe is measured in the test laboratory at the manufacturing plant using a statistically significant sampling technique.

Vitrified clay pipes are installed under various bedding conditions. Different bedding conditions provide varying levels of support around vitrified clay pipes and, hence, give different bedding factors. Currently used bedding conditions and their corresponding bedding factors in the United States are given in ASTM Standards (*3*), as shown in Figure 1. These bedding factors, except that for crushed stone encasement, are based on the research conducted in the early part of this century by Spangler (*4*) and Schlick (*5*). Since then, there have not been any changes in these bedding factors in the United States.

In addition, the loads used on these clay pipes in the United States are still based on the worst possible predictions by the old Marston theory. The authors calculated much lower loads in comparison to Marston loads and these results were reported recently in another paper (*1*), in which details of the finite element model used, distributions of soil pressures around the pipe for various bedding conditions, and locations of critical stresses and strains in the clay pipe wall were provided. Thus, in U.S. design practice, conservative bedding factors and Marston loads resulted in conservative designs of clay pipe installations. During these 50 years of conservative design practice, several advances have taken place in the field of soil-pipe interaction. Large-scale laboratory research on the bedding factors of vitrified clay pipes has been conducted by Bland et al. (*6*) and Sikora (*7*). The soil-pipe interaction problems have been successfully analyzed using the finite element method by Duncan et al. (*8-11*), Jeyapalan et al. (*12-17*), Katona (*18*), Krizek et al. (*19*), and Leonards (*20*). Thus, the finite element method can provide an accurate method of evaluating bedding factors for vitrified clay pipes under various bedding conditions.

The purpose of this paper is to present the bedding factors of buried vitrified clay pipes under different bedding conditions as computed by finite element analyses.

MATERIAL PROPERTIES

The properties of three different sizes of vitrified clay pipes used in the analyses are presented in Table 1 based on published data (*20*). The Young's modulus for vitrified clay pipe listed in Table 1 is based on the test results reported by Sikora (*7*).

Four types of backfill and bedding conditions were used in the analyses; two degrees of compaction level were chosen for each type, as follows:

1. Well-graded gravel compacted to 85 and 95 percent of standard AASHTO dry density (GW85 and GW95).
2. Silty sand at 80 and 95 percent (SM80 and SM95).

Wisconsin Hazardous Waste Management Center, 2304 Engineering Building, University of Wisconsin, Madison, Wis. 53706.

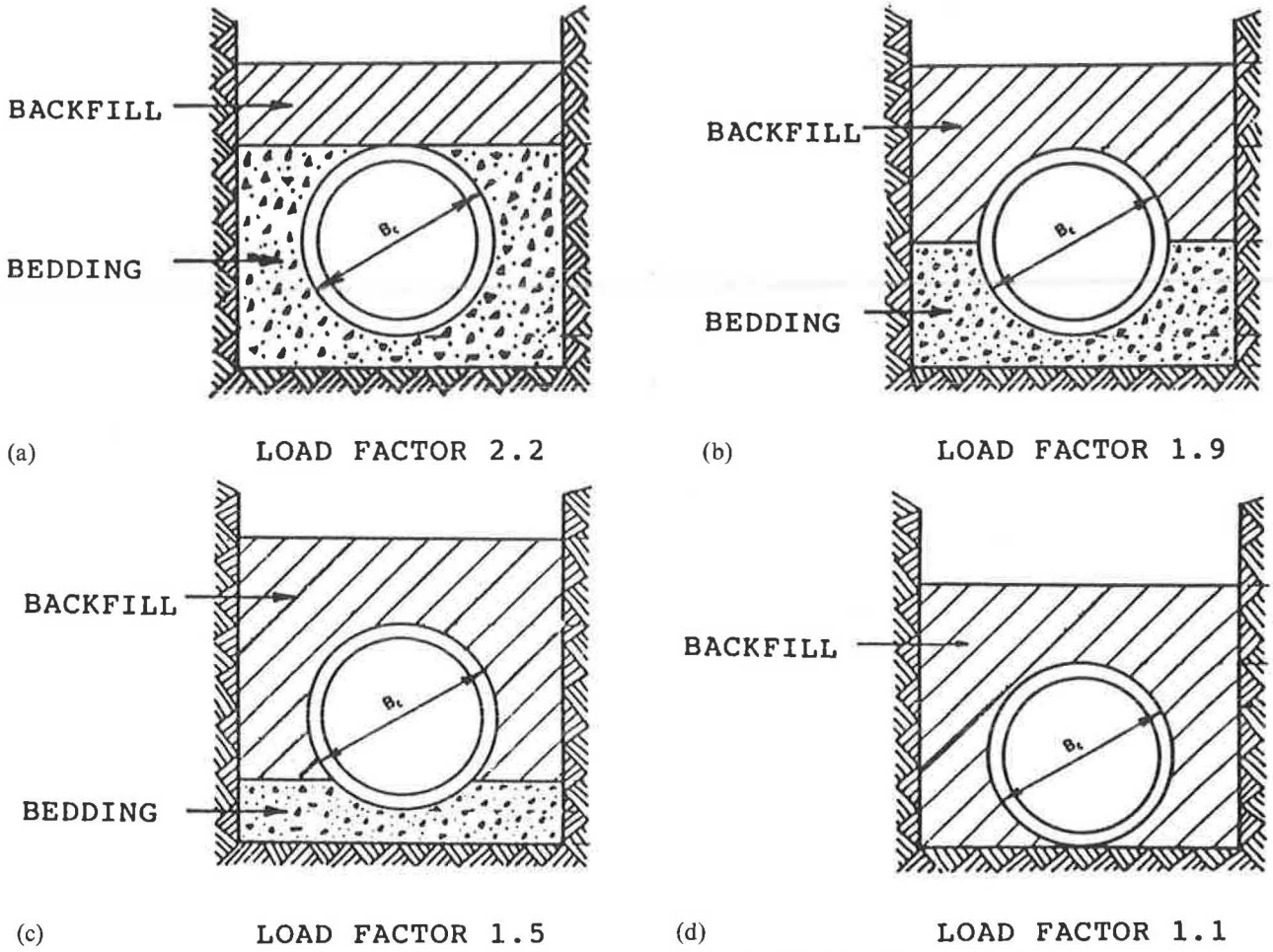

FIGURE 1 Current bedding conditions and their bedding factors for buried vitrified clay pipes: (a) Crushed stone encasement, (b) Class B, (c) Class C, and (d) Class D.

TABLE 1 PROPERTIES OF VITRIFIED CLAY PIPES USED IN ANALYSES

Pipes	Inner Diameter (in.)	Outer Diameter (in.)	Thickness (in.)	Area (ft^2/ft)	Moment of Inertia (ft^4/ft)	Young's Modulus (ksf)
6-in.	6	7.375	0.6875	0.05729	0.00001567	835,200
21-in.	21	25.5	2.25	0.1875	0.0005493	835,200
42-in.	42	51	4.5	0.3750	0.004395	835,200

3. Sand-clay-silt mixture at 80 and 95 percent (SM-SC80 and SM-SC95).
4. Low-plastic clay at 80 and 95 percent (CL80 and CL95).

Native soil used in all the analyses is low-plastic clay at 90 percent (CL90). The hyperbolic soil model parameters of soils used in the analyses are presented in Table 2.

FINITE ELEMENT ANALYSES

The interaction between the vitrified clay pipe and the surrounding soils was studied using the finite element method. The computer program used in the analyses is a plane-strain soil-pipe interaction finite element program. The hyperbolic stress-strain relationship of soils developed by Duncan et al. (*11*) was used in the program to approximate the nonlinear and stress-dependent stress-strain properties of the soils. The actual sequence of construction operation was simulated by a number of construction layers. The geometry of the trench was simulated in the analyses by using a finite width for the soil elements placed in each compaction lift. The load from the construction lift was applied in the analyses by converting the soil weight to equivalent nodal point forces.

A typical finite element mesh used in the analyses is shown in Figure 2. This mesh was used to model a 42-in. vitrified clay pipe with a backfill height of 50 ft and a trench width of 8 ft.

TABLE 2 SOIL PROPERTIES

Unified Classification	RC Standard AASHTO	γ kcf	C ksf	φ degrees	Δφ degrees	K	n	R_f	K_b	m	K_o
CW	85	0.130	0	30	2	100	0.4	0.7	25	0.2	0.5
	95	0.140	0	36	5	300	0.4	0.7	75	0.2	0.5
SM	80	0.115	0	28	1	75	0.25	0.7	50	0	0.5
	95	0.130	0	34	6	450	0.25	0.7	350	0	0.5
SM-SC	80	0.115	0.1	33	0	50	0.6	0.7	25	0.5	0.5
	95	0.130	0.4	33	0	200	0.6	0.7	100	0.5	0.5
CL	80	0.115	0.05	30	0	30	0.45	0.7	20	0.2	0.5
	95	0.130	0.3	30	0	120	0.45	0.7	110	0.2	0.5

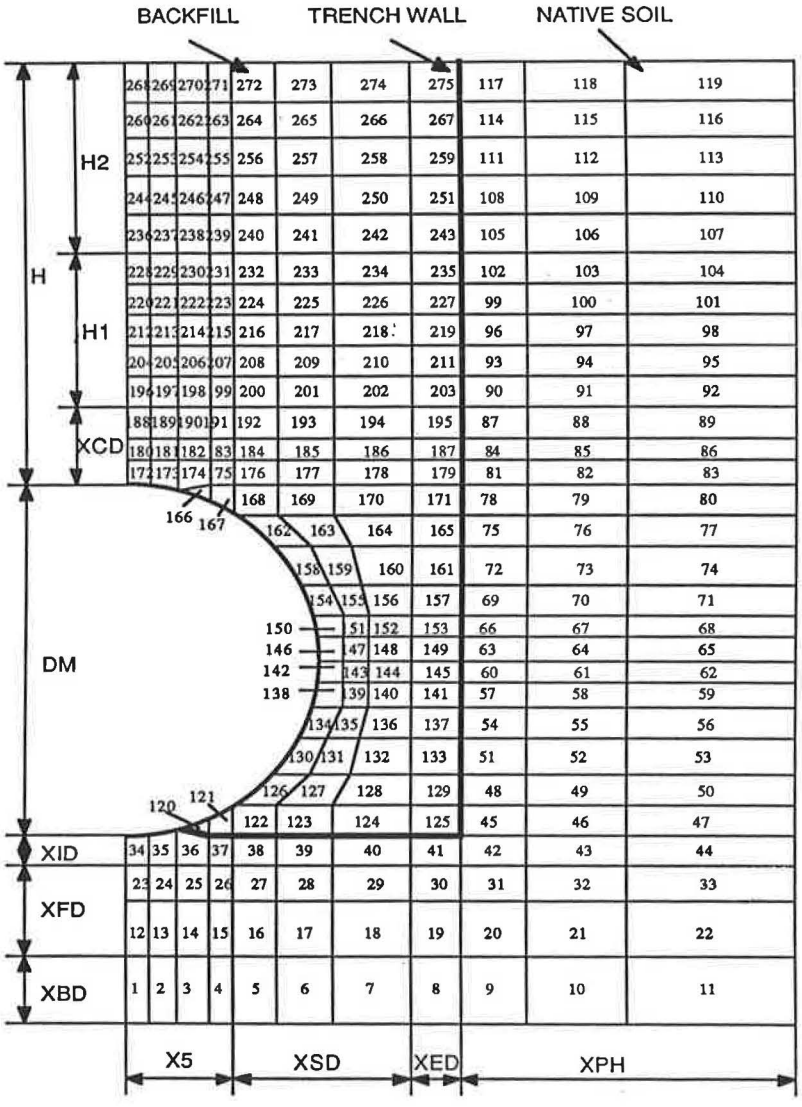

FIGURE 2 Typical finite element mesh used in analyses.

Because of the symmetry, only half of the soil-pipe system was analyzed. Half of the 42-in. vitrified clay pipe was divided into 18 circular curved beam elements and half of the soil was divided into 275 two-dimensional isoparametric soil elements with 318 nodes. To obtain sufficiently accurate results, 14 construction layers were used to simulate the actual construction sequence in the field. Similar finite element meshes were used to model 6- and 21-in. vitrified clay pipes under various installation conditions. The soil load acting on the pipe was calculated from the finite element analyses by adding up the normal and shear stress resultants acting at the centroids of the soil elements over the pipe wall. The soil load was then applied as a concentrated load to the pipe in the simulated three-edge bearing strength test where a structural analysis of the vitrified clay pipe was performed by the computer program under the simulated supporting and loading conditions of the three-edge bearing test. The bedding factor was estimated as the ratio of the maximum tensile strain in the simulated three-edge bearing test to that in the finite element analyses of the soil-pipe system. The maximum strains due to bending occurred at the crown and invert of the pipe in all cases. The ratio of the soil load causing failure in the buried pipe to that load causing failure in the three-edge load test might be a better definition of the bedding factor. Due to the fact that the clay pipe industry is committed to the definition based on strains, the authors used the maximum strains for computing the bedding factors. However, the clay pipe industry relied on comparison of strains for computing the bedding factor because strains were easier to measure than loads on the pipe in both field tests and controlled laboratory tests. Therefore, the strain ratio was selected for defining the bedding factor in the present research. It should be noted that the bedding factors calculated by both methods yield exactly the same results when the strain level is under the failure value of about 500 microstrain.

NEW BEDDING FACTORS

The bedding factors computed by comparing the maximum strains from the finite element analyses with those from the simulated ASTM-specified three-edge loading test are given in Figures 3-17. The variations of the bedding factor with backfill height for 6-, 21-, and 42-in. clay pipes are shown in Figures 3-5. The trench width used for these three figures ranges from 1.5 to 8 ft. The bedding factor depends significantly on the backfill height for the smallest diameter pipe. Even for the large-diameter pipes, the dependence on the backfill height is significant enough to consider this variable as an important parameter governing the choice of the bedding factor in clay pipe design. It is also clear from these figures that the level of compaction and the soil type play important roles in the determination of bedding factors for clay pipe installations. The ASTM-specified bedding factors vary from 1.1 to 2.2, whereas the bedding factors from the finite element analyses vary from 1.6 to 3.6 in these figures. The bedding factor, in general, increases as the backfill height increases. This is probably because the sidefill loading, which can increase the bedding factor (*7*), increases as the backfill height increases. Due to the fact that the overly celebrated Marston theory makes much of the trench width, the influence of trench width on the bedding factor was studied in great detail in this research program with typical results shown in Figures 6-14. The variations of bedding factor with trench width for three backfill heights are shown in Figures 6-8 for the 6-in. pipe. These figures show that for the small-diameter pipe, the bedding factor decreases as the trench width increases. However, this rate of decrease is somewhat independent of the backfill height but controlled by soil type and compaction density. The variations of bedding factor with trench width are shown in Figures 9-11 for three levels of soil cover depth on a 21-in. pipe. In some cases of soil type, the bedding factor increases with trench width, but in others it decreases with trench width. This inconsistency could be explained by the stiffness and the unit weight of the trench soil in comparison to those of the native soil. In the cases where the soil in the trench is heavier or is only about the same stiffness as that of the native soil, the bedding factor tends to decrease with an increase in trench width. Variations of bedding factor with trench width for three depths of cover are shown in Figures 12-14 for the 42-in. pipe. In almost all cases, the bedding factor increases with trench width. Variations of bedding factor with pipe diameter are shown in Figures 15-17 for three depths of cover. In almost all cases, the bedding factor tends to increase with diameter of the clay pipe.

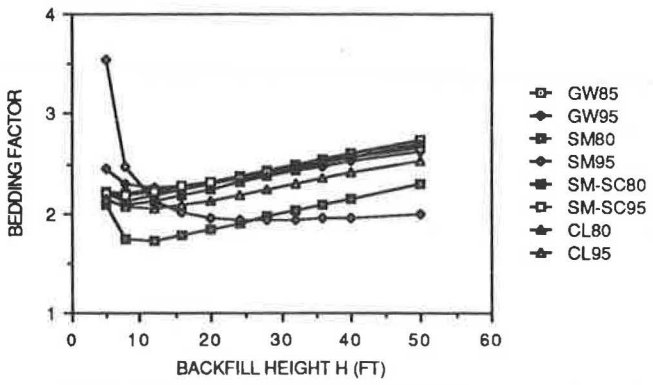

FIGURE 3 Bedding factor versus backfill height: D = 6 in. and B_d = 5 ft.

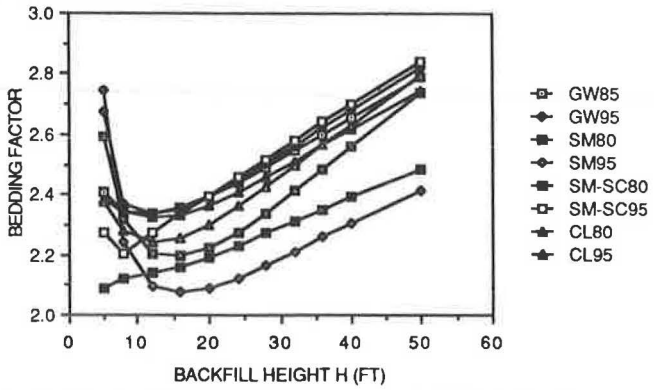

FIGURE 4 Bedding factor versus backfill height: D = 21 in. and B_d = 5 ft.

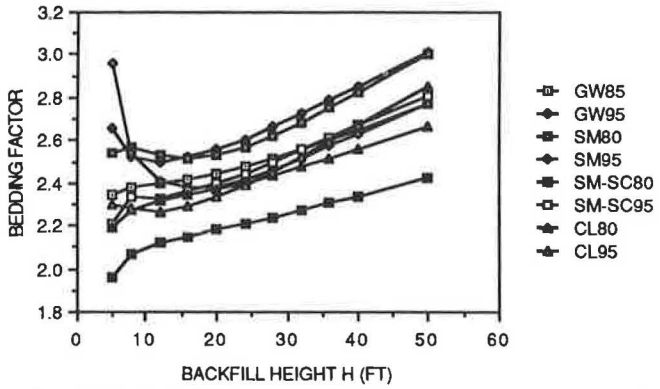

FIGURE 5 Bedding factor versus backfill height: D = 42 in. and B_d = 8 ft.

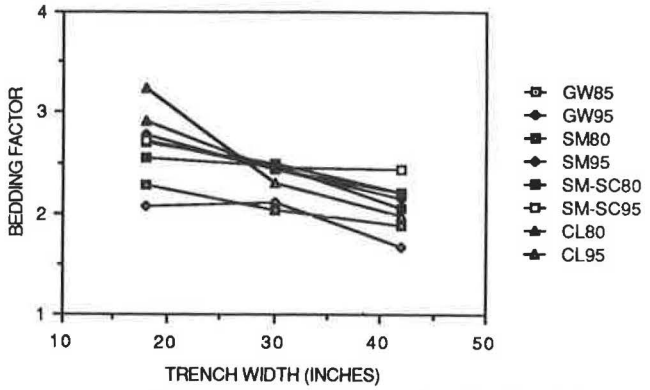

FIGURE 8 Bedding factor versus trench width: D = 6 in. and H = 32 ft.

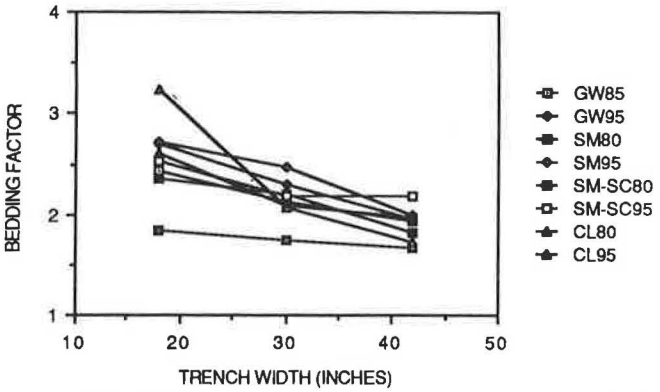

FIGURE 6 Bedding factor versus trench width: D = 6 in. and H = 8 ft.

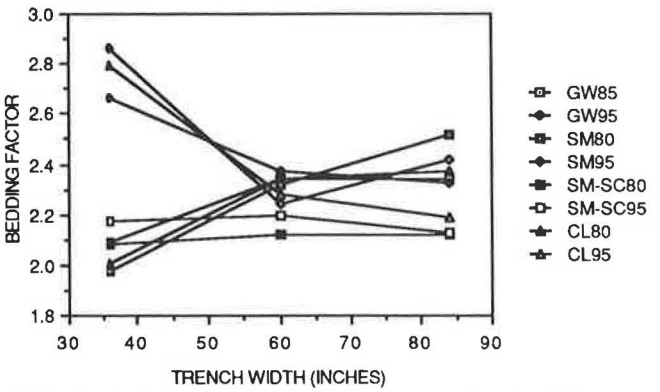

FIGURE 9 Bedding factor versus trench width: D = 21 in. and H = 8 ft.

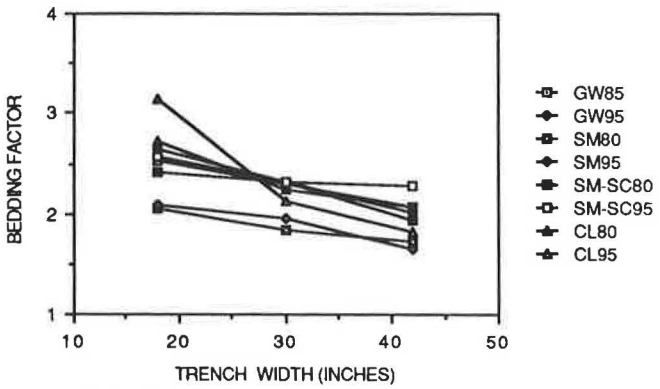

FIGURE 7 Bedding factor versus trench width: D = 6 in. and H = 20 ft.

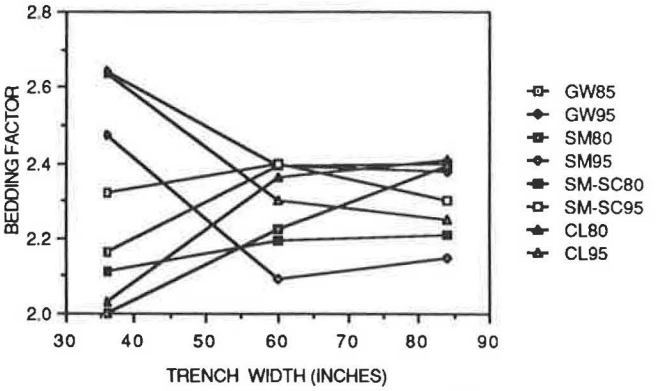

FIGURE 10 Bedding factor versus trench width: D = 21 in. and H = 20 ft.

INTERNATIONAL CLAY PIPE DESIGN PRACTICE

At the conclusion of this research program, the senior author visited a number of clay pipe design engineers and manufacturing facilities in Europe to review the procedures in effect in Europe and other countries for the design of underground clay pipes. During these visits, it was apparent that several countries had abandoned the use of Marston's load theory and its resulting conservative bedding factors. A summary of the bedding factors used by the various countries is given in Table 3. Australia is the only country using compaction density as one of the parameters controlling the choice of the bedding factor used in the design of clay pipes. In the U.S.S.R. bedding factors significantly higher than those in the United States are used. The bedding factor used in the U.S.S.R. for the weakest bedding system is 2.8, which is higher than the 2.2 used in the United States for the strongest bedding system. The loads used by the designers in the U.S.S.R. are also lower than those used in the United States. A review of safety factors used by various countries also

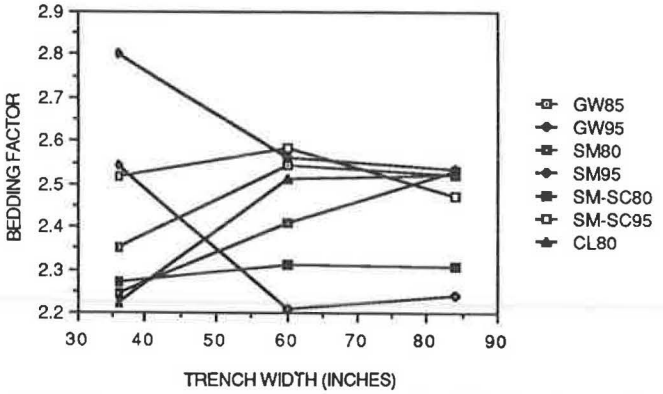

FIGURE 11 Bedding factor versus trench width: D = 21 in. and H = 32 ft.

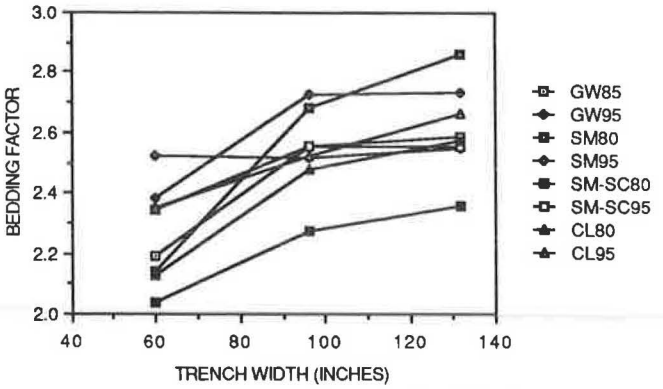

FIGURE 14 Bedding factor versus trench width: D = 32 in. and H = 32 ft.

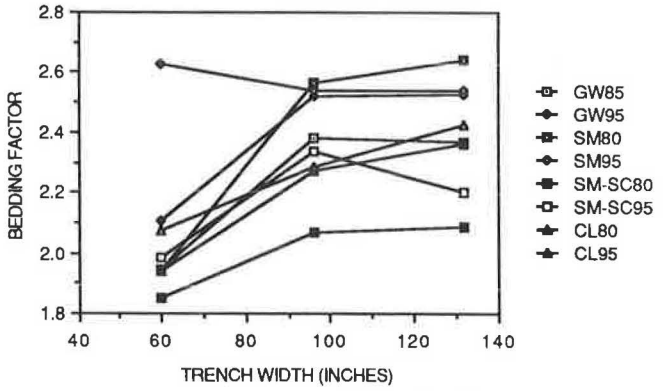

FIGURE 12 Bedding factor versus trench width: D = 42 in. and H = 8 ft.

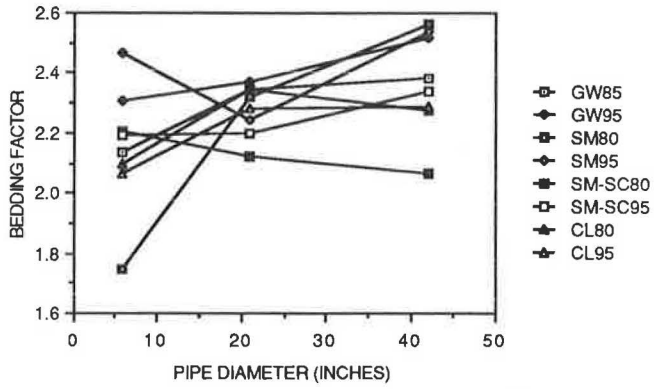

FIGURE 15 Bedding factor versus pipe diameter: H = 8 ft.

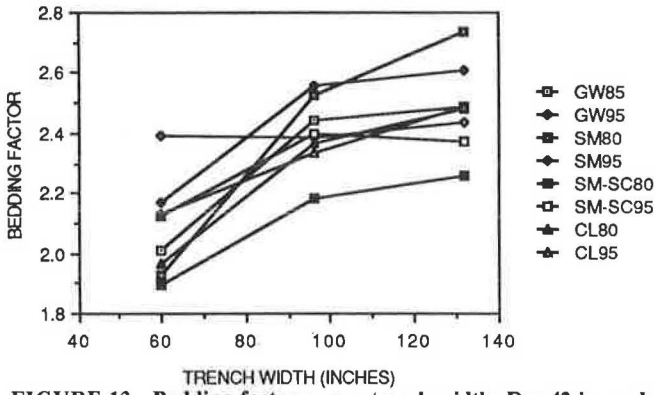

FIGURE 13 Bedding factor versus trench width: D = 42 in. and H = 20 ft.

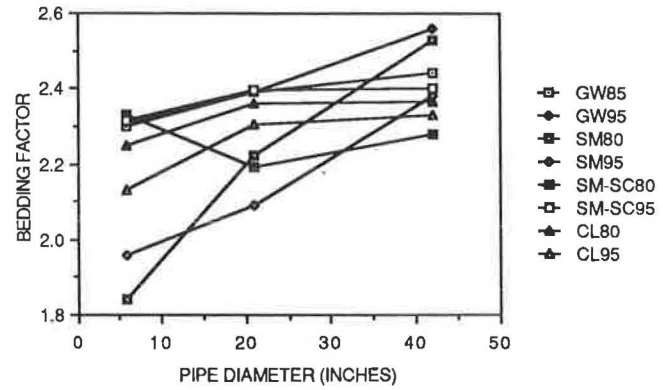

FIGURE 16 Bedding factor versus pipe diameter: H = 20 ft.

revealed some interesting information, as presented in Table 4. In Table 4, the new West German ATV rigorous design method is used as the standard in arriving at the relative margins of safety. In the United States, a factor of safety of 1.5 is used relative to the ATV rigorous method, and in the U.S.S.R., the factor of safety used is 0.9. Switzerland uses a factor of safety of 2.0, but it should be recognized that the loads used on clay pipes are only half as high as those calculated by the Marston load theory.

CONCLUSIONS

Based on the results of this research study, the following conclusions can be made:

1. The bedding factor is dependent on the type of backfill and bedding materials used. Well-graded gravel material gives the highest bedding factors, while silty sand or sand-clay-silt materials give the lowest bedding factors. The degree

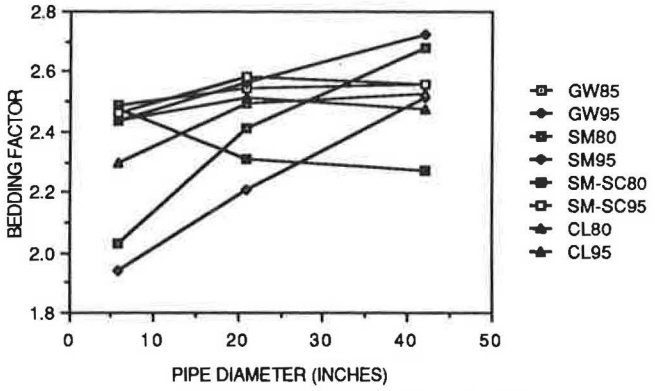

FIGURE 17 Bedding factor versus pipe diameter: H = 32 ft.

of compaction of the backfill and bedding materials is also an important parameter.

2. The bedding factor is affected by the backfill height. The bedding factor generally increases as the backfill height increases.

3. The bedding factor increases with the diameter of the pipe. The trench width also controls the magnitude of the bedding factor to be used in design.

4. The loads used for the design of clay pipes in the United States based on the Marston load theory are too high, and improved loads are given by the authors in another paper elsewhere (*1*). The loads used by several other countries around the world compare better with the loads reported by the authors than with those developed by Marston.

TABLE 3 SUMMARY OF BEDDING FACTORS USED INTERNATIONALLY

Bedding Class	U.K. (Marston load theory)	U.S. (Marston load theory)	Australia (Marston load theory)	India (Marston load theory)	Japan (France) (Marston load theory)	Switzerland (Wetzorke load theory)	W. Germany Clay pipe ind	W. Germany ATV	Russia (Emilianov load theory)	Sweden (Marston load theory)
S	2.2	2.2	/	/	2.31	1.5	/	/	3.2	/
B	1.9	1.9	2.5 - 1.9	1.9	2.03	/	/	2.18	3.1	1.88
C	/	1.5	1.9 - 1.5	1.5	1.68	/	1.5	1.59	3.0	/
D	1.1	1.1	1.1	1.1	1.08	/	/	/	2.8	/

/ Bedding not applicalbe.

TABLE 4 RELATIVE MARGIN OF SAFETY FOR VARIOUS DESIGN PROCEDURES

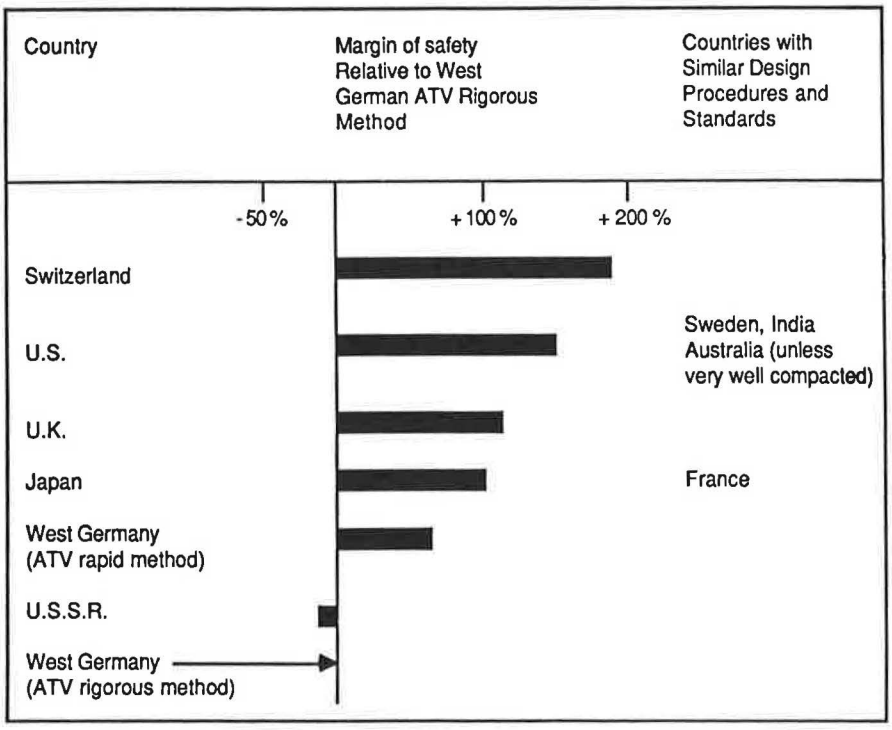

5. The factor of safety used in U.S. practice is also high, particularly when the low bedding factors in effect are taken into consideration. Thus, use of higher bedding factors, lower factors of safety, or lower loads on these vitrified clay pipes are more appropriate. These procedures would enable pipe design engineers to use materials more efficiently while the United States is undergoing a major infrastructure rehabilitation program in many of its oldest cities.
6. Based on the available information, it appears that a bedding factor of 3.5 for crushed stone encasement and 2.5 for Class D beddings could be used when the loads calculated for the pipe are based on Marston theory.
7. Although the research and conclusions thereof are for vitrified clay pipes, the results would also be applicable for concrete pipes with some minor modifications.

ACKNOWLEDGMENTS

The results reported in this paper were obtained as part of an ongoing research program on vitrified clay pipes funded by the National Clay Pipe Institute at the University of Wisconsin, Madison. A major field observation program is being planned at the time of writing this paper to verify the results of the finite element analyses. In this field test program, a series of strain-gauged vitrified clay pipes will be monitored at actual installations under varying backfill and load conditions, and the results will be compared with those obtained from the finite element analyses. The results of this field test program will be reported in another paper at a later date. The technical assistance provided by Edward Sikora and Howard Lund is greatly appreciated. Audrey Miller typed the manuscript.

REFERENCES

1. J. K. Jeyapalan and N. Jiang. Load Reduction Factors for Buried Clay Pipes. *Journal of Transportation Engineering, ASCE*, Vol. 112, No. 3, May 1986, pp. 236-249.
2. *Standard Methods of Testing Vitrified Clay Pipe*. Annual Book of ASTM Standards, Vol. 4.05, Philadelphia, Pa., 1983.
3. *Standard Practice for Installing Vitrified Clay Pipe Lines*. Annual Book of ASTM Standards, Vol. 4.05, Philadelphia, Pa., 1983.
4. M. G. Spangler. *The Supporting Strength of Rigid Pipe Culverts*. Bulletin 112, Iowa State College, 1933.
5. W. J. Schlick. *Supporting Strength of Cast Iron Pipe for Water and Gas Service*. Bulletin 146. Iowa Engineering Experimental Station, 1940.
6. C. E. G. Bland and K. J. Sheppard. Investigation into the Structural Performance of Clay Pipes. *Proc., International Conference on Advances in Underground Pipeline Engineering*, University of Wisconsin, Madison, Aug. 1985, 610 pp.
7. E. J. Sikora. Load Factors and Non-Destructive Testing of Clay Pipes. *Journal of Water Pollution Control Federation*, Vol. 52, No. 12, Dec. 1980.
8. J. M. Duncan. Behavior and Design of Long Span Metal Culverts. *Journal of the Geotechnical Engineering Division, ASCE*, Vol. 105, No. GT3, 1977, pp. 399-418.
9. J. M. Duncan and J. K. Jeyapalan. *Design Studies for Kaiser Aluminum Elliptical Culvert Structures Pinson Mounds, Jackson, Tennessee*. Preprint for the State of Tennessee Department of Transportation, 1979.
10. J. M. Duncan and J. K. Jeyapalan. Deflection of Flexible Culverts Due to Backfill Compaction. In *Transportation Research Record 878*, TRB, National Research Council, Washington, D.C., Dec. 1982, pp. 10-17.
11. J. M. Duncan, P. M. Byrne, K. S. Wong, and P. N. Mabry. *Hyperbolic Volume Change Parameters for Nonlinear Finite Element Analysis of Stresses and Movements in Soil Masses*. Geotechnical Engineering Report, University of California, Berkeley, 1978.
12. J. K. Jeyapalan. Geofabric Stabilization of Soft Backfill Materials for Plastic Sewer Pipe Installation. *Proc., International Conference on Pipeline in Adverse Environments II*, San Diego, Calif., 1983.
13. J. K. Jeyapalan and A. M. Abdelmagid. Significance of Pipe-Soil Stiffness Ratio in Flexible Pipe Design. Paper presented at the California Water Pollution Control Association Annual Meeting, Palo Alto, May 3 and 4, 1984.
14. J. K. Jeyapalan and A. M. Abdelmagid. Analysis and Design of Large Diameter Plastic Sewer Pipes. Paper presented at the 1984 ASCE Spring Convention, Atlanta, Ga., 1984.
15. J. K. Jeyapalan and B. A. Boldon. Performance and Selection of Rigid and Flexible Pipes. *Journal of Transportation Engineering, ASCE*, Vol. 112, No. 5, Sept. 1986, pp. 507-524.
16. J. K. Jeyapalan, F. Oseguedu, and W. J. Horn. *Soil-Structure Interaction Analyses of Plastic Pipes*. ASCE Convention and Exhibit, Preprint 82-511, New Orleans, La., Oct. 1982.
17. M. G. Katona, J. M. Smith, R. J. Odello, and J. R. Allgood. *CANDE: Engineering Manual—A Modern Approach to the Structural Design and Analysis of Buried Culverts*. FHWA, U.S. Department of Transportation, Civil Engineering Laboratory, Port Hueneme, Calif., 1976.
18. R. J. Krizek and P. V. McQuade. Behavior of Buried Concrete Pipes. *Journal of the Geotechnical Engineering Division, ASCE*, Vol. 104, No. GT7, July 1978, pp. 815-836.
19. G. A. Leonards, C. H. Juang, T. H. Wu, and R. E. Stetkar. Predicting Performance of Buried Metal Conduits. In *Transportation Research Record 1008*, TRB, National Research Council, Washington, D.C., 1985, pp. 42-52.
20. *Vitrified Clay Pipe Engineer's Handbook*. Southern Clay Pipe Institute, Atlanta, Ga., 1960.
21. *Clay Pipe Engineering Manual*. National Clay Pipe Institute, Washington, D.C., 1982.

APPENDIX

Notations

The following symbols are used in this paper:

B_c = outer diameter of vitrified clay pipes,
B_d = horizontal width of trench at top of vitrified clay pipes,
D = inner diameter of vitrified clay pipes,
H = backfill height,
K_b = bulk modulus number,
K_o = coefficient of earth pressure at rest,
m = bulk modulus exponent,
n = modulus exponent,
R_f = failure ratio,
γ = unit weight of backfill materials,
$\Delta\phi$ = friction angle parameter, and
ϕ = friction angle.

Design of Buried Culverts With Stress-Relieving Joints

MICHAEL G. KATONA AND ADEL Y. AKL

Circumferentially slotted bolt hole connections, a new concept for corrugated metal culverts, have proven to be effective in reducing thrust stress (ring compression) in deep embankment installations. Pragmatically, this means that slotted-joint culverts can be buried deeper than standard-joint culverts, or lighter-gauge metal can be used. However, because of the present lack of design tables and guidelines, this economical innovation has far from reached its full application potential. In an attempt to fill this need, a complete design methodology employing an experimentally verified culvert-joint-soil system model with analytical solutions along with a set of realistic design criteria is offered in this paper. The design methodology is used to generate a sequence of design tables for 6- × 2-in. corrugated steel pipes with slotted joints, in which the tables specify the maximum allowable fill height cover as a function of pipe diameter, wall thickness (gauge), and soil stiffness. Even though the design methodology is conservative, the slotted-joint pipes can, in some cases, sustain fill heights more than twice those of standard pipes if good-structural-quality soil is used. On the other hand, when poor-quality soil is used, the slotted-joint pipes do not provide a gain in allowable fill height.

The purpose of slotted bolt hole connections for corrugated metal culvert installations is to relieve the thrust stress and, thereby, achieve a deeper allowable burial depth, or alternatively reduce the required wall thickness. Said another way, by removing little bits of metal next to the bolt holes, the design capacity of the culvert is significantly improved. Quite remarkable, is it not?

The concept is simple. Rather than attempting to bolt corrugated structural plate segments into a continuous unit, the bolt holes are slotted in the circumferential direction to permit relative circumferential contraction of the plates (i.e., after the thrust force exceeds a predetermined frictional bolt-clamping resistance). As the culvert circumferentially contracts from joint slippage, the surrounding soil envelope is forced into a compression arch that in turn carries a greater portion of additional soil loading (i.e., positive soil arching). When all joint slippage is complete, the culvert again acts as a continuous unit so that further overburden loading will be carried by both the structure and the soil arch. Ultimate failure in thrust typically occurs by seam failure, that is, bearing failure, but at a burial depth significantly greater than a standard culvert without slotted joints.

In a recent paper (*1*), results of a comprehensive research program sponsored by the FHWA (*2*) on the analysis and behavior of buried culverts with slotted joints were discussed. Developments included instrumented field data from functional and experimental installations, laboratory data on load-deformation behavior of slotted joints, analytical model developments for slotted joints and incorporation into soil-structure analysis, parametric studies, and comparison of analytical predictions with experimental results. The major conclusion, supported experimentally and analytically, is that the slotted-joint concept really works; for example, fill height gains or increased burial depths on the order of 50 ft were achieved.

In this paper, attention is devoted to design considerations. The objective is to provide a set of design tables similar to the AISI Handbook, listing the maximum allowable fill height for 6- × 2-in. corrugated steel pipes with slotted joints and, for comparative purposes, with standard joints as well. Such design tables are needed before widespread application of this cost-saving concept can realize its full potential. In the following sections, a review of slotted-joint behavior and modeling assumptions is followed by the analytical treatment of the complete pipe-joint-soil system, and finally the design methodology (coupling the analysis procedure with the design criterion) that leads to the design tables.

SLOTTED-JOINT BEHAVIOR AND MODELING

Attention is focussed on the so-called "keyhole" slot configuration shown in Figure 1. In practice, the keyhold shapes are punched into mating pairs of 6- × 2-in. corrugated structural plate segments and lap-joined in the field with 3/4-in. bolts torqued to 200 ft-lb. Each joint, so formed, has a net slot travel length of 1 in., that is, a 1/2-in. contribution for each keyhole slot.

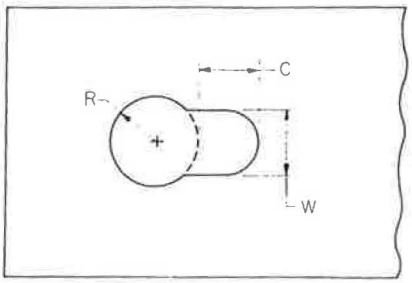

R = Bolt Hole Radius (7/16 in)
C = Key-Slot Length (1/2 in)
W = Slot Width (5/8 in)

FIGURE 1 Standard keyhole slot dimensions.

M. G. Katona, TRW Defense Systems Group, P.O. Box 1310, San Bernardino, Calif. 92402. A. Y. Akl, Structural Engineering Department, Cairo University, Cairo, Egypt.

Experimental Observations

Highlighted in the following are some observations and findings obtained from a comprehensive laboratory investigation on the load and deformation behavior of slotted-joint test specimens loaded in axial compression with and without load eccentricity (*2*). The typical nature of the load-deformation effect is shown in Figure 2. The response is characterized by four piecewise-linear zones of behavior: the elastic zone (stiff) represents the initial elastic response prior to joint slippage; the slipping zone (soft) begins when the axial load overcomes the bolt clamping resistance and continues until the slots are closed; the postslipping zone (stiff) begins at joint closure, that is, when the bolt shank comes into contact with the ends of the slots, and continues to maximum load; and, the failure zone (flat) exhibits plastic-like deformation until ultimate metal bearing failure is reached.

Although physical factors such as slot width, slot length, surface treatment, bolt torque, and so forth influence the size, slope, and magnitude of each response zone, the basic piecewise linear approximation remains valid. For the standard keyhole slot configuration, this piecewise description will be subsequently quantified in terms of a stress-strain model simulating slotted-joint behavior. The experimental results revealed that eccentric loading did not influence the load-deformation response; in other words, only thrust load, not the applied moment, influences the joint response. These findings are inherent in the following slotted-joint model.

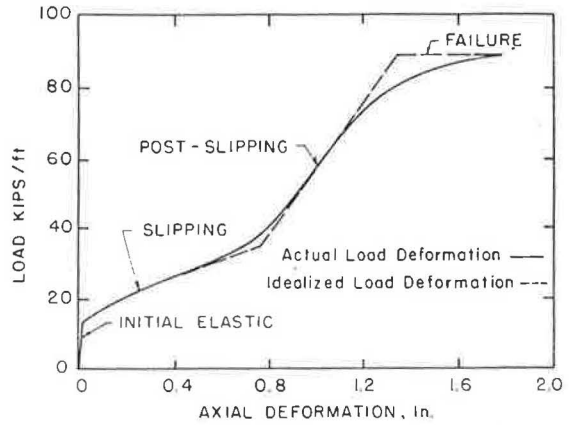

FIGURE 2 Typical load-deformation response of a slotted-joint test specimen in axial compression.

Stress-Strain Model

Figure 3 shows the five-parameter stress-strain idealization of slotted-joint behavior characterized by three tangent moduli values E_e, E_s, and E_p representing elastic, slipping, and postslipping zones, respectively, and two stress measures σ_e and σ_f representing the elastic limit or initial slipping stress and failure stress, respectively. Of course, this model is not a classical description of stress and strain. Rather, the parameters are artificial measures of stress and strain that provide a convenient way to unify the experimental data and to facilitate model development using the following definitions.

Joint stress is defined by the thrust (axial load) divided by the cross-sectional area of one corrugated plate. Joint strain is defined as the change in joint length divided by the joint length, where joint length is defined as the net slot length per joint (e.g., 1 in. for standard keyhole slots). By this definition, the joint strain at the end of the slipping zone is unity.

With regard to the load-deformation experiments, the definition of joint strain is important because it eliminates the influence of the length of the test specimen that contains the joint length as a subcomponent. By decomposing the overall specimen deformation into joint and nonjoint contributions, the response of the joint can be isolated to get the stress-strain response of the joint and hence model parameters E_e, E_s, E_p, σ_e, and σ_f.

To summarize, the slotted-joint stress-strain model is a piecewise linear relationship, incrementally defined by

$$\Delta\sigma = E_j \Delta\varepsilon_j \tag{1}$$

where $\Delta\sigma$ is an increment of thrust stress, $\Delta\varepsilon_j$ is a corresponding increment of joint strain, and E_j is the current joint modulus dependent on the zone of loading. That is, E_j is defined in four loading zones by the conditions

$$E_j = \begin{cases} E_e = & \text{initial elastic modulus when } 0 \le \varepsilon_j < \varepsilon_e; \\ E_s = & \text{slipping modulus when } \varepsilon_e \le \varepsilon_j < \varepsilon_s; \\ E_p = & \text{postslipping modulus when } \varepsilon_s \le \varepsilon_j < \varepsilon_p; \text{ and} \\ E_f = & 0 \text{ (failure zone) when } \varepsilon_p \le \varepsilon_j; \end{cases} \tag{2}$$

where the zone strain limits are inherently determined by the five model parameters. Because this paper is concerned only with monotonic loading, unloading characteristics are not addressed.

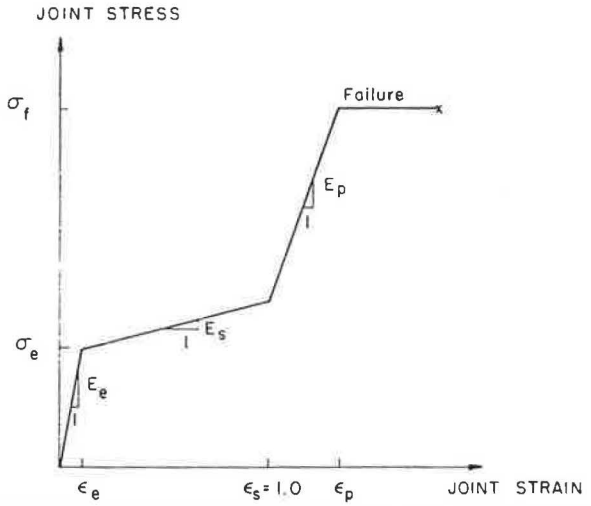

FIGURE 3 Five-parameter, pseudo stress-strain model for slotted joints.

For standard keyhole slot configurations punched in 6- × 2-in. corrugated steel plates with galvanized coating and joined with four 3/4-in. bolts per foot of seam length each torqued to 200 ft-lb, the recommended model parameters are $E_e = 30 \times 10^6$ psi, $E_s = 9{,}000$ psi, $E_p = 15 \times 10^6$ psi, $\sigma_e = 5{,}000$ psi, and $\sigma_f = 33{,}000$ psi. Note that the initial elastic modulus E_e is identical to the modulus of structural steel, and the joint failure stress is identical to the yield stress of structural steel. These recommended parameter values are

applicable to all standard wall thicknesses (gauges) and are in conformance with experimental results with some degree of conservatism employed.

SOIL-STRUCTURE ANALYSIS

In a previous paper (*1*), two solution methods for soil-culvert systems incorporating the slotted-joint stress-strain model were presented; an incremental elasticity solution based on extending the work of Burns (*3*), and a general finite element procedure using the CANDE program (*4, 5*). Both methods assume plane-strain geometry; however, the finite element approach offers a much wider scope of modeling flexibility (e.g., nonlinear soil models and arbitrary shapes) and its predictive capabilities allowed matching of experimental field data for both slotted-joint and standard-joint installations.

Although the incremental elasticity solution is more limited in scope, it was in surprisingly good agreement with the finite element solution for idealized soil-structure models with and without slotted joints. Further, by appropriate choice of elastic soil properties, the incremental elasticity solution reasonably and conservatively approximated nonlinear finite element solutions using hyperbolic soil models. Based on these studies, it was concluded that the incremental elasticity solution could be used to conservatively design circular pipes with (or without) slotted joints in deep, homogeneous embankment installations.

With this understanding and motivation, the development and assumptions of the incremental elasticity solution are briefly reviewed in preparation for the design methodology.

Incremental Elasticity Solution

Burns's theory as originally presented (*3*) provides an exact solution for an elastic, circular pipe encased in an isotropic, homogeneous, infinite, elastic material (soil) with a uniformly distributed overburden pressure acting on a horizontal plane far above the pipe. Thin-shell theory is assumed for the pipe and continuum elastic theory is used for the surrounding soil. Two solutions are offered depending on the pipe-soil interface assumption—completely bounded or frictionless.

Table 1 presents Burns's solutions for the key responses of the pipe for both interface assumptions. However, the solutions are cast in a different notation from that originally

TABLE 1 ELASTICITY SOLUTION EQUATIONS FOR PRESSURES ON PIPE RESPONSES FOR BONDED AND FRICTIONLESS INTERFACES

Structural Response of pipe 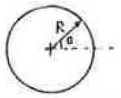	Common Factor	Bonded Interface $A^* = (1+K) + 3(5-K)\beta + (3+K)\alpha + 12(3-K)\alpha\beta$	Frictionless Interface $A^* = (1+K) + 3(5-K)\beta$
Radial Presure on Pipe P_r	P_0	$\alpha/(1+\alpha) - \{(1-K)(-2\alpha+18\beta+24\alpha\beta)/A^*\}\cos 2\theta$	$\alpha/(1+\alpha) - \{18(1-K)\beta/A^*\}\cos 2\theta$
Tang. Pressure on Pipe P_θ	P_0	$\{(1-K)(4\alpha+21\alpha\beta)/A^*\}\sin 2\theta$	0.0
Radial Disp. of Pipe w	$P_0 \frac{R(1-K)}{2G}$	$1/((1-K)(1+\alpha)) - \{(2+4\alpha)/A^*\}\cos 2\theta$	$1/((1-K)(1+\alpha)) - \{2/A^*\}\cos 2\theta$
Tang. Disp. of Pipe v	$P_0 \frac{R(1-K)}{2G}$	$\{(2+2\alpha+6\beta)/A^*\}\sin 2\theta$	$\{1/A^*\}\sin 2\theta$
Moment in Pipe Wall M	$P_0 R^2$	$\beta/(1+\alpha) + \{(6\beta(1-K)+12\alpha\beta(1-K))/A^*\}\cos 2\theta$	$\beta/(1+\alpha) + \{6(1-K)\beta/A^*\}\cos 2\theta$
Thrust in Pipe Wall N	$P_0 R$	$\alpha/(1+\alpha) + \{(1-K)(2\alpha+6\beta+24\alpha\beta)/A^*\}\cos 2\theta$	$\alpha/(1+\alpha) + \{6(1-K)\beta/A^*\}\cos 2\theta$
Shear Resultant in Pipe Q	$P_0 R$	$\{(1-K)(-12\beta-24\alpha\beta)/A^*\}\sin 2\theta$	$\{-12(1-K)\beta/A^*\}\sin 2\theta$

(a) soil lateral pressure coeff. is related to Poisson ratio by $K = \nu_S/(1-\nu_S)$

(b) plane-strain modulus of pipe, $E = E_{steel}/(1-\nu^2)$

NOTE: Definitions are as follows:

Soil Properties

- G = shear modulus
- K = lateral pressure coeff. (a)
- P_0 = overburden pressure

Pipe Properties

- E = plane-strain Young's modulus (b)
- I = moment of inertia
- A = thrust area
- R = average radius

Dimensionless Parameters

- α = $EA/2GR$
- β = $EI/2GR^3$

presented by Burns. Two dimensionless parameters α and β are defined as follows:

α = $EA/2GR$, the relative circumferential stiffness, and (3)

β = $EI/2GR^3$, the relative flexural stiffness. (4)

Here, α is the ratio of the pipe's circumferential stiffness EA to a corresponding measure $2GR$ of circumferential soil stiffness, where G is the soil shear modulus and R is the pipe radius. Similarly, β is a ratio of the pipe's flexural stiffness EI to a measure $2GR^3$ of flexural soil stiffness. For typical pipe-soil systems without slotted joints, $\alpha >> 1$, and $\beta << 1$. In other words, circumferential stiffness is dominated by the pipe, and flexural stiffness is dominated by the soil. To illustrate the use of Table 1, the average thrust force occurs at $\theta = 45°$, and its value is $N = P_0R\alpha/(1 + \alpha)$, for either set of interface conditions. Only the parameter α is influenced by joint behavior, and during joint slippage $\alpha << 1$, thereby reducing the thrust force.

In adapting the elasticity solutions to simulate slotted-joint behavior, the equations are applied in an incremental fashion to accommodate changes in the circumferential stiffness E^*A, as overburden pressure increases. E^*A, which is a smeared average of the elastic pipe wall and all slotted joints, has four possible values corresponding to the four zones of slotted-joint behavior. Initially, E^* is the elastic steel modulus E_e. When the average thrust stress exceeds σ_e (the initial slipping stress), E^* is reduced to represent joint slipping (shown subsequently); this value is retained until the total circumferential contraction of the pipe is equal to the sum of all slot lengths. Upon further loading, E^* is increased to represent postslipping until the average thrust stress reaches σ_f (joint failure), after which the incremental modulus is zero.

In developing the expression for E^*, use is made of the geometric ratio

$$J_r = C_{max}/2\pi R \quad (5)$$

where C_{max} is the sum of all slot lengths. Thus, J_r is the fraction of the pipe circumference containing slots. E^* is given by

$$E^* = E_j/[(1 - J_r)(E_j/E_e) + J_r] \quad (6)$$

where E_j is the load-dependent joint modulus of Equation 2 and E_e is the elastic steel modulus. (If $E_j = E_e$ or $J_r = 0$, $E^* = E_e$.)

The derivation of Equation 6 is based on the smeared-joint approximation. That is, any differential segments of the pipe circumference are assumed to be composed of two subparts, a joint portion $s_j = J_r s$ and an elastic, pipe-wall portion $s_e = (1 - J_r)s$. By taking the modulus of the joint portion as E_j and of the elastic portion as E_e, the net effective modulus E^* for the differential segment can be determined as given by Equation 6.

Summarizing, increments of overburden pressure are prescribed, and incremental responses (e.g., thrusts, moments, and displacements) are computed from Table 1 using the current value of E^* to define α (β remains constant). The incremental responses are summed into running totals to give the net response values throughout the loading schedule.

The bonded and frictionless interface conditions represent two extreme cases for the coefficient of friction at the pipe-soil interface $\mu = \infty$ and 0, respectively. By comparison with finite element solutions, it was found that an intermediate friction coefficient $\mu = 0.3$ (considered to be a realistic value) could be simulated by taking a weighted average of the bonded and frictionless solutions. Specifically, the weighted solutions are formed by adding w times the bonded solutions to $(1 - w)$ times the frictionless solutions, where $w = 0.7$ was found to be the proper weight to simulate a friction coefficient of $\mu = 0.3$. These weighted solutions are used to develop the design tables presented in a later section.

Model Behavior

In order to properly set the stage for the design procedure, a discussion is warranted on the maximum values of thrust, moment, and vertical deflection. From Table 1 it can be readily deduced that for any pipe-soil system (slotted or unslotted, frictionless or bonded) the maximum thrust and maximum moment always occur at the springline location ($\theta = 0°$), and the maximum radial displacement always occurs at the crown location ($\theta = 90°$). The latter displacement represents one-half of the diametrical shortening between the crown and invert, or more simply, one-half of the vertical deflection.

For standard unslotted pipes, these key structural responses increase in direct proportion to overburden pressure, whereas for slotted-joint pipes, the structural responses typically exhibit the behavior shown in Figure 4. Here and in all subsequent discussions, overburden pressure is related to fill height by the conventional relationship

$$P_0 = H\gamma \quad (7)$$

where H is the fill height cover above the crown and γ is the soil density. Hence, H is taken to be a monotonically increasing loading variable.

As shown in Figure 4, the springline thrust N, nondimensionalized by the material yield thrust N_y, exhibits a sharp reduction in rate of increase during that portion of loading in which the slotted joints are contracting. After the slotted joints are fully contracted, the thrust rate sharply increases again. The potential fill-height gain ΔH is defined as the difference between the fill height at which the slotted joints become closed and the fill height of a corresponding standard unslotted pipe experiencing the same amount of thrust, as shown in Figure 4. In other words, if the design criterion was based solely on some allowable thrust level, say $N/N_y = 0.5$, then, potentially, the slotted pipe could be buried at a depth ΔH greater than a standard pipe.

Using this definition, the incremental elasticity solution can be manipulated to provide a general expression for the potential fill height gain valid for all conditions, that is,

$$\Delta H = 2GJ_r(1 - E_s/E_e)/\gamma \quad (8)$$

This simple yet rather remarkable result shows that the potential gain is directly proportional to the soil shear modulus G and to the ratio J_r of all slot lengths to pipe circumference. However, whether or not the full potential gain can be realized depends on whether or not complete joint closure is achieved before the thrust stress limit is exceeded. More important, it depends on the interaction of other design criteria. For example, the center graph in Figure 4 shows that the springline moment normalized by the yield moment increases at a greater rate during slot closure than the corresponding moment rate of a standard pipe. Consequently, if a moment criterion, say flexure strain, controls the design, then no fill height gain will be achieved. This undesirable and perhaps unexpected response characteristic of slotted-pipe behavior is caused by a shift in the moment distribution, that is, during joint closure the springline moment increases while the crown moment decreases in comparison to the moment responses of a standard pipe.

The last graph in Figure 4 shows that vertical displacement (normalized by diameter) increases its rate of deflection during joint closure. This behavior, as should be anticipated, is caused by the uniform circumferential contraction of the periphery of the pipe during joint closure, thereby producing an additional vertical deflection superimposed on the standard ovaling deformation mode due to flexural bending. Unlike the moment behavior, this increased deflection does not compromise the design integrity of the slotted pipe, as explained in the following design methodology.

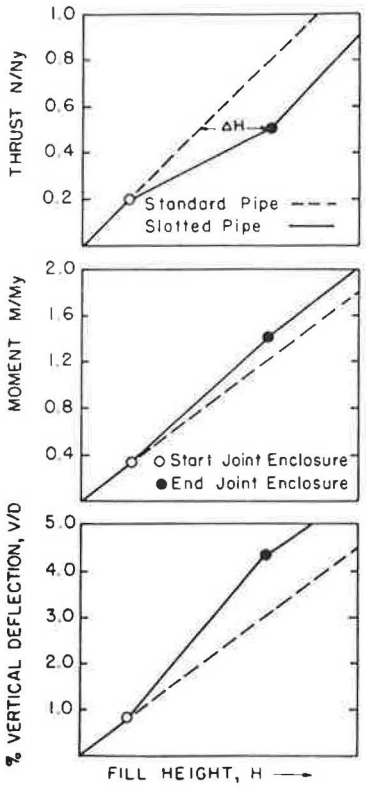

FIGURE 4 Typical response behavior for thrust, moment, and deflection with increasing fill height.

DESIGN METHODOLOGY

The goal of the ensuing design methodology is to establish design tables that specify the maximum allowable fill height for round, 6- × 2-in. corrugated steel pipes with slotted joints. Like the AISI (*6*) design tables for standard (unslotted) pipes, the maximum allowable fill heights will be given as a function of pipe diameter and steel gauge (thickness). However, unlike AISI (*6*) a sequence of tables that accounts for varying degrees of soil quality (stiffness) is presented herein.

The design methodology can be discussed in terms of design criteria and analytical procedures along with assumptions and limitations. Design criteria form a set of maximum allowable structural responses or acceptable standards for which the pipe-soil system is considered functionally safe. Correspondingly, the analytical procedure determines the maximum allowable load (fill height) such that the predicted structural responses do not exceed the design criteria.

Design Criteria

The design criteria adopted here are for the most part in conformance with the traditional criteria used for flexible pipe design. They are as follows:

$$\text{Thrust stress} \leq \sigma_y/2.0, \tag{9a}$$
$$\text{Percent vertical deflection} \leq 5 \text{ percent} + 100J_r, \tag{9b}$$
$$\text{Flexural strain} \leq 2.0\varepsilon_y, \tag{9c}$$
$$\text{Buckling pressure} \leq P_{cr}/2.0, \text{ and} \tag{9d}$$
$$\text{Flexibility factor } D^2/EI \leq FF = 0.02. \tag{9e}$$

Thrust stress is usually the controlling design criterion when good-quality backfill soil is used. This criterion limits the maximum allowable thrust stress anywhere in the pipe wall or in any joint to one-half the steel yield stress σ_y. This limit implies a safety factor of 2.0 against complete wall yielding or joint failure.

Vertical deflection, that is, the relative flattening between the crown and invert of the pipe, is traditionally limited to 5 percent of the diameter. This criterion is intended to be a safeguard against excessive ovaling deformation. (Twenty percent ovaling is considered tantamount to failure due to reversal of curvature that promotes a complete collapse.) For pipes with slotted joints, vertical deflection is caused by ovaling and uniform circumferential contraction of the joints. Because the latter deformation mode does not cause structural distress, the vertical deflection criterion is increased by the percentage of diametrical shortening due to joint contraction, that is, $100J_r$, where J_r is the fraction of the pipe circumference containing slots (Equation 5). Typically, this is an increase of 1.5 to 2.0 percent.

The criterion for flexural strain due to bending moments is usually not used in the design of steel culverts because flexural yielding of the pipe wall, even to the extent of complete plastic hinging, does not produce a collapse mechanism because of the support of the surrounding soil envelope. Indeed, some amount of flexural yielding is expected to occur in many standard pipe installations. As previously discussed, however, pipes with slotted joints

experience somewhat greater moments locally than standard pipes. Thus, in the spirit of conservatism, a flexural strain criterion is used that limits the maximum outer fiber flexural strain to no more than twice the yield strain ($\varepsilon_y = \sigma_y/E$). In effect, this condition limits the maximum plastic penetration to 50 percent of the corrugated cross section.

For the buckling pressure criterion, a conservative formula is adopted from Chelapati and Allgood (*7*) in which the critical hydrostatic pressure causing local instability of a plane-strain cylinder in an elastic soil medium is given by

$$P_{cr} = 3G(2\beta)^{1/2} \tag{10}$$

where G is the soil shear modulus and β is the relative pipe-soil flexural stiffness (Equation 4). Thus, the maximum buckling pressure $P_{cr}/2.0$ infers a safety factor of 2. This design criterion is satisfied by requiring that the predicted buckling pressure, that is, the average radial pressure as predicted from the incremental elasticity solution does not exceed $P_{cr}/2.0$.

Finally, the flexibility factor, which is an a priori requirement on the robustness of the pipe to sustain handling and erection loads, is taken in accordance with conventional practice. For each gauge of pipe, this criterion immediately establishes an upper limit on the pipe diameter independent of installation and soil conditions. The worth and justification of this criterion remains controversial; nonetheless, it is retained here.

Design Scope and Assumptions

The design investigation is restricted to circular pipes fabricated from 6- × 2-in. corrugated steel plates with slotted joints. It is assumed that the soil envelope is homogeneous, representative of a deep embankment installation without a stiff bedding, and further, it is assumed that live loads are insignificant. Nonsaturated soil conditions are presumed, such that the soil retains its shear stiffness.

System parameters to be varied include the complete set of standard pipe diameters and wall gauges as listed in the AISI Handbook (*6*). These diameters range from 5.0 to 26.0 ft in increments of 0.5 ft, and for each diameter there are seven standard gauges available that provide a range of circumferential and flexural wall stiffnesses EA and EI, respectively.

For each combination of pipe diameter and gauge, four different soil moduli (E_{soil} = 4,000, 2,000, 1,000, and 500 psi, along with Poisson's ratio = 1/3) are used to assess the influence of soil stiffness.

The number of slotted joints around the pipe's circumference varies from 4 to 16 depending on the pipe's diameter, and the characteristics of each joint are patterned after the keyhole slot configuration. The following list presents the values of all the parameters used in this study.

Pipe Parameters

Diameters D = 5.0 to 26.0 ft, in 0.5-ft increments.
Wall sections = 6- × 2-in. corrugation; gauges = 12, 10, 8, 7, 5, 3, and 1; section properties I and A; as taken from AISI handbook.
Steel modulus $E = 30 \times 10^6$ psi.
Poisson's ratio $\nu = 0.33$.
Yield stress σ_y = 33,000 psi.

Soil Properties

Young's modulus E_{soil} = 4,000, 2,000, 1,000, and 500 psi.
Poisson's ratio $\nu_{soil} = 0.333$.
Density $\gamma_R = 120$ lb/ft^3.

Joint Properties

Total number of joints N = 4 to 16, depending on pipe diameter (see Design Tables).
Slot length per joint l_j = 1.0 in.
Initial slipping stress σ_e = 5,000 psi.
Slipping modulus E_s = 9,000 psi.
Post slipping modulus $E_p = 15 \times 10^6$ psi.
Joint failure stress σ_f = 33,000 psi.

Soil-Pipe Interface

Simulated friction coefficient $\mu = 0.3$.

Design Procedure

The design procedure, that is, determining the maximum allowable fill height for a particular pipe-joint-soil system, is conceptually straightforward. That is, each pipe-joint-soil system is analyzed using the incremental elasticity solution in the preslip, slip, and postslip regions. At each stage in the loading sequence, the predicted thrust stress, vertical deflection, flexural strain, and buckling pressure are checked against the corresponding design criteria, Equations 9a to 9d. The exact load level at which any one of these measures becomes equal to the allowable design value establishes the allowable fill height as well as the controlling design criterion. Overall, there are 43 different pipe diameters, 7 pipe gauges, and 4 soil moduli, inferring 1,204 design solutions. However, because the flexibility factor criterion (Equation 9e) precludes certain combinations of large-diameter pipe with light gauges, the actual number of design solutions is 936. Of course, the design solutions were obtained with the aid of a computer, and a detailed description of this special-purpose program is available (*2*).

Clearly, the design criteria and procedures could also be applied to standard unslotted pipes with considerable ease by holding the pipe's axial stiffness constant at its initial value. For comparative purposes, design solutions for slotted and unslotted pipes are given in the next section.

DESIGN TABLES AND GUIDELINES

Tables 2 through 5 list the allowable fill heights for both slotted-joint (Sld.J) and standard-joint (Std.J) construction based on the preceding design methodology and assumptions.

The four tables correspond to the four cases of soil stiffness (E_{soil} = 4,000, 2,000, 1,000, and 500 psi), and the format of each table is patterned after the AISI (*6*) height-of-cover tables in which the pipe diameter increases with row number and pipe-wall thickness increases with column number (in terms of gauge measures, the column correspond to gauge Nos. 1, 3, 5, 7, 8, 10, and 12).

Upon inspecting these tables, it is observed that the slotted pipes permit a substantially larger fill height than standard pipes when the D/t (diameter-to-thickness) ratio is relatively high. Conversely, when the D/t ratio is relatively low, the slotted pipes do not provide a gain in allowable fill height. This is denoted by a dash in the tables that indicates that slotted pipes should not be used. An explanation of these results along with the influence of soil stiffness follows.

Discussion of Tables

To better understand and interpret the design tables, Figure 5 shows the domain (diameter and gauge) of the tables subdivided into regions that identify the controlling design criterion. For good-quality soil, say $E_{soil} \geq 2{,}000$ psi, the thrust stress criterion dominates the domain, however, less so for slotted pipes than for standard pipes. The moment criterion, that is, flexural strain, controls in the region of low D/t ratios, that is, the upper right corner of the domain, and this region grows as the soil stiffness decreases. Whenever the moment criterion governs, the slotted pipes do not provide a gain in the allowable fill height because, as previously explained, the maximum bending moment is increased by introducing slotted joints.

The deflection criterion does not become significant unless poor-quality soil is employed (e.g., $E_{soil} < 1{,}000$ psi), and the buckling criterion does not control any of the design solutions because it is masked by the flexibility factor limit (the handling criterion). That is, the handling criterion automatically excludes consideration of pipes with large D/t ratios for all soil conditions. If this criterion were not used, then the buckling criterion would control in the lower left corner of the domain where the D/t ratios are large, and this region would grow as soil stiffness decreases.

Figure 6 provides an overall assessment of the increased fill height that can be achieved with slotted pipes as compared to standard pipes. Specifically, the ratios of allowable fill heights, slotted to standard, are plotted as contours over the diameter-gauge domain for each soil condition. For good-quality soil and large D/t ratios, the benefits from slotted-joint pipes are tremendous; burial depths of more than twice that of standard pipes can be achieved. On the other hand, for poor-quality soil the benefits are marginal.

The allowable fill heights for standard unslotted pipes are more conservative than those of the AISI Handbook (*6*), even for the stiffest soil condition of 4,000 psi. In part, this result is due to the additional design criterion for flexure; but more generally it is due to AISI's (*6*) use of ring compression theory, which gives a lower estimation of maximum thrust stress than the present soil-structure analysis. With regard to slotted pipes, the allowable fill heights derived herein are significantly greater than the AISI (*6*) fill heights for standard pipes, providing that good-quality soil and large D/t ratios are used. Thus, because the designs for unslotted pipes are conservative with respect to the AISI (*6*) designs, it is concluded that the designs for slotted pipes are also conservative.

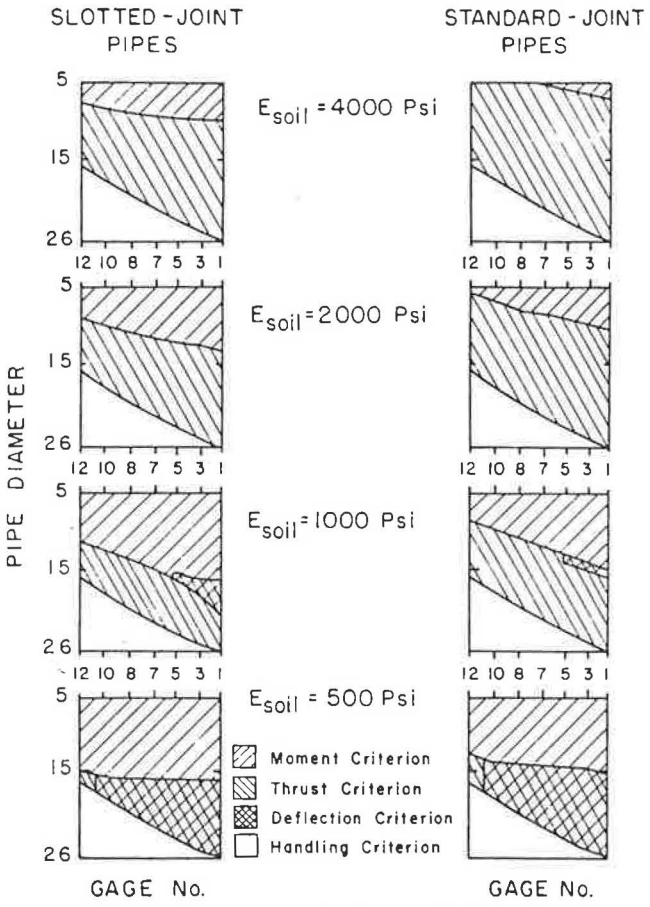

FIGURE 5 Regions of governing design criteria for four cases of soil stiffness.

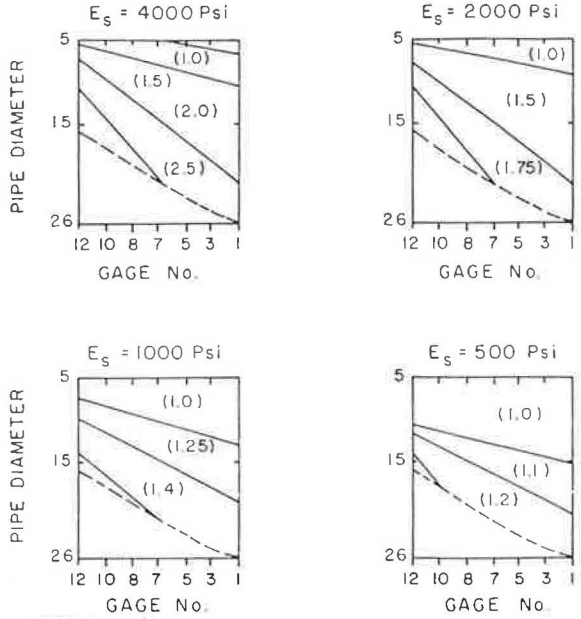

FIGURE 6 Contours of fill height ratios, slotted divided by standard, for four cases of soil stiffness.

TABLE 2 MAXIMUM FILL HEIGHT COVER FOR STRUCTURAL PLATE PIPES (E_{SOIL} = 4,000 PSI; 6- × 2-IN. CORRUGATION)

Diameter of Pipe		No. of Joints	Maximum Fill Cover in Feet													
			Specified Thickness in Inches													
			0.109		0.138		0.168		0.188		0.218		0.249		0.280	
In Ft.	In In		Std. J.	Sld. J.	Std. J.	Sld. J.	Std. J.	Sld. J.	Std. J.	Sld. J.	Std. J.	Sld. J.	Std. J.	Sld. J.	Std. J.	Sld. J.
5.0	60	4	71	103	91	110	111	117	121	122	136	–	151	–	165	–
5.5	66		65	103	83	115	101	121	113	125	129	131	142	–	155	–
6.0	72		60	99	77	112	94	124	104	129	121	134	135	139	147	–
6.5	78		56	96	71	108	87	119	97	126	112	138	128	143	140	147
7.0	84		52	92	66	105	81	115	90	122	105	133	120	143	134	151
7.5	90	6	49	102	62	112	76	122	84	128	98	138	112	147	126	151
8.0	96		46	98	58	110	71	119	79	125	92	134	105	143	118	152
8.5	102		43	93	55	105	67	117	75	122	87	131	99	139	112	148
9.0	108		41	88	52	100	64	111	71	118	83	128	94	136	106	144
9.5	114		39	84	50	94	60	105	67	112	78	123	89	134	100	141
10.0	120		37	80	47	90	57	100	64	107	75	118	85	128	96	139
10.5	126		35	76	45	86	55	96	61	102	71	112	81	122	91	132
11.0	132	8	34	85	43	95	52	104	58	110	68	120	78	130	87	139
11.5	138		32	82	41	91	50	100	56	106	65	115	74	124	84	133
12.0	144		31	78	40	87	48	96	54	101	63	110	71	119	80	128
12.5	150		30	75	38	84	46	92	52	97	60	106	69	115	77	123
13.0	156		29	72	37	80	45	89	50	94	58	102	66	110	74	118
13.5	162		28	70	35	78	43	85	48	90	56	98	64	106	71	114
14.0	168		27	67	34	75	41	82	46	87	54	95	61	103	69	110

TABLE 2 *continued*

Diameter of Pipe		No. of Joints	Maximum Fill Cover in Feet													
			Specified Thickness in Inches													
			0.109		0.138		0.168		0.188		0.218		0.249		0.280	
In Ft.	In In		Std. J.	Sld. J.	Std. J.	Sld. J.	Std. J.	Sld. J.	Std. J.	Sld. J.	Std. J.	Sld. J.	Std. J.	Sld. J.	Std. J.	Sld. J.
14.5	174	10	26	75	33	82	40	89	45	94	52	101	59	109	67	116
15.0	180		25	72	32	79	39	86	43	91	50	98	57	105	64	112
15.5	186		24	70	31	77	38	84	42	88	49	95	56	102	62	109
16.0	192		23	68	30	74	36	81	41	85	47	92	54	99	61	106
16.5	198				29	72	35	79	39	83	46	89	52	96	59	102
17.0	204				28	70	34	76	38	80	45	87	51	93	57	99
17.5	210				27	68	33	74	37	78	43	84	49	91	55	97
18.0	216	12			27	74	32	80	36	84	42	90	48	96	54	102
18.5	222						32	78	35	82	41	87	47	93	52	99
19.0	228						31	76	34	79	40	85	46	91	51	97
19.5	234						30	74	33	77	39	83	44	89	50	94
20.0	240						29	72	33	76	38	81	43	86	49	92
20.5	246								32	74	37	79	42	84	47	90
21.0	252								31	72	36	77	41	82	46	88
21.5	258	14							30	77	35	82	40	87	45	92
22.0	264										35	80	39	85	44	90
22.5	270										34	78	39	83	43	88
23.0	276										33	77	38	81	42	86
23.5	282												37	80	42	84
24.0	288												36	78	41	83
24.5	294												36	77	40	81
25.0	300	16											35	81	39	85
25.5	306														38	83
26.0	312														38	82

Std. J = Standard Joints, Sld. J = Slotted Joints

TABLE 3 MAXIMUM FILL HEIGHT COVER FOR STRUCTURAL PLATE PIPES (E_{SOIL} =. 2,000 PSI; 6- × 2-IN. CORRUGATION)

Diameter of Pipe		No. of Joints	Maximum Fill Cover in Feet													
			Specified Thickness In Inches													
			0.109		0.138		0.168		0.188		0.218		0.249		0.280	
In Ft.	In In		Std. J.	Sld. J.	Std. J.	Sld. J.	Std. J.	Sld. J.	Std. J.	Sld. J.	Std. J.	Sld. J.	Std. J.	Sld. J.	Std. J.	Sld. J.
5.0	60	4	67	-	82	-	92	-	96	-	102	-	108	-	114	-
5.5	66		64	67	77	-	90	-	94	-	99	-	104	-	109	-
6.0	72		59	69	73	75	85	-	92	-	98	-	102	-	106	-
6.5	78		55	68	70	77	81	81	88	-	99	-	102	-	105	-
7.0	84		51	66	65	76	78	83	84	86	94	-	102	-	105	-
7.5	90	6	48	69	61	79	74	82	81	85	90	-	100	-	106	-
8.0	96		45	67	57	76	70	85	78	87	87	90	96	-	105	-
8.5	102		42	65	54	74	66	83	74	88	85	93	93	95	101	-
9.0	108		40	64	51	72	62	80	70	86	81	94	91	98	98	100
9.5	114		38	60	49	71	59	79	66	83	77	91	88	99	96	103
10.0	120		36	58	46	68	56	77	63	82	73	89	84	96	94	103
10.5	126		34	55	44	65	54	74	60	80	70	87	80	94	90	101
11.0	132	8	33	59	42	68	51	78	57	82	67	89	76	95	86	102
11.5	138		31	56	40	65	49	74	55	80	64	87	73	94	82	100
12.0	144		30	54	39	63	47	71	53	77	62	86	70	92	79	98
12.5	150		29	52	37	60	45	68	51	74	59	82	68	91	76	96
13.0	156		28	50	36	58	44	66	49	71	57	79	65	87	73	95
13.5	162		27	48	35	56	42	64	47	68	55	76	63	84	70	92
14.0	168		26	46	33	54	41	61	45	66	53	74	60	81	68	89

TABLE 3 *continued*

Diameter of Pipe In Ft.	Diameter of Pipe In In	No. of Joints	Maximum Fill Cover In Feet													
			Specified Thickness In Inches													
			0.109		0.138		0.168		0.188		0.218		0.249		0.280	
			Std. J.	Sld. J.	Std. J.	Sld. J.	Std. J.	Sld. J.	Std. J.	Sld. J.	Std. J.	Sld. J.	Std. J.	Sld. J.	Std. J.	Sld. J.
14.5	174	10	25	50	32	57	39	64	44	69	51	76	58	83	66	91
15.0	180		24	48	31	55	38	62	42	67	49	74	57	81	64	88
15.5	186		23	47	30	53	37	60	41	64	48	71	55	78	62	85
16.0	192		23	45	29	52	36	58	40	62	46	69	53	76	60	82
16.5	198				28	50	35	56	39	61	45	67	51	73	58	80
17.0	204				27	49	34	55	38	59	44	65	50	71	56	78
17.5	210				27	47	33	53	36	57	43	63	49	69	55	75
18.0	216	12			26	50	32	56	35	60	41	66	47	71	53	77
18.5	222						31	54	34	58	40	64	46	70	52	75
19.0	228						30	53	34	56	39	62	45	68	50	73
19.5	234						29	52	33	55	38	61	44	66	49	72
20.0	240						29	50	32	54	37	59	43	64	48	70
20.5	246								31	52	36	58	42	63	47	68
21.0	252								30	51	36	56	41	61	46	66
21.5	258	14							30	53	35	58	40	63	45	68
22.0	264										34	57	39	62	44	67
22.5	270										33	56	38	60	43	65
23.0	276										32	55	37	59	42	64
23.5	282												36	58	41	63
24.0	288												36	57	40	61
24.5	294												35	56	39	60
25.0	300	16											34	57	38	62
25.5	306														38	60
26.0	312														37	59

TABLE 4 MAXIMUM FILL HEIGHT COVER FOR STRUCTURAL PLATE PIPES (E_{SOIL} =. 1,000 PSI; 6- × 2-IN. CORRUGATION)

Diameter of Pipe		No. of Joints	Maximum Fill Cover in Feet													
			Specified Thickness In Inches													
			0.109		0.138		0.168		0.188		0.218		0.249		0.280	
In Ft.	In In		Std. J.	Sld. J.	Std. J.	Sld. J.	Std. J.	Sld. J.	Std. J.	Sld. J.	Std. J.	Sld. J.	Std. J.	Sld. J.	Std. J.	Sld. J.
5.0	60	4	52	-	59	-	65	-	69	-	75	-	82	-	88	-
5.5	66		51	-	56	-	61	-	64	-	70	-	75	-	80	-
6.0	72		51	-	55	-	59	-	62	-	66	-	70	-	74	-
6.5	78		49	-	54	-	58	-	60	-	64	-	70	-	70	-
7.0	84		46	-	55	-	58	-	59	-	62	-	68	-	68	-
7.5	90	6	45	45	54	-	58	-	59	-	62	-	64	-	67	-
8.0	96		43	47	52	-	59	-	60	-	62	-	64	-	66	-
8.5	102		41	48	52	51	58	-	61	-	62	-	64	-	66	-
9.0	108		39	46	49	52	56	-	61	-	63	-	65	-	66	-
9.5	114		37	45	48	53	55	56	59	-	65	-	66	-	67	-
10.0	120		35	44	46	51	53	57	58	59	65	-	67	-	68	-
10.5	126		34	43	43	50	52	57	56	60	63	-	68	-	69	-
11.0	132	8	32	44	42	51	51	57	55	60	62	62	68	-	70	-
11.5	138		31	43	40	50	49	56	54	60	60	64	66	-	72	-
12.0	144		30	42	38	49	47	55	52	59	59	65	65	66	70	-
12.5	150		29	40	37	48	45	54	50	58	58	63	63	68	69	69
13.0	156		27	39	35	46	53	48	48	57	56	62	62	68	68	71
13.5	162		26	37	34	45	42	52	46	56	54	61	61	66	66	72
14.0	168		26	36	33	43	40	51	45	55	52	60	60	65	65	70

TABLE 4 *continued*

Diameter of Pipe		No. of Joints	Maximum Fill Cover in Feet													
			Specified Thickness in Inches													
			0.109		0.138		0.168		0.188		0.218		0.249		0.280	
In Ft.	In In		Std. J.	Sld. J.	Std. J.	Sld. J.	Std. J.	Sld. J.	Std. J.	Sld. J.	Std. J.	Sld. J.	Std. J.	Sld. J.	Std. J.	Sld. J.
14.5	174	10	25	37	32	44	39	51	43	56	51	60	58	65	64	70
15.0	180		24	36	31	43	38	50	42	54	49	60	56	64	62	69
15.5	186		23	35	30	41	36	48	41	52	47	59	54	64	61	68
16.0	192		22	34	29	40	35	47	39	51	46	57	52	62	59	67
16.5	198				28	39	34	45	38	49	45	56	51	61	57	65
17.0	204				27	38	33	44	37	48	43	54	49	59	56	64
17.5	210				26	37	32	43	36	46	42	52	48	58	54	62
18.0	216	12			26	38	31	43	35	47	41	53	47	58	53	63
18.5	222						30	42	34	46	40	52	45	57	51	61
19.0	228						30	41	33	45	39	50	44	56	50	60
19.5	234						29	40	32	44	38	49	43	54	49	59
20.0	240						28	39	32	43	37	48	42	53	47	58
20.5	246								31	41	36	47	41	52	46	57
21.0	252								30	40	35	46	40	51	45	56
21.5	258	14							29	41	34	46	39	51	44	56
22.0	264										34	45	38	50	43	55
22.5	270										33	44	37	49	42	54
23.0	276										32	43	37	48	41	52
23.5	282												36	47	40	51
24.0	288												35	46	40	50
24.5	294												34	45	39	49
25.0	300	16											34	45	38	50
25.5	306														37	48
26.0	312														36	47

TABLE 5 MAXIMUM FILL HEIGHT COVER FOR STRUCTURAL PLATE PIPES (E_{SOIL} = 500 PSI; 6- × 2-IN. CORRUGATION)

Diameter of Pipe		No. of Joints	Maximum Fill Cover in Feet													
			Specified Thickness in Inches													
			0.109		0.138		0.168		0.188		0.218		0.249		0.280	
In Ft.	In In		Std. J.	Sld. J.	Std. J.	Sld. J.	Std. J.	Sld. J.	Std. J.	Sld. J.	Std. J.	Sld. J.	Std. J.	Sld. J.	Std. J.	Sld. J.
5.0	60	4	38	-	45	-	51	-	55	-	62	-	68	-	75	-
5.5	66		35	-	41	-	46	-	49	-	55	-	60	-	65	-
6.0	72		34	-	38	-	42	-	45	-	50	-	54	-	58	-
6.5	78		32	-	36	-	40	-	42	-	46	-	50	-	53	-
7.0	84		32	-	35	-	38	-	40	-	43	-	46	-	50	-
7.5	90	6	32	-	34	-	37	-	39	-	42	-	44	-	47	-
8.0	96		32	-	34	-	36	-	38	-	40	-	43	-	45	-
8.5	102		32	-	34	-	36	-	37	-	39	-	41	-	43	-
9.0	108		33	-	34	-	36	-	37	-	39	-	41	-	42	-
9.5	114		33	-	35	-	36	-	37	-	39	-	40	-	42	-
10.0	120		32	-	35	-	37	-	38	-	39	-	40	-	41	-
10.5	126		31	32	36	-	37	-	38	-	39	-	40	-	41	-
11.0	132	8	30	32	37	-	38	-	38	-	39	-	40	-	41	-
11.5	138		30	33	36	-	39	-	39	-	40	-	41	-	42	-
12.0	144		29	32	35	35	39	-	40	-	41	-	41	-	42	-
12.5	150		28	31	34	36	40	-	41	-	41	-	42	-	42	-
13.0	156		27	31	34	36	39	-	41	-	42	-	42	-	43	-
13.5	162		26	30	33	35	38	39	41	-	43	-	43	-	44	-
14.0	168		25	30	32	35	37	40	46	40	43	-	44	-	44	-

TABLE 5 *continued*

Diameter of Pipe In Ft.	Diameter of Pipe In In	No. of Joints	Maximum Fill Cover in Feet													
			Specified Thickness in Inches													
			0.109		0.138		0.168		0.188		0.218		0.249		0.280	
			Std. J.	Sld. J.	Std. J.	Sld. J.	Std. J.	Sld. J.	Std. J.	Sld. J.	Std. J.	Sld. J.	Std. J.	Sld. J.	Std. J.	Sld. J.
14.5	174	10	24	30	31	35	36	40	39	41	42	-	43	-	44	-
15.0	180		24	29	30	34	35	39	38	42	42	42	43	43	43	44
15.5	186		23	29	29	34	34	38	37	41	41	43	42	44	43	45
16.0	192		22	28	28	33	33	37	36	41	40	44	42	45	42	45
16.5	198				28	32	32	37	35	39	39	44	41	46	42	46
17.0	204				27	31	32	36	34	39	39	43	41	45	41	47
17.5	210				26	30	31	35	34	39	38	42	40	44	41	46
18.0	216	12			25	30	30	35	33	38	37	42	40	44	41	46
18.5	222						30	34	32	37	36	41	40	44	40	45
19.0	228						29	33	32	36	35	40	39	43	40	45
19.5	234						29	33	31	35	35	39	38	43	40	44
20.0	240						28	32	31	34	34	38	38	42	40	44
20.5	246								30	34	33	38	37	41	39	43
21.0	252								29	33	33	37	36	40	39	43
21.5	258	14							29	33	32	37	36	40	38	43
22.0	264										32	36	35	40	37	42
22.5	270										31	35	34	39	36	42
23.0	276										31	35	33	38	35	40
23.5	282												33	37	34	39
24.0	288												32	36	33	38
24.5	294												31	35	33	37
25.0	300	16											31	35	32	37
25.5	306														31	36
26.0	312														31	35

Design Guidelines and Recommendations

To use the design tables, the following guidelines and recommendations are offered.

1. The design tables are based on a reference soil density of $\gamma_R = 120$ lb/ft^3. For an actual soil density γ_A, the allowable fill heights may be scaled by the ratio γ_R/γ_A.
2. For optimum performance, well-graded, granular soils should always be used for backfill. Recommended values for E_{soil} are given in Figure 7 as a function of percent compaction. Allowable fill heights may be linearly interpolated between tabled values for intermediate values of E_{soil}.
3. If the actual total available slot travel length C_A (= number of joints × slot length) is less than the reference value C_R given in the design tables, then the actual fill height gain (ΔH, increase above the standard pipe) can be found by scaling down the reference fill height gain with the ratio C_A/C_R. Note, if $C_A/C_R > 1$, this technique should not be used to scale up the fill height gain unless it is known that the controlling design criterion will not change.
4. Finally, for pipe-joint-soil installations outside of the scope considered here (e.g., noncircular pipes and nonhomogeneous soil zones), the CANDE computer program can be used to obtain a design solution using finite element techniques. The program and documentation are available, free of charge, from the FHWA.

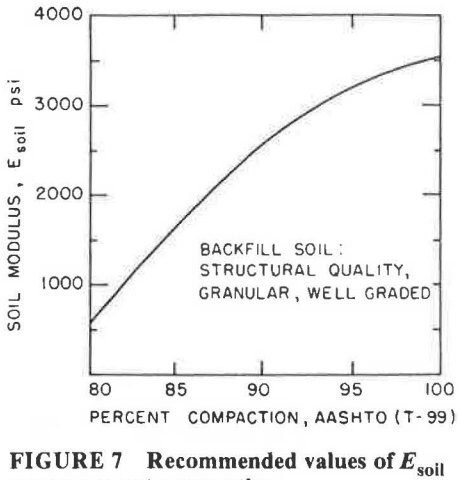

FIGURE 7 Recommended values of E_{soil} versus percent compaction

SUMMARY AND CONCLUSIONS

Use of slotted-bolt-hole joints in large-diameter corrugated-pipe culverts permits substantial increases of burial depth up to a factor of 2 or more over that of unslotted pipes providing that good-quality backfill soil is employed. For poor-quality soil or smaller diameter-to-thickness ratios, the benefits of slotted-joint construction are marginal.

The maximum allowable fill-height tables presented here can be used with conservative confidence providing that the slotted-joint culvert system conforms to the stated guidelines and assumptions. For other installations (e.g., noncircular shapes and stiff inclusions), direct use of the CANDE program is recommended.

Lastly, this design methodology, which is based on sound soil-structure interaction theory and backed by experimental data, is also applicable to standard unslotted pipes and is more rational than the design approach used in national standards, such as those of AISI and AASHTO. However, the design criterion for flexural strain may be overly conservative for standard pipes.

ACKNOWLEDGMENT

Deep appreciation is extended to the FHWA for sponsoring and encouraging this research effort. Thanks are also extended to the National Science Foundation through its Presidential Young Investigator Award for providing further support of the general design methodology.

REFERENCES

1. M. G. Katona and A. Y. Akl. Analysis and Behavior of Buried Culverts with Slotted Joints. In *Transportation Research Record 1008*. TRB, National Research Council, Washington, D.C., 1985, pp. 22-32.
2. M. G. Katona and A. Y. Akl. Metal Culverts with Slotted Bolt Holes. FHWA, U.S. Department of Transportation, Aug. 1984.
3. J. Q. Burns. *An Analysis of Circular Cylindrical Shells Embedded in Elastic Media*. Ph.D. thesis, University of Arizona, Tucson, 1965.
4. M. G. Katona et al. *CANDE: A Modern Approach for the Structural Design of Buried Pipe Culverts*. Report FHWA-RD-77-5. FHWA, U.S. Department of Transportation, Oct. 1976.
5. M. G. Katona et al. *CANDE: Box Culverts and Soil Models*. Report FHWA-RD-80-172. FHWA, U.S. Department of Transportation, May 1981.
6. *Handbook of Steel Drainage and Highway Construction Products*. American Iron and Steel Institute, Washington, D.C., 1971.
7. C. V. Chelapati and J. R. Allgood. Buckling of Cylinders in a Confining Medium. In *Highway Research Record 413*. HRB, National Research Council, Washington, D.C., 1972, pp. 77-88.

Wheel-Load-Induced Earth Pressures on Box Culverts

RAY W. JAMES AND DALE E. BROWN

A full-scale 8- by 8-ft reinforced-concrete box culvert was constructed and instrumented with earth pressure cells. Dead loads caused by backfill and up to 8 ft of cover were applied in 2-ft increments. Live loads were applied at each level of cover by a test vehicle loaded to represent the alternate interstate design load, consisting of two 24,000-lb axles spaced 4 ft apart. Measured live-load earth pressures on the top slab are compared to various theoretical solutions for concentrated and distributed wheel loads and to pressures predicted by a finite element model. Empirical equations are presented that for shallow covers more accurately model the measured data than do the analytical and numerical methods studied.

The prediction of live-load-induced earth pressures on culverts under shallow fill is accomplished in design by empirical methods such as the AASHTO pyramid loading (*1*), in which the vertical pressure caused by a concentrated or distributed load on the surface is calculated by dividing the load by the area of the base of a four-sided pyramid having sides with specified slopes and apex at the location of the concentrated load or truncated top at the rectangular distributed surface load. Applicable theoretical methods (*2-5*) are generally based on elasticity solutions, usually involving simplifying assumptions of linearly elastic, isotropic behavior. In addition, such methods are cumbersome for application in design. Finite element methods using such programs as CANDE (*6*) and SST1PN (a code written at the University of California at Berkeley) have become widely used in design for prediction of earth pressures accounting for nonlinear material behavior, soil-structure interaction, and complex geometries that cannot be easily modeled with the analytical methods. Essential to any finite element model are data for testing the validity of assumptions regarding material properties and soil-structure interaction mechanisms. Anand (*7*) describes the need for reliable full-scale model data as follows: "Most of all, experimental data from full-scale models of shallow buried rigid pipes are desperately needed to verify the proposed analysis." While some recent data (*8*) have been developed concerning blast loading of concrete structures under shallow earth covers, few data for wheel-load-induced pressures have been reported.

R. W. James, Department of Civil Engineering, Texas A&M University, College Station, Tex. 77843-3136. D. E. Brown, Engineering Department, Chandler, Ariz. 85224.

DESCRIPTION OF EXPERIMENT

Culvert and Instrumentation

An 8- by 8- by 44-ft-long (2.44- by 2.44- by 13.41-m) reinforced-concrete box culvert was constructed in February 1982. Thicknesses of the side walls and slabs were 8 in. (20.3 cm) and 7 in. (17.8 cm), respectively. The culvert was constructed according to current Texas SDHPT standard specifications for SC-NB Type 3 single culverts—normal. The selected 44-ft (13.41-m) length was designed to allow construction of a 12-ft (3.66-m) roadway with 2:1 side slopes across the culvert. Twelve Terra Technology Model T-9010 total pressure cells were installed in the top slab flush with the top surface at locations described in Figure 1. The pressure cells had a full-scale range of 250 psi (1,720 kPa) and a manufacturer's specified accuracy of 0.1 percent full scale. The readings were taken with a 50-psi (7.3-kPa) full-scale pressure gauge and a resolution of 0.1 psi (0.7 kPa). Other instrumentation included pressure cells on the side walls and resistance strain gauges bonded to the reinforcing steel of the top slab. Measurements of top-slab deflection were made with a deflection dial gauge. The top-slab pressure cells were arranged in two banks of six cells each. The pressure cells

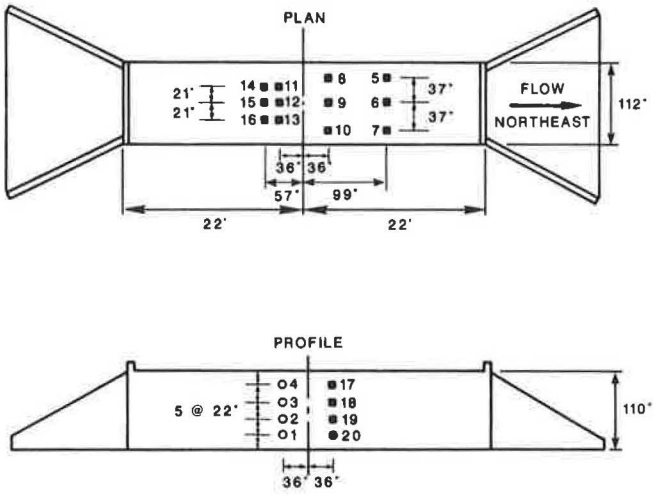

FIGURE 1 Test culvert and instrumentation.

used were static devices, incapable of indicating dynamic loads.

During February 1982 through September 1984, backfill and cover were placed, and measurements of dead- and live-load-induced earth pressures and strains in reinforcing steel were made. The measured live-load pressures on the top slab are presented herein. Live loads were applied by parking a test vehicle at a designated location above the culvert, and recording the static earth pressures applied to the culverts. Testing was repeated at various cover depths from 8 in. (20.3 cm) to 8 ft (2.44 m). The soil used to backfill and to cover the culvert was obtained at the test site, and has been classified as SC-SP, according to the Unified Soil Classification System. The liquid limit and plasticity index were 37.5 and 21.3 percent, respectively. The effective stress parameters C and ϕ were 0 and 31.8°, respectively. The soil properties and construction sequence are described in detail by James et al. (*9*).

Test Procedure

The test vehicle was a five-axle tractor-semitrailer combination vehicle, having the geometry and axle weights shown in Figure 2. The test vehicle essentially simulated the alternate interstate design load, a tandem of two 24-kip (107-kN) axles spaced 4 ft (1.22 m) apart. The effects of the lightly loaded tractor tandem and the steering axle were observed to be insignificant in comparison to the effect of the heavily loaded rear tandem.

The test vehicle was parked with the loaded tandem in various locations, as presented in Table 1. The pressure cells were pressurized according to the manufacturer's specifications, and the indicated pressures recorded. Three separate readings were taken for averaging, unless the first two readings were in agreement within 0.1 psi (0.7 kPa).

Data Reduction and Presentation

The recorded data were reduced and plotted using a microcomputer. Data reduction consisted of subtracting the indicated pressure with no live load applied from the indicated pressure with live load applied. No temperature correction

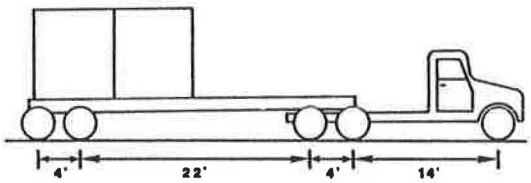

APRIL 1983					
LEFT SIDE	11,600	11,720	3,810	4,100	4,500
RIGHT SIDE	12,340	12,770	3,930	4,170	4,500
TOTAL	24,140	24,490	7,740	8,270	9,000
JUNE 1984					
LEFT SIDE	11,480	11,300			
RIGHT SIDE	12,980	12,870	NO DATA TAKEN		NO DATA TAKEN
TOTAL	24,430	24,250			

FIGURE 2 Test vehicle geometry and axle weights.

was required because the only observed effect of temperature on the cells was a change in the zero pressure offset. The effect of this variable offset was eliminated by subtracting the indicated pressure for the dead load as long as the temperature of the cell did not change between the two measurements. Because indicated pressures for the dead load were usually measured immediately before application of the live load, this temperature requirement was satisfied. The dead-load pressures, discussed by James et al. (*9*), did indicate a significant dependence on temperature, attributed to differential thermal expansion of the culvert and soil system.

MEASURED EARTH PRESSURES

The measured live-load earth pressures are presented in Table 1.

EMPIRICAL PRESSURE PREDICTION EQUATIONS

A number of functions were fit to the data of Table 1 in an attempt to develop an empirical equation for use in predicting design pressures under shallow covers. Existing theoretical equations for concentrated loads on the surface, such as Boussinesq's equation and Westergaard's equation, are not applicable for depths of cover that are not significantly greater than some characteristic dimension of the loaded area (*10*). In addition, these theoretical equations are based on a linearly elastic behavior within the soil, and the validity of this simplification is not certain. However, these equations were included in the set of candidate functions.

$$P_{VL} = W_i F(r, z) \quad (1)$$

where

P_{VL} = live-load vertical pressure,
W_i = wheel load, and
$F(r, z)$ = reciprocal area that depends on radial distance r and vertical distance z.

The functions considered included the following:

$$F(r, z) = (1.5/\pi)(Az)^3[(Br)^2 + (Az)^2]^{-2.5} \quad (2a)$$

$$F(r, z) = [\pi(Az)^2]^{-1}[1 + 2(Br/Az)^2]^{-1.5} \quad (2b)$$

$$F(r, z) = (\pi r_0^2)^{-1} \exp(-z/z_0)\exp\{-[\exp(-z/z_0)](r/r_0)^2\} \quad (2c)$$

and several members of the family

$$F(r, z) = \exp[-(Br/r_0)^2] \quad (2d)$$

including functions $r_0(z)$ such as

$$r_0(z) = (z/z_0) \quad (2e)$$

$$r_0(z) = (z/z_0)^{0.5} \quad (2f)$$

$$r_0(z) = \exp[(z/z_0)^2] \quad (2g)$$

$$r_0(z) = \exp(0.5z/z_0) \quad (2h)$$

Equation 2a is a form of Boussinesq's equation, as adapted to soils engineering by Jurgenson (*3*) and here modified by the dimensionless parameters A and B that multiply the z and r position variables, respectively. Equation 2b is a form of Westergaard's equation (*11*), modified here by the dimensionless parameters A and B. Equation 2c is an empirical equation that satisfies equilibrium and appropriate boundary conditions and that has been suggested as a model of the vertical live-load earth pressures (*9*). The parameters z_0 and r_0 are constant characteristic lengths that can be determined to best fit the data. Equation 2d is a family of functions that also satisfy equilibrium and the appropriate boundary conditions, but that are expressed in terms of a constant length parameter z_0 and a function $r_0(z)$ that depends on the dimensionless variable z/z_0. Functions $r_0(z)$ that were considered are listed in Equations 2e through 2h.

These theories do not include the effect of soil-structure interaction, and are therefore expected to predict pressures slightly greater than the actual pressures.

Regression Method

The best-fit parameters A, B, r_0, and z_0 for the equations listed were determined approximately by nonlinear regression. The error norm minimized was

$$\left|(P_t - P_m)\exp(-r/0.5)\right|$$

where P_t and P_m were theoretical and measured earth pressures, respectively.

The weighted error norm was calculated for the various equations and local minimums were identified. The weighting function was arbitrarily chosen so that pressures near points beneath an applied load were more heavily weighted than pressures at points some horizontal distance from an applied load. The corresponding values of the parameters and the ranges checked are presented in Table 2.

Discussion of Results

The results of the regression analysis are presented in Figures 3-11, which show the predicted pressures along a wheel path for each of the equations evaluated. The pressures indicated for the six pressure cells along either wheel path are presented for comparison. The earth pressures predicted from Equations 2e through 2h are not presented because the regression analysis results in Table 2 indicate relatively poor fits. Also shown for comparison are curves representing Boussinesq's equation integrated over four uniformly loaded 10- by 20-in. (25.4- by 50.8-cm) AASHTO footprints. No parameters were introduced to fit these curves to the data.

The Boussinesq equation (2a) and the Westergaard equation (2b) are shown as nearly identical curves, as expected. For shallow covers however, these two equations greatly overestimate the peak pressure directly beneath the wheel footprint. Because both equations are based on theories of earth pressure beneath concentrated loads, this observation is not unexpected. Because the maximum earth pressure beneath a wheel is limited to pressures not much more than the tire pressure, which is approximately 70 psi (482 kPa), the predicted pressures of over 170 psi (1,160 kPa) at 8-in. (20.3-

TABLE 1 MEASURED EARTH PRESSURES

EARTH COVER in feet	LOAD LOC. in feet	MEASURED EARTH PRESSURE IN PSI CELL NO. 5	6	7	8	9	10	11	12	13	14	15	16
(1)	(2)	(3)	(4)	(5)	(6)	(7)	(8)	(9)	(10)	(11)	(12)	(13)	(14)
1	0.0	0.2	0.3	-0.1	-0.3	-0.1	3.9	34.1	-0.1	17.4	0.1	-0.6	-0.3
2	3.0	0.1	-0.2	0.0	0.0	7.4	3.1	0.3	5.7	6.2	-0.2	3.4	3.0
2	-4.7	0.1	0.0	0.0	0.1	0.0	11.1	0.3	0.1	7.5	0.0	-0.5	2.3
2	0.0	0.1	-0.1	0.4	7.1	2.5	6.0	13.2	2.1	11.6	2.2	0.0	3.5
2	4.7	0.1	0.0	0.5	10.5	0.0	0.0	8.5	0.6	0.2	1.8	-0.4	-0.2
4	0.0	0.2	-0.2	0.1	3.3	1.5	2.9	4.1	1.5	2.2	1.8	1.6	2.1
4	3.0	-0.2	-0.4	0.0	3.5	0.6	0.3	3.3	1.1	-0.1	1.4	0.7	0.1
6	0.0	-0.2	-0.4	0.2	1.2	0.5	1.2	1.9	0.5	0.7	0.8	0.5	0.7
8	0.0	0.7	0.0	0.6	1.9	0.9	1.6	1.7	0.6	1.3	0.7	0.8	0.9

Note: Load location is the distance from the culvert centerline, measured along the perpendicular roadway centerline to the center of the loaded tandem. The axle spacing is 4 ft and the tread width is approximately 6.33 ft. The tandem is centered with respect to the roadway centerline.

cm) cover are clearly erroneous. The peak pressure predicted by Equation 2c is in much better agreement with the measured pressures and the upper bound approximated by the tire pressure. The curve corresponding to the empirical Equation 2c fits the measured data at 2 ft better than the Boussinesq and Westergaard theories, although the qualitative fit of all three curves to the data at this cover depth is judged to be acceptable. The Boussinesq equation applied to the uniformly loaded AASHTO footprints fits the data much better than the simpler equations corresponding to concentrated loads; however, the derivations from the measured pressures are consistently unconservative, in spite of the expected conservative deviation due to the neglect of soil-structure interaction. The proposed Equation 2c fits the data better, and deviations would result in conservative designs.

Also shown in Figure 6 is a comparison to a pretest two-dimensional prediction of live-load pressure distribution over the top slab for an equivalent live-load distribution (*13*). Although direct comparison of the numerical solution to measurements is hampered by the difference in modeled and actual loadings, it can be seen that the SSTIPN finite element solution obtained in this instance results in unconservative pressures on the top slab. The assumptions in the method of distributing wheel loads along the length of the structure are thought to be conservative; however, the resulting predicted earth pressures are unconservative. A similar comparison is shown in Figure 8 for 4-ft (1.22-m) cover. The finite element solution for this cover depth more closely approximates the measured data, when the difference in the loadings is taken into consideration.

At depths of cover equal to or exceeding 4 ft (1.22 m), the Boussinesq and Westergaard equations (2a and 2b) fit the data better than Equation 2c. The differences in predicted and measured pressures are slight for all three equations; however, the data indicate locally higher pressures beneath each wheel, as predicted by the Boussinesq and Westergaard theories for depths as great as 8 ft (2.44 m). The curve corresponding to Equation 2c predicts a single local maximum pressure along the wheel path for depths of 4 ft (1.22 m) or more. The Boussinesq equations for uniformly loaded AASHTO footprints again are consistently unconservative compared to the measured pressures.

Several factors account for the comparatively poor predicted pressures by the Boussinesq and Westergaard equations at shallow cover depths. First, the actual wheel loads are distributed over a finite area, approximated in design by the 10- by 20-in. (25.4- by 50.8-cm) rectangular AASHTO footprint. The Boussinesq and Westergaard equations predict the pressure beneath a concentrated load, resulting in a pressure that approaches infinity as the radial and vertical coordinates approach zero. For practical purposes, this means the theoretical equations should not be used to predict earth pressures in the immediate vicinity of the finite footprint, a limitation that has long been recognized. Also shown in Figure 4 is a pressure distribution calculated using the Boussinesq equation applied to a uniformly distributed pressure distributed over the tire contact areas. This curve, labeled "Boussinesq (distributed load)" in Figures 4-7, shows that the peak earth pressures predicted by this method are significantly less than the measured earth pressures. Second, the soil is neither linear elastic nor isotropic as is assumed in both theories. Some compensation for these differences is made by the parameters introduced in the regression analysis. Both the Boussinesq and the Westergaard theories were modified by changing variables from r and z to Br and Az, with factors A and B determined by regression to provide the best fit. In both cases, the data led to values for A and B different from 1.

The measured data may include random and systematic errors, characteristic of the transducers used. The physical

TABLE 2 RESULTS OF REGRESSION ANALYSIS

Equation No. (1)	Parameter (2)	Range Checked (3)	Value for Best Fit (4)	Ave. Error in psi (5)
(2a)	A	0.5-3.0	0.76	1.8
	B	0.5-3.0	1.50	
(2b)	A	0.5-3.0	0.61	1.4
	B	0.5-3.0	1.25	
(2c)	r_o	0.6-1.4 ft	0.62 ft	0.7
	z_o	0.6-1.4 ft	1.28 ft	
(2e)	A	0.5-3.6	3.0	45
	z_o	0.3-2.0 ft	1.2 ft	
(2f)	A	0.02-3.0	0.12	45
	z_o	0.5-8.0 ft	4.5 ft	
(2g)	A	0.02-3.0	0.1	50
	z_o	1-20 ft	12.5 ft	
(2h)	A	0.02-3.0	0.09	45
	z_o	1-20 ft	8.5 ft	

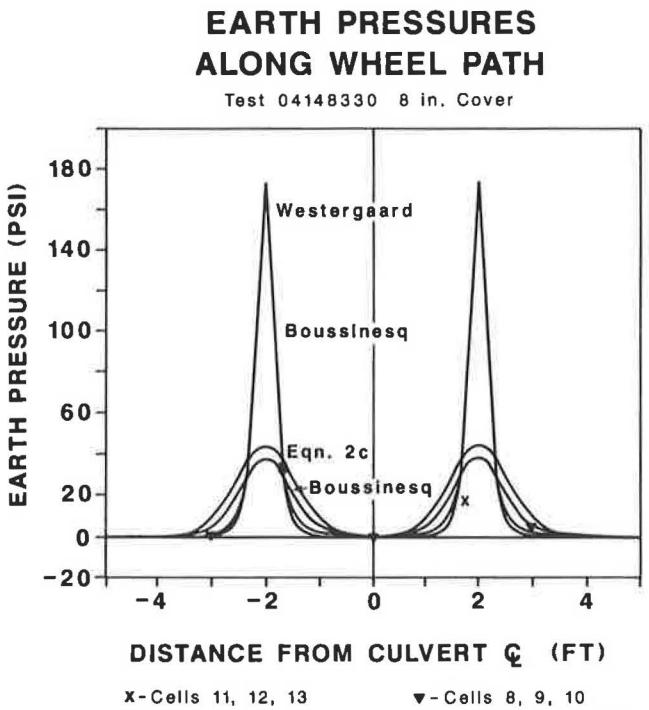

FIGURE 3 Comparison of empirical pressure prediction equations with data from Test 04148330.

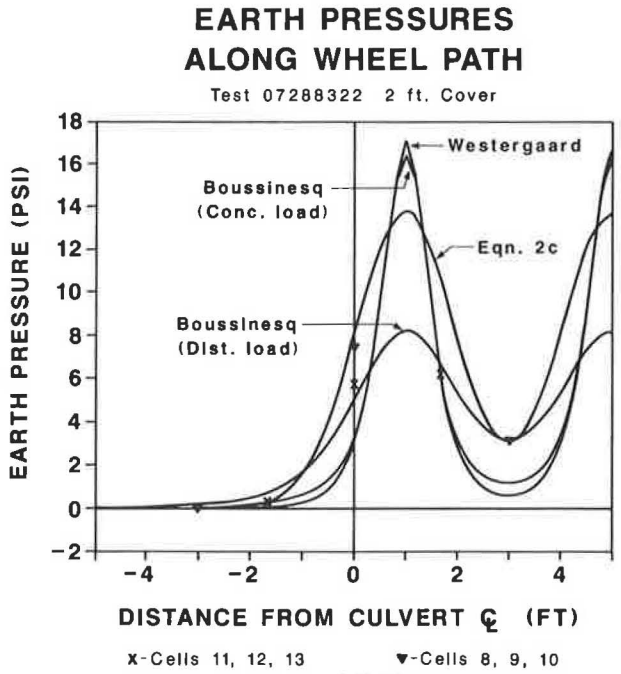

FIGURE 5 Comparison of empirical pressure prediction equations with data from Test 07288322.

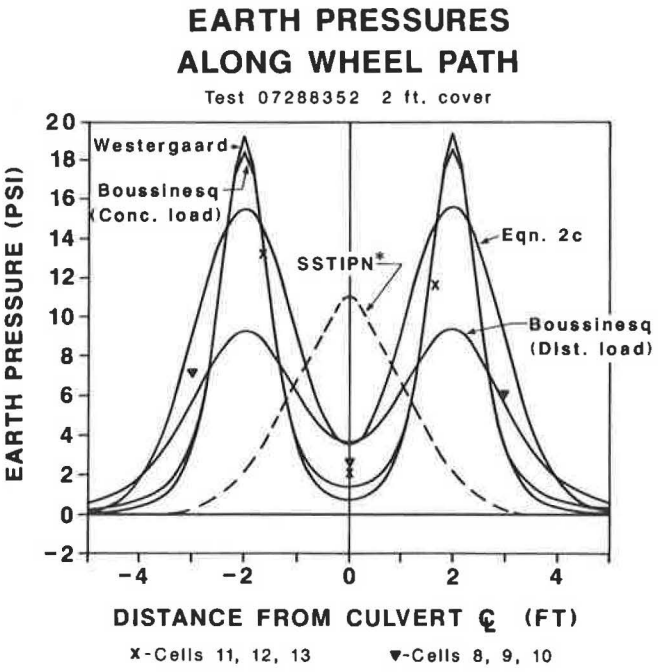

FIGURE 4 Comparison of empirical pressure prediction equations with data from Test 07288352.

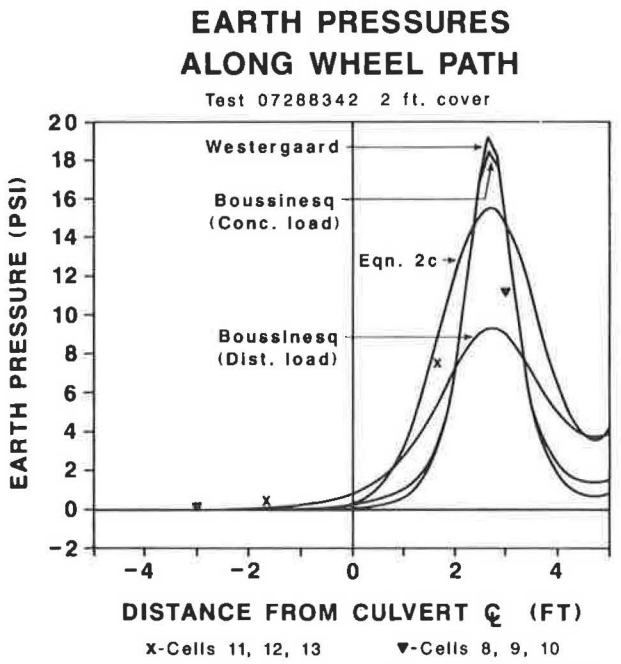

FIGURE 6 Comparison of empirical pressure prediction equations with data from Test 07288342.

size of the pressure cells results in an averaging of the earth pressure over an area approximately 6 in. (15.2 cm) square. Locally, high pressures caused by the wheel load may not be accurately reflected in the measured pressures, an effect that is more significant at shallow earth covers. This effect would result in indicated pressures less than actual pressures for cells located exactly at the point of maximum earth pressure, and indicated pressures more than actual pressures for cells located exactly at the point of minimum earth pressure. The measured earth pressures are typically several inches from local maximum theoretical pressures, at which points the errors due to the size of the transducer are expected to be negligible. Several data points lie at the location of theoretical minimum pressure, and the actual earth pressure may be slightly less than the indicated pressure at such points. Because the earth pressure gradients are not as great near the

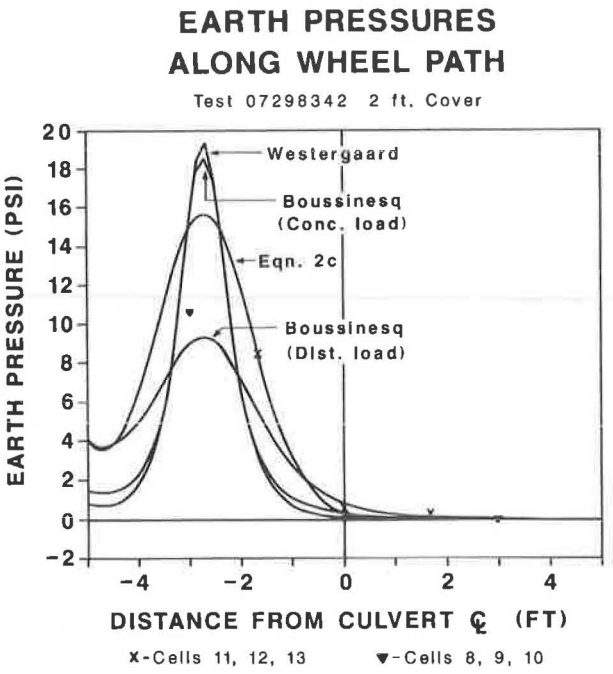

FIGURE 7 Comparison of empirical pressure prediction equations with data from Test 07298342.

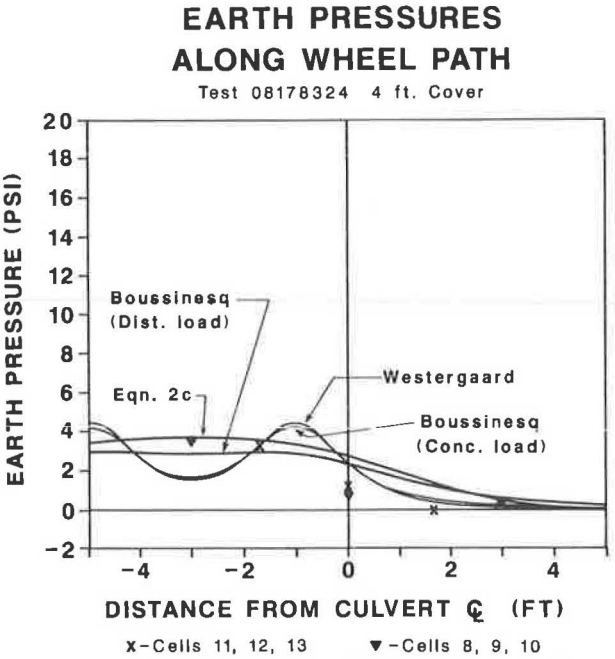

FIGURE 9 Comparison of empirical pressure prediction equations with data from Test 08178324.

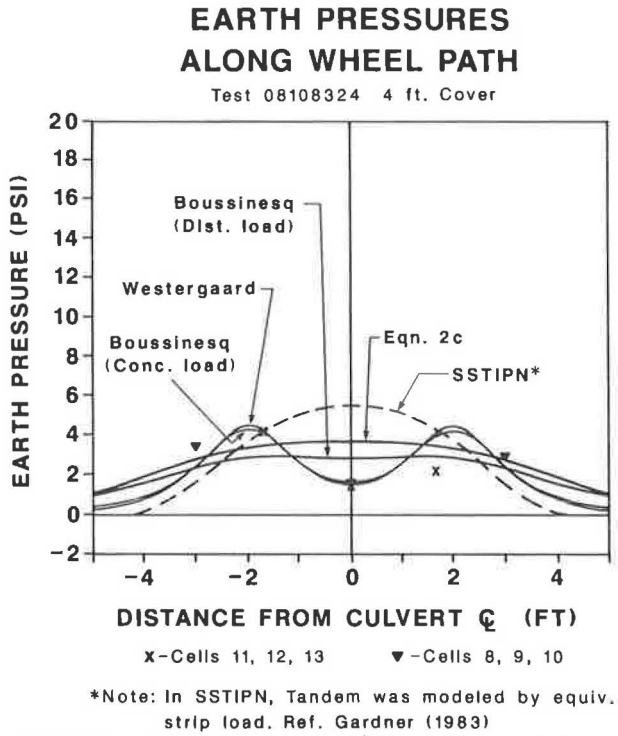

FIGURE 8 Comparison of empirical pressure prediction equations with data from Test 08108324.

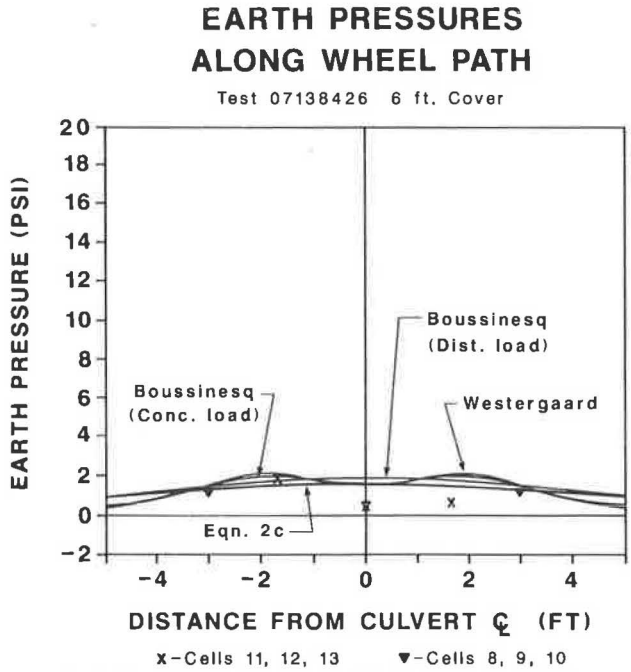

FIGURE 10 Comparison of empirical pressure prediction equations with data from Test 07138426.

local minimums, this systematic error is not as important near the minimum theoretical pressures as near the maximum theoretical pressures.

Hvorslev (*12*) discusses the effect of eccentricity of loading on a pressure cell. The presence of earth pressure gradients is equivalent to an eccentric loading because the center of pressure does not coincide with the geometric center of the cell. For a 6-in. (15.2-cm) diameter cell, Hvorslev (*12*) reports an average error of 7 percent underregistration for a 33 percent earth pressure variation across the face of the cell. For some of the extreme cases of shallow covers reported here, the pressure may experience variations on the order of 100 percent across the face of the cell. The result is that even in regions of uniform pressure gradient without the complicating factor of local pressure maxima, the pressure readings may include a systematic error, perhaps underregistering on the order of 20 percent.

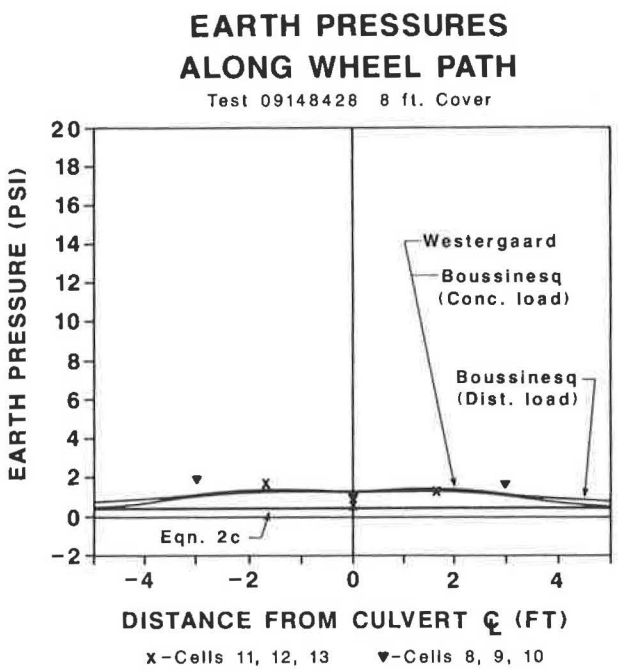

FIGURE 11 Comparison of empirical pressure prediction equations with data from Test 09148428.

Hvorslev (*12*) also discusses the effect of incomplete embedment of the pressure cell in the concrete slab. The cells were placed in the plastic concrete of the top slab as nearly flush as possible with the top surface. In spite of installation difficulties, protrusions of the cells were generally less than 0.25 in. (0.64 cm). Hence, any error caused by protrusion was expected to be underregistration in an amount dependent on the cell-soil modular ratio.

CONCLUSIONS

Data for measured live-load earth pressures is compared to existing theoretical and numerical methods, and to proposed empirical equations for predicting live-load earth pressures. The theoretical equations due to Boussinesq and Westergaard can be modified to satisfactorily model the measured earth pressure data when the depth of fill is 4 ft (1.22 m) or greater. For measured data at depths of cover up to 2 ft (1.22 m), the theoretical equations, even with empirical scaling parameters chosen for best fit, do not fit the data satisfactorily. The empirically determined Equation 2c appears to fit the data much better, particularly with respect to prediction of maximum earth pressure. The Boussinesq and Westergaard theoretical earth pressure equations for concentrated loads predict earth pressures considerably greater than the tire pressure at 8 in. (20.3 cm) of earth cover, whereas the Boussinesq equation applied to a uniformly distributed AASHTO footprint loading predicts pressures significantly less than measured. The potential systematic errors discussed probably result in underregistration of maximum earth pressures, and the suggested empirical equation appears to generally overestimate the measured earth pressures for covers up to 2 ft (0.61 m). Because the regression parameters in the proposed empirical equation are determined based on a data set including cover depths up to 8 ft (2.44 m), a better fit of the measured data for covers of 2 ft (0.61 m) or less could be determined. However, the apparent conservativism of the proposed equation is considered advantageous in the light of the potential systematic measurement errors.

The predicted wheel-load-induced pressures can be compared to the uniform pressures used in the AASHTO design procedure. Table 3 provides a comparison of the peak pressures calculated by Equation 2c and the AASHTO uniform design pressure for the 12-kip (53-kN) wheel loads of the test. Impact has not been included, and the 9.33-ft (2.84-m) width of the culvert top slab has been used as the limiting width of the AASHTO design area. From Table 3, it can be shown that the proposed equation predicts considerable higher pressures at 2 ft (0.61 m) of cover than does the AASHTO method. The deviation of the two methods is considerably less at greater depths of cover.

The proposed empirical equation offers the advantages of simplicity and accuracy for prediction pressures at cover depths of 2 ft (0.61 m) of less, with deviations from measured pressures generally resulting in conservative designs. It should be noted that the proposed equation does not provide a different pressure distribution transverse to traffic, as would be expected because of the shape of the wheel footprints.

The finite element solution compares acceptably with the measured data at depths of fill of 4 ft (1.22 m) (*13*), but at shallow covers of 2 ft (0.61 m) or less the finite element model resulted in unconservative predicted pressures. The finite element method is a two-dimensional solution, and direct comparison with the three-dimensional measured and theoretical earth pressures is difficult. In addition, the finite element solution used a single axle carrying 32 kip (142 kN) instead of the actual tandem 24-kip (107-kN) axles tested. The finite element simulation was made in advance of the tests, using soils data from laboratory tests at the site and proven modeling techniques.

TABLE 3 COMPARISON OF PEAK EARTH PRESSURES TO AASHTO METHOD

Cover (ft)	AASHTO Pressure (psi)	Equation (2c) Pressure (psi)
0.67	---	40
2	6.8	15.6
4	2.7	3.6
6	2.1	1.6
8	1.8	0.5

Note: Impact is neglected.

PRACTICAL APPLICATIONS

The measured data are applicable to designers of box culverts for service under less than approximately 2 ft (0.61 m) of cover. Extension of the results to box geometries or soils significantly different from those tested should be done with caution. The data or the empirical equations presented can be used for design or as a test case for evaluation of finite element methods to soil-structure interaction for culverts or similar structures.

ACKNOWLEDGMENTS

The research was funded by the Texas State Department of Highways and Public Transportation, to whom the authors are grateful. Other researchers contributing substantially included Harry M. Coyle, Richard E. Bartoskewitz, and Robert L. Lytton. The assistance and encouragement of the TSDHPT personnel, particularly Charles Terry, is appreciated. Assistance with construction and instrumentation by the Construction Equipment Training Division and the Texas Transportation Institute Instrument Shop is acknowledged.

REFERENCES

1. *Standard Specifications for Highway Bridges*. 13th ed., AASHTO, Washington, D.C., 1983.
2. N. M. Newmark. *Influence Charts for Computation of Stresses in Elastic Foundations*. Bulletin 338. University of Illinois Engineering Experiment Station, 1942 (reprinted June 1964).
3. L. Jurgenson. The Application of Theories of Elasticity and Plasticity to Foundation Problems. *Journal of the Boston Society of Civil Engineers*, July 1954.
4. E. J. Yoder and M. W. Witczak. *Principles of Pavement Design*. 2nd ed., Wiley, New York, 1975, 711 pp.
5. *Design Manual: Soil Mechanics, Foundations, and Earth Structures*. DM-7, NAFAC, Department of the Navy, 1971, 223 pp.
6. M. G. Katona and J. M. Smith. *CANDE: User Manual*. FHWA, U.S. Department of Transportation, Oct. 1976.
7. S. C. Anand. Stress Distributions Around Shallow Buried Rigid Pipes. *Journal of the Structural Division, ASCE*, Vol. 100, No. ST1, Proc. Paper 10258. Jan. 1974, pp. 161-174.
8. T. Krauthammer. Shallow-Buried RC Box-Type Structures. *Journal of the Structural Division, ASCE*, Vol. 110, No. 3, March 1984, pp. 637-651.
9. R. W. James, D. E. Brown, R. E. Bartoskewitz, and H. M. Coyle. *Earth Pressures on Reinforced Concrete Box Culverts*. Research Report 294-2F. Texas Transportation Institute, Texas A&M University System, College Station, Aug. 1985.
10. G. B. Sowers and G. F. Sowers. *Introduction to Soil Mechanics and Foundations*. 3rd ed. Macmillan, New York, 1970.
11. H. M. Westergaard. *A Problem of Elasticity Suggested by a Problem of Soil Mechanics: Soft Material Reinforced by Numerous Strong Horizontal Sheets*. Contributions to the Mechanics of Solids. Macmillan, New York, 1938.
12. M. J. Hvorslev. *The Changeable Interaction Between Soils and Pressure Cells; Tests and Reviews at the Waterways Experiment Station*. Technical Report S-76-7. Soils and Pavements Laboratory, U.S. Army Engineer Waterways Experiment Station. Vicksburg, Miss., June 1976.
13. M. P. Gardner, J. K. Jeyapalan, and R. W. James. *The Behavior of Reinforced Concrete Box Culverts Under Symmetrical and Unsymmetrical Live Loads*. Research Report 326-2F, Texas Transportation Institute, Texas A&M University System, College Station, Sept. 1983 (revised Aug. 1985), 161 pp.

Passive Lateral Earth Pressure Development Behind Rigid Walls

S. BANG AND H. T. KIM

An analytical solution procedure is described to estimate the developed passive lateral earth pressures behind a vertical rigid retaining wall rotating about its toe or top into a mass of cohesionless soil. Various stages of wall rotation, from an at-rest state to an initial passive state to a full passive state, are considered in the analysis. A condition of failure defined by a modified Mohr-Coulomb criterion and equilibrium conditions are used to obtain the necessary equations for solution. The development of friction along the wall surface at various stages of wall rotation is also taken into account in the analysis. Finally, the results predicted by the developed method of analysis are compared with those obtained from the experimental model tests on loose and dense sand. The comparisons show good agreements at various stages of wall movement.

The estimation and prediction of the lateral earth pressure development have been among the most important aspects in geotechnical engineering. The development of active lateral earth pressures in particular has received a considerable amount of attention, because a majority of retaining structures are designed based on the active lateral earth pressures due to the tendency of outward movement. However, design of many geotechnical structures requires consideration of passive lateral earth pressures. Several analytical and experimental studies have been made in the past to investigate the magnitude and distribution of passive lateral earth pressures developed behind the retaining walls (*1-5*). These studies have been helpful for understanding the mechanism of the development of passive lateral earth pressures. However, most of the analytical studies fail to provide adequate comparisons with experimental model test results. This failure may be in part due to the uncertainties associated with the variations of the soil strength and the wall friction with respect to the magnitude of wall movement. A need for an analytical solution that takes into account the variation of material properties at various stages of wall movement therefore has been realized.

This paper presents an analytical solution method that describes the transition of the passive lateral earth pressures from an at-rest state to an initial passive state to a full passive state behind a vertical rigid wall rotating about its toe or top into a mass of cohesionless soil. The at-rest state is defined as a stage of no wall movement. The initial passive state refers to a stage of wall rotation when only the soil element either at the top or at the toe of the wall, depending upon the location of rotation center, experiences a sufficient amount of deformation (limiting deformation) to achieve a limiting passive condition. The full passive state occurs when the entire zone of soil elements from the top to the toe of the wall is in the limiting passive condition.

When the retaining wall rotates about its toe, the initial passive state will be developed initially at the top of the wall, whereas the wall rotation about its top produces the initial passive state at the toe of the wall first. The original concept of this approach and the theoretical formulation and the numerical procedures applied to the solution of active lateral earth pressure development have already been described by the authors (*6*).

The analytical method developed has been applied to estimate the passive lateral earth pressures behind a rigid retaining wall experiencing rotations about its toe and top at various stages of rotation. The results are compared with those of experimental model tests and show in general good agreements, indicating the effectiveness of the proposed method of analysis.

THEORETICAL BACKGROUND

Full details of the formulation have been presented by Bang and Kim (*6*) previously; therefore only a brief summary of the principal features is given in the following paragraphs.

The fundamental equations governing the behavior of the system are those for two-dimensional plane-strain equilibrium (*7*).

$$\partial\sigma_x/\partial x + \partial\tau_{xz}/\partial z = 0$$

$$\partial\tau_{xz}/\partial x + \partial\sigma_z/\partial z = \gamma \qquad (1)$$

where γ indicates the unit weight of the soil. The center of the coordinate is located at the top of the retaining wall with x and z axes being taken positive toward the backfill and downward, respectively. It is obvious from Equation 1 that an additional equation is necessary to solve for the three unknown stresses. Using any familiar failure criterion for this purpose will lead to the solution at the limiting state, that is, at failure. Sokolovskii (*8*) solved this problem with a Mohr-Coulomb failure criterion in 1965. In this paper, however, to describe the transition of the passive stresses from the at-rest to the full passive state (the limiting state), a relationship

Department of Civil Engineering, South Dakota School of Mines and Technology, Rapid City, S. Dak. 57701-3995.

between the major and minor principal stresses has been assumed:

$$\text{Principal stress ratio} = (1 - \sin\psi)/(1 + \sin\psi) \quad (2)$$

In Equation 2, the angle ψ describes the slope of the line tangent to the stress Mohr's circle (Figure 1). Note that if the angle ψ equals $-\phi$ (the internal soil friction angle), Equation 2 reduces to Rankine's passive lateral earth pressure expression.

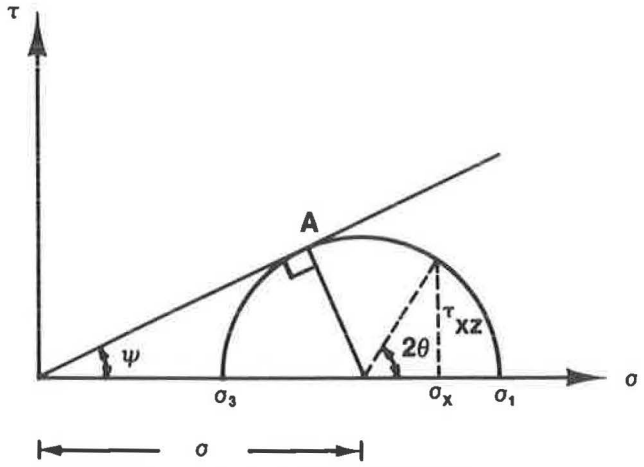

FIGURE 1 Mohr-Coulomb stress relationship.

The angle ψ is assumed to vary in magnitude from ϕ_0 to $-\phi$, where ϕ_0 indicates the inclination angle relating σ_1 and σ_3 in the at-rest state. Note that a negative magnitude of friction angle is used for the purpose of developing a general formulation, that is, a positive friction angle describes the transition of active lateral pressures. The value of ϕ_0 can be easily obtained if the at-rest lateral earth pressure coefficient K_0 is known.

$$\phi_0 = \sin^{-1}[(1 - K_0)/(1 + K_0)] \quad (3)$$

By varying the angle ψ from ϕ_0 to $-\phi$, Equation 2 could represent both the at-rest and full passive states. However, when the wall experiences movements other than translational, the resulting rotation may produce different stress ratios at different depths. In other words, a portion of the backfill soil may experience deformations exceeding the limiting value, whereas the remaining portion may not. The former case would then achieve the $\psi = -\phi$ state and the latter case the $\phi_0 > \psi > -\phi$ state. Therefore, the angle ψ describing the relationship between the major and minor principal stresses may have to be described as a function of the depth z.

Based on this assumption and Mohr's circle relationship, three unknown stresses can be expressed as

$$\begin{aligned}\sigma_x &= \sigma[1 + \sin\psi(z)\cos 2\theta] \\ \sigma_z &= \sigma[1 - \sin\psi(z)\cos 2\theta] \\ \tau_{xz} &= \sigma\sin\psi(z)\sin 2\theta\end{aligned} \quad (4)$$

where

σ = $(\sigma_1 + \sigma_3)/2$ at any depth z, and
θ = rotation angle from the x-axis to the direction of σ_1 measured clockwise positive (Figure 2).

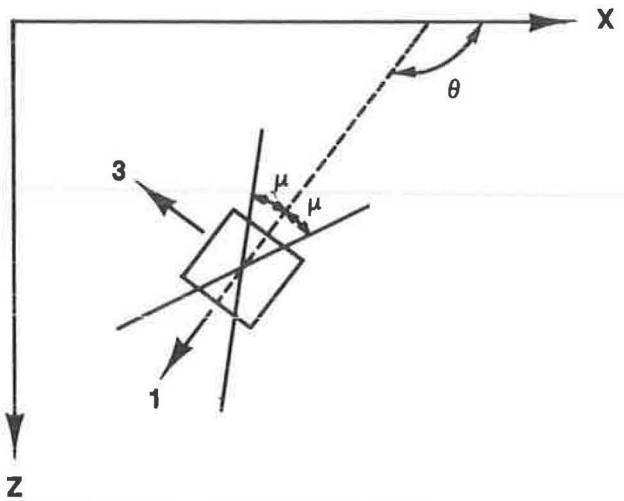

FIGURE 2 Orientation of pseudoslip lines.

Substitution of Equations 4 into Equations 1 leads to the following pair of differential equations (*6*):

$$d\sigma + 2\sigma\tan\psi(z)d\theta = \gamma\,(dz + \tan\psi(z)dx) + \sigma\,[\partial\psi(z)/\partial z]\,dx \quad (5)$$

$$d\sigma - 2\sigma\tan\psi(z)d\theta = \gamma\,(dz - \tan\psi(z)dx) - \sigma\,[\partial\psi(z)/\partial z\,]dx \quad (6)$$

Equations 5 and 6 contain the four unknowns x, z, σ, and θ. Additional two equations for the necessary solutions can be obtained from the geometry of the slope of pseudoslip lines as shown in Figure 2. As can be seen from the figure, the slopes can be expressed as

$$dz/dx = \tan(\theta \pm \mu) \quad (7)$$

where μ indicates a rotation angle from the direction of σ_1 to the pseudoslip lines. It is obvious from the Mohr-Coulomb stress circle relationship (Figure 1) that

$$\mu = \pi/4 - \psi(z)/2 \quad (8)$$

Equations 5-8 can be solved simultaneously with appropriate boundary conditions. A backward finite difference method has been applied for the solution. The resulting expressions are as follows:

$$z_{i,j} - z_{i-1,j} = (x_{i,j} - x_{i-1,j})\tan(\theta_{i-1,j} - \mu_{i-1,j}) \quad (9)$$

$$z_{i,j} - z_{i,j-1} = (x_{i,j} - x_{i,j-1})\tan(\theta_{i,j-1} + \mu_{i,j-1}) \quad (10)$$

$$\begin{aligned}&(\sigma_{i,j} - \sigma_{i-1,j}) - 2\sigma_{i-1,j}(\theta_{i,j} - \theta_{i-1,j})\tan\psi_{i-1,j} \\ &= \gamma[(z_{i,j} - z_{i-1,j}) - (x_{i,j} - x_{i-1,j})\tan\psi_{i-1,j}] \\ &\quad - \sigma_{i-1,j}(x_{i,j} - x_{i-1,j})\partial\psi/\partial z|_{i-1,j}\end{aligned} \quad (11)$$

$$(\sigma_{i,j} - \sigma_{i,j-1}) + 2\sigma_{i,j-1}(\theta_{i,j} - \theta_{i,j-1})\tan\psi_{i,j-1}$$
$$= \gamma[(z_{i,j} - z_{i,j-1}) + (x_{i,j} - x_{i,j-1})\tan\psi_{i,j-1}]$$
$$+ \sigma_{i,j-1}(x_{i,j} - x_{i,j-1})\partial\psi/\partial z\,|_{i,j-1} \quad (12)$$

Equations 9-12 completely describe recurrence formulas for the determination of the pseudoslip line coordinates $x_{i,j}$ and $z_{i,j}$, the pseudoslip line slope ($\theta_{i,j} \pm \mu_{i,j}$), and the associated average stress ($\sigma_{i,j}$) in terms of previous values at coordinates i-1,j and i,j-1. The solution process starts from the backfill ground surface whose coordinates and stress values are known and proceeds to the back face of the wall (*8*).

However, the detailed solution steps require a description of the function $\psi(z)$ and its derivative, which define the transition of lateral earth pressures from the at-rest to the full passive state. As discussed before, the function varies from ϕ_0 in the at-rest state to $-\phi$ in the full passive state. The variation between these two extreme values is assumed to be as follows:

1. Rotation about the toe. Let β denote the stage of wall rotation so that $\beta = 0$ for the at-rest state, $\beta = 1.0$ for the initial passive state, and $\beta = 2.0$ for the full passive state. In other words, for values of β between 0 and 1.0, transition from an at-rest to an initial passive state is described with β directly proportional to the deformation of the wall, that is, in the elastic range.

Values of β between 1.0 and 2.0 describe the transition from an initial passive to a full passive state, that is, in the elastoplastic range. Figure 3 shows the schematic variation of $\psi(z)$. At $\beta = 1.0$, the variation of $\psi(z)$ is assumed to be $\psi(z) = -\phi$ at $z = 0$ and $\psi(z) = \phi_0$ at $z = H$, because by definition the initial passive state describes a stage of wall rotation when only the soil element at $z = 0$ reaches a limiting passive condition. The original concept of this approach was first proposed by Dubrova as reported by Harr (*9*) in his method of redistribution of pressures.

The variations of $\psi(z)$ at various values of β assumed in the analysis are shown in Figure 3. They can be expressed, for $0 \leq \beta \leq 1.0$, as

$$\psi(z) = \phi_0 - (\phi + \phi_0)(1 - z/H)\beta$$

$$\partial\psi(z)/\partial z = \beta(\phi + \phi_0)/H \quad (13)$$

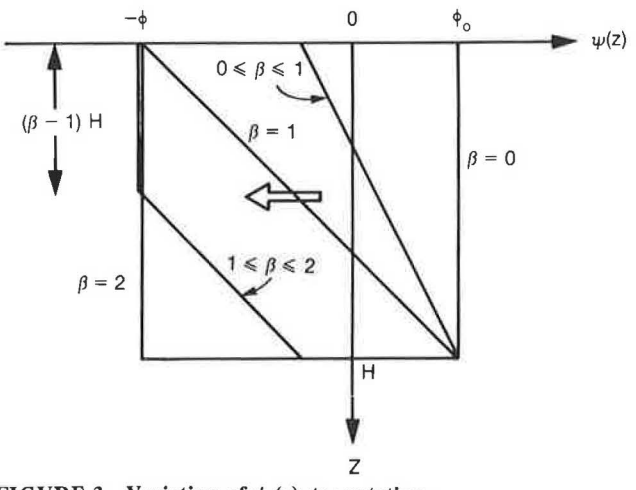

FIGURE 3 Variation of ψ (z), toe rotation.

For $1.0 < \beta \leq 2.0$, within a zone already in the limiting passive condition $[0 \leq z \leq (\beta - 1)H]$,

$$\psi(z) = -\phi$$

$$\partial\psi(z)/\partial z = 0 \quad (14)$$

Within a zone not yet in the limiting passive condition $[(\beta - 1)H \leq z \leq H]$,

$$\psi(z) = \phi_0 - (\phi + \phi_0)(\beta - z/H)$$

$$\partial\psi(z)/\partial z = (\phi + \phi_0)/H \quad (15)$$

2. Rotation about the top. The description of ψ variation in this mode of retaining wall movement remains the same as for the case of toe rotation, except the initial passive state occurs at the toe of the retaining wall. Applying the same logic, one obtains for $0 \leq \beta \leq 1.0$,

$$\psi(z) = \phi_0 - (\phi + \phi_0)z/H\beta$$

$$\partial\psi(z)/\partial z = -\beta(\phi + \phi_0)/H \quad (16)$$

For $1.0 < \beta \leq 2.0$, within a zone already in limiting passive condition $[(2 - \beta)H < z \leq H]$,

$$\psi(z) = -\phi$$

$$\partial\psi(z)/\partial z = 0 \quad (17)$$

Within a zone yet to reach the limiting passive condition $[0 \leq z \leq (2 - \beta)H]$,

$$\psi(z) = \phi_0 - (\phi + \phi_0)(\beta - 1 + z/H)$$

$$\partial\psi(z)/\partial z = -(\phi + \phi_0)/H \quad (18)$$

The variation of the angle $\psi(z)$ in this mode of retraining wall movement is schematically illustrated in Figure 4.

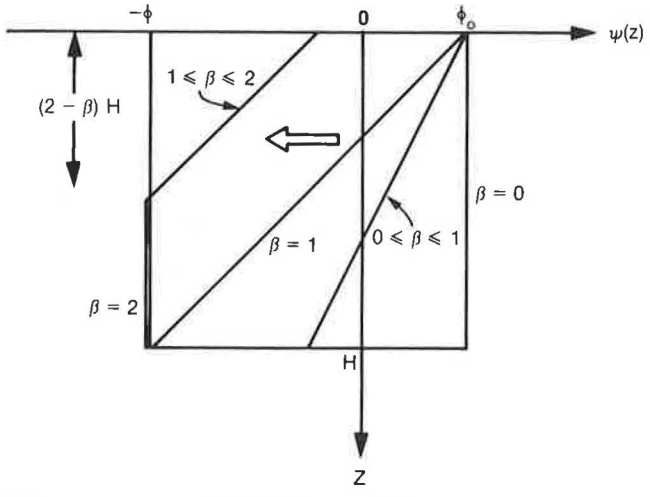

FIGURE 4 Variation of ψ (z), top rotation.

COMPARISON WITH MODEL TESTS

The results from the proposed method of analysis were compared with those from model test results reported by Narain et al. (*4*). The height of the wall was 1.5 ft and hand tamping was used to obtain the desirable soil densities. The tests were performed on dry Ranipur sand using a model wall made of steel. Included were two types of passive wall movement, rotations about the toe and the top. The normal pressures developed on the wall at different displacements were measured using three soil pressure transducers, located at depths of 0.33, 0.88, and 1.33 ft from the top of the backfill. The displacements of the wall shown in Figures 5-8 were measured at its midheight.

Figures 5-8 show the detailed comparisons of predicted and measured passive lateral earth pressures on the wall at various stages of wall rotation. The internal friction angle ϕ of sand and the wall friction angle δ reported by Narain et al. (*4*) with other pertinent soil properties used in the analysis are also included in the figures. The values of initial at-rest lateral earth pressure coefficient K_0 were obtained from the measured earth pressure distributions at rest, which were essentially constant with depth. The unit weights γ of the sand, however, were backcalculated from the relationship between the soil density and its angle of internal friction reported by Sherif et al. (*10*) (because Narain et al. did not report these properties). The values of β indicating the various stages of wall rotation as shown in the figures were obtained from limiting deformations defining the passive state. The limiting deformations were calculated by assuming that at β of 1.8 or greater the passive earth pressures were close to the largest measured values.

As shown in Figures 5 and 6, in general the agreements are good for the cases when the wall rotates about its toe with loose or dense sand backfill, except near the toe of the wall with relatively large deformations. When the wall experiences a rotation about its top, the comparison shows good agreement for loose sand (Figure 7) but not as good for dense sand (Figure 8), particularly at the pressure cell located near the midheight. It is highly unlikely that, as the middle pressure cell measurements in Figure 8 indicate, the passive pressure decreases as the wall rotation increases. Overall, the calculated lateral earth pressures predict measured values reasonably well, considering the uncertain variations in measurements. It is also noted that when the wall rotates about its toe, parabolically-shaped pressure distributions are obtained during transition periods from both analytical and experimental results (Figures 5 and 6). Similar observations have been made during the study of active lateral earth pressure transition, supporting many previous researchers' findings, both analytical and experimental, that suggest a similarly shaped pressure distribution.

CONCLUSIONS

A numerical solution method has been developed to estimate the magnitude and distribution of the passive lateral earth

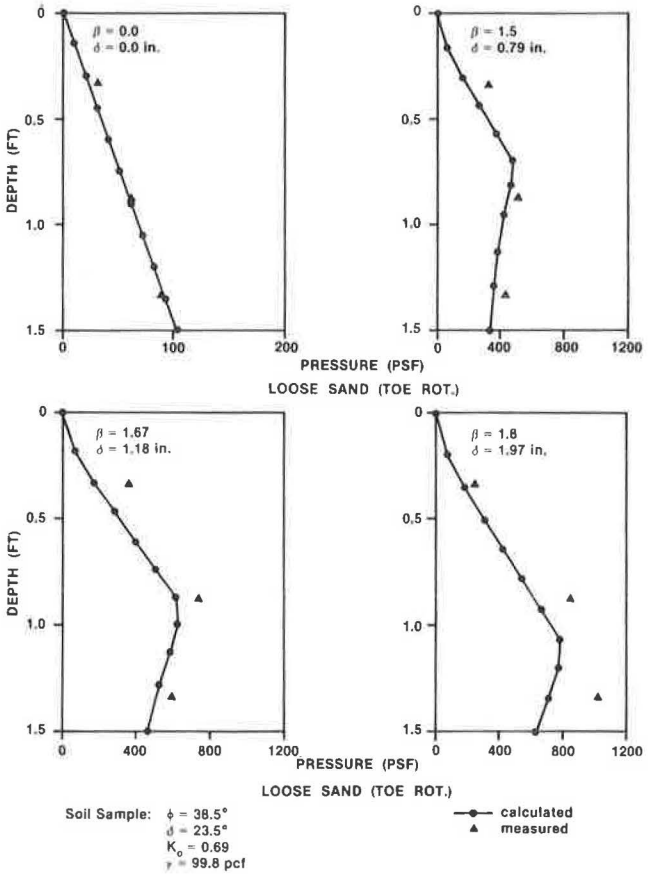

FIGURE 5 Model test comparison for loose sand, toe rotation.

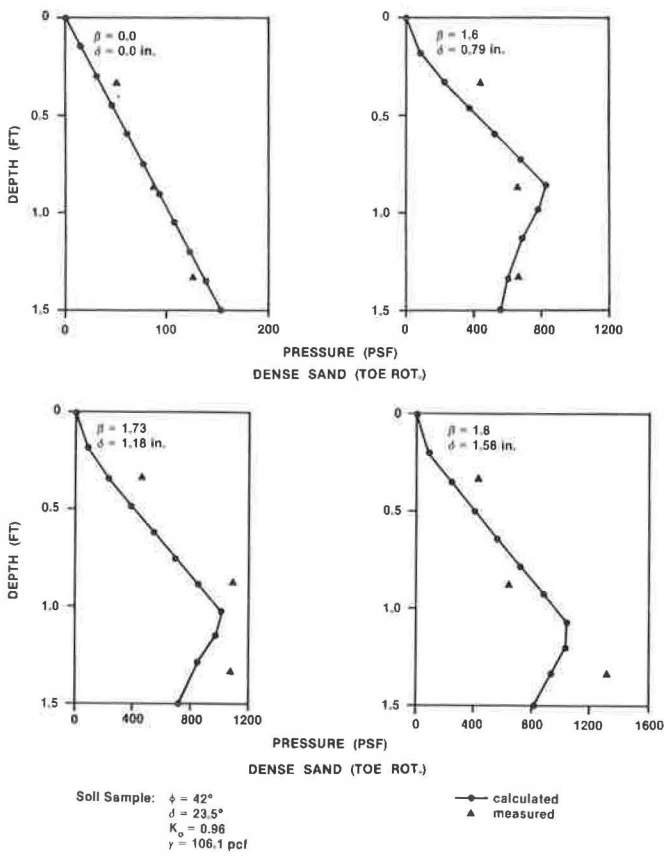

FIGURE 6 Model test comparison for dense sand, toe rotation.

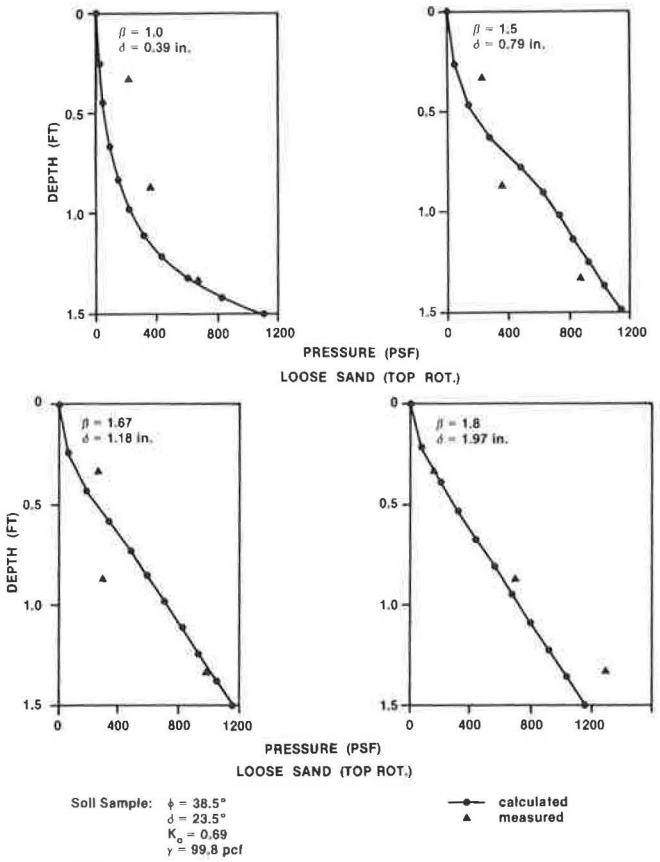

FIGURE 7 Model test comparison for loose sand, top rotation.

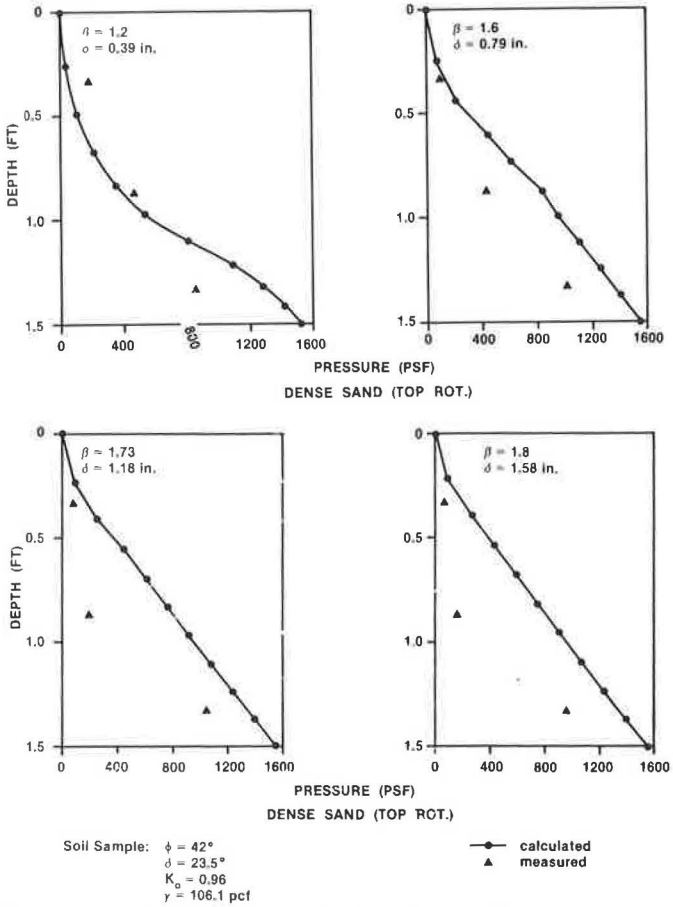

FIGURE 8 Model test comparison for dense sand, top rotation.

pressures behind a vertical rigid wall supporting cohesionless backfill soil. Included are various stages of wall rotation about either the top or the toe. The developed method is capable of predicting the transition of the passive lateral earth pressures, starting from the at-rest state associated with no wall movement to the initial-passive to the full-passive state when the entire soil mass is in limiting equilibrium state. Comparisons with several experimental model test results have also been made and good agreements are observed.

The proposed solution method can be further improved without difficulty to take into consideration the depth-dependent strength and material characteristics, the sloping backfill, and the layered soil deposits. It can also be expanded to analyze the transition of lateral earth pressures associated with various types of wall movement, including the translation and the rotation about the midheight under an active or passive condition.

The developed solution method includes many assumptions; namely, the limiting deformation to achieve a passive state, the validity of Mohr-Coulomb failure criterion, and the relationship between major and minor principal stresses. These assumptions should therefore be studied further, as additional experimental data become available, so that the true behavior of the lateral earth pressure transition can be modeled effectively. The effects of various parameters defining the system can then be analyzed in detail through an analytical parametric study.

REFERENCES

1. K. S. Wong. *Elasto-Plastic Finite-Element Analyses of Passive Earth Pressure Tests.* Ph.D. dissertation, University of California, Berkeley, 1978.
2. R. G. James and P. L. Bransby. Experimental and Theoretical Investigations of a Passive Earth Pressure Problem, *Geotechnique,* Vol. 20, No. 1, 1970.
3. J. Graham. Calculation of Passive Pressure in Sand. *Canadian Geotechnical Journal*, Vol. 8, 1971.
4. J. Narain, S. Saran, and P. Nandakumaran. Model Study of Passive Pressure in Sand. *Journal of the Soil Mechanics and Foundations Division, ASCE,* Vol. 95, No. SM4, July 1969.
5. P. W. Rowe and K. Peaker. Passive Earth Pressure Measurements. *Geotechnique,* Vol. 15, No. 1, 1965.
6. S. Bang and H. T. Kim. At-Rest to Active Earth Pressure Transition. In *Transportation Research Record 1105,* TRB, National Research Council, Washington, D.C., 1986, pp. 41-47.
7. S. P. Timoshenko and J. N. Goodier. *Theory of Elasticity.* 3rd ed., McGraw-Hill, New York, 1970.
8. V. V. Sokolovskii. *Statics of Granular Media.* Pergamon, Oxford, 1965.
9. M. E. Harr. *Foundations of Theoretical Soil Mechanics.* McGraw-Hill, New York, 1966.
10. M. A. Sherif, I. Ishibashi, and C. D. Lee. *Dynamic Earth Pressures Against Retaining Structures.* Soil Engineering Research Report 21. University of Washington, Seattle, Jan. 1981.